

SUPPLEMENTARY FIGURE LEGENDS

Fig. S1. Optimal ssDNA sequence length – 25nt – for stem-loop structure prediction. **a)** Loop stability scores (ΔG , kcal/mol) with gradually increased sequence length of ssDNA (starting from 13nt, 4nt increase per escalation, centred on the mutation site) considering 6 passenger mutations. Passengers include 4 silent mutations, 1 mutation within transit peptide and 1 missense mutation on gene with an absence of mRNA expression in bladder cancer. Colours represent different passenger mutations. Solid and dashed arrows represent the completion of primary and occurrence of neighbouring/secondary stem-loop structures, respectively. **b)** Examples of predicted stem-loop structures for *PDE3A* L275L mutation across series of ssDNA lengths. *In PDF file page 4.*

Fig. S2. The frequency of all mutations in 602 bladder cancers follows a long-tail distribution **(a)** and identification of the optimal frequency threshold (counts ≥ 4) for 130 hotspot mutations **(b)**. Ratios of the number of mutations with a count larger than this integer ($n(c>x)$) to the number of mutations with a count equal to this integer ($n(c=x)$). Details of these hotspot mutations are summarised in Supplementary Tables 1. Related to Figure 1a and Table 1. *In PDF file page 5.*

Fig. S3. Identification of 44 APOBEC-associated hotspot mutations in BCa. Hotspot mutations corresponding to an APOBEC-type motif (TCN \rightarrow T[G/T]N mutations, N = any base) were considered as candidate APOBEC-associated hotspot mutations ($n=59$). Comparisons were made for the fraction score of APOBEC-mediated mutagenesis in tumours bearing one of the given candidate APOBEC-associated hotspot mutation with tumours free of any these hotspot mutations. *P* value: Wilcoxon test. ***, $P<0.001$; **, $P<0.01$; *, $P<0.05$ and N.S. for not significant. Color scale for *P* value from lowest to highest. X axis: 44 APOBEC-associated hotspot mutations are in red and others in black. Related to Figure 1a and Table 1. *In PDF file page 6.*

Fig. S4. Attributable mutagenic process to each of 130 hotspot mutations identified from 602 bladder cancers using Letouzé *et al.* algorithm **(a)** 44 hotspot mutations classified as APOBEC-associated one according to our initial method and **(b)** 86 other hotspot mutations. Red represents tumour sample bearing the given mutation that was attributed to APOBEC mutagenesis; Blue for Age-associated mutagenesis; Green for ERCC2-related mutagenesis. *In PDF file page 7.*

Fig. S5. *AID/APOBEC* gene expression (RSEM, log2) in relation to APOBEC-associated mutations – tumours with vs. without any of 44 APOBEC-associated mutations in 602 bladder cancers. *P* value: Wilcoxon test between two groups. *In PDF file page 8.*

Fig. S6. APOBEC-mediated mutagenesis confers special characteristics to its target mutations, containing 43 figures in total from **a)** to **aq)**. Plots related to Figure 2a-c. For each of the included 43 APOBEC-associated hotspot mutations (mapping to 32 genes) identified in bladder cancer, we show replication fork directionality (RFD) during DNA replication in the HeLa cell line (upper panel),

predicted stem-loop structure (middle panel) and the mutation spectrum of the corresponding gene (lower panel). DNA stem-loop structures were predicted with 25 nt length ssDNA centred on mutated site. The interpretation of the results is similar to that of the example of *ERBB2* S310F shown in the main figures (Figure 2e-g). The RFDs of eight other cell lines are summarised in Supplementary Table 1. *In PDF file page 10-52.*

Fig. S7. Mutation spectra for the 55 APOBEC-target genes identified from other cancer types, including 55 figures in total. Related to Figure 3c. Red rectangles indicate APOBEC-associated hotspot mutations. The other cancer types corresponded to 3,751 tumours from patients with cervical, head and neck, breast and lung cancer. Most of the over-represented mutations are associated with APOBEC-mediated mutagenesis within its target genes. *In PDF file page 54-108.*

Fig. S8. mRNA levels (RSEM, log₂) for (a) known and (b) suspected tumour suppressor genes (TSGs) according to the APOBEC-associated mutations of these TSGs – tumours with a given APOBEC-associated hotspot mutation vs. tumours with wild-type alleles for each known/suspected TSG in bladder cancer. *RREB1* as a suspected TSG. RNA-Seq data are available in 406 bladder cancers from The Cancer Genome Atlas (TCGA). *P* value: Wilcoxon test between two groups. *In PDF file page 109.*

Fig. S9. Evaluation for the stringency of expression and loop stability for cancer gene and likely passenger mutation. **a)** Distribution comparison of mRNA levels between known cancer genes and all genes at the whole-transcriptome scale (as background) across 32 cancer types from The Cancer Genome Atlas (TCGA). All genes' expression was rank-transformed and functional annotation for cancer genes are curated from a recent publication (Method). Cancer genes' expression ranks in 32 cancer types were shown in Supplementary Table 3. **b)** Stem-loop deltaG distribution of 1000 expression-matched non-recurrent mutations and the 7 known passenger mutations. 1000 mutations were randomly selected from non-recurrent mutations (mutated only once in the cohort) in genes with matched expression level ($\pm 1\%$) to the genes hosting the known passengers ($n = 7$) (Methods). *In PDF file page 110.*

Fig. S10. Permutation-based FDR estimation for predicted APOBEC-associated drivers and passengers. Benjamin-Hochberg adjustment was applied for multiple testing to produce the corrected final FDR estimation (Methods). Predictions with FDR < 0.05 were considered as confident. *In PDF file page 111.*

Fig. S11. Oncoprint (A) and interaction plot (B) of the 26 driver mutations. Driver mutations include the known drivers ($n=9$) and predicted ones ($n=17$). *P*-value for probability of mutations being co-occurred or mutual exclusive. *In PDF file page 112.*

Fig. S12. Functionality evaluation for *TBC1D12* mutations in bladder cancer (BCa). **a)** *TBC1D12* Mutation spectrum in BCa. Red rectangle marked *TBC1D12* (c.-1G>A) 5'-UTR mutation which was APOBEC-associated. **b)** Computed selection intensity of *TBC1D12* mutations. Selection intensity was calculated by cancer effect size algorithm that estimates functional importance of each mutation (Method). Red dot marked *TBC1D12* (c.-1G>A) 5'-UTR mutation which was APOBEC-associated and showed a very low intensity, indicating less important function of this mutation. *In PDF file page 113.*

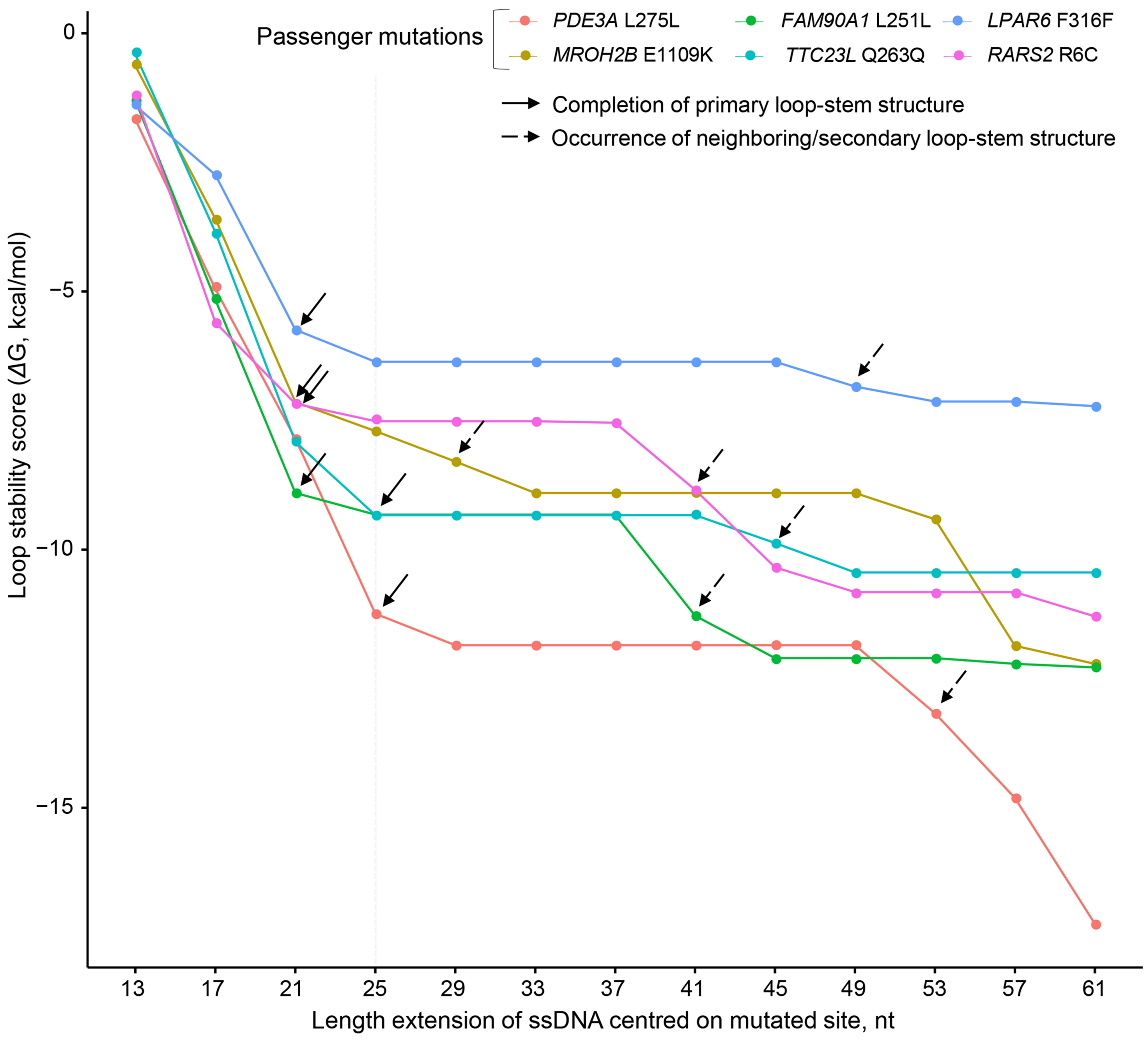
Fig. S13. Distribution of the fraction of APOBEC signature mutations between tumors of luminal and non-luminal subtypes. *P*-value for wilcoxon rank-sum test. *In PDF file page 114.*

Fig. S14. Correlation between *AHR* gene expression and GRISPR-mediated AhR knock-out effect. TPM, transcripts per million . *In PDF file page 115.*

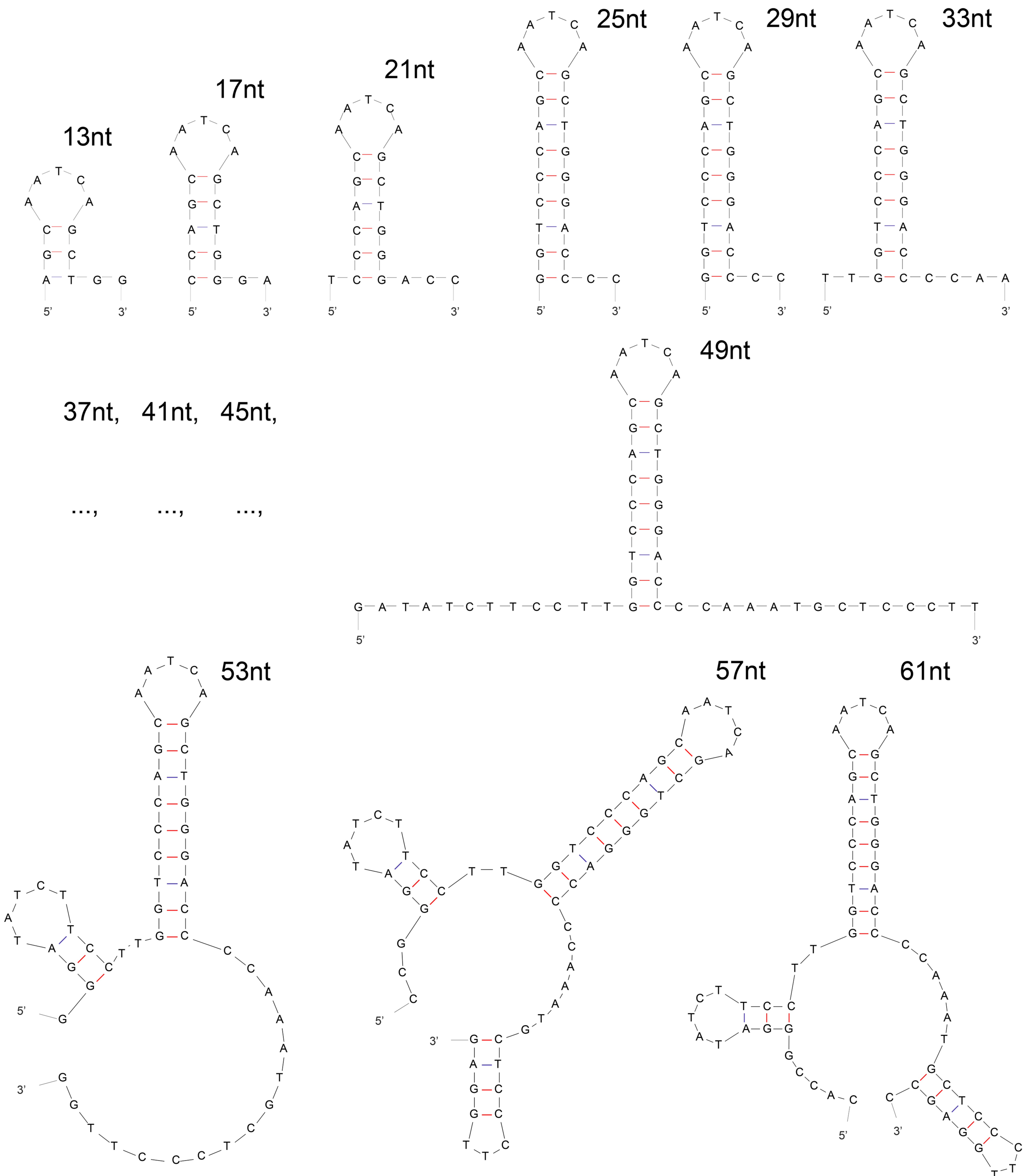
Fig. S15. Scatter plot showing BCa cell lines' AHR/ARNT dependency scores against corresponding cumulative fractions by subtype. *P*-value from Wilcoxon signed-rank test comparing luminal cell lines' dependency scores and their quantile counterparts in nonLuminal cell lines, either directly extracted or obtained by localized linear interpolation. *In PDF file page 116.*

Fig. S16. GLR (generalized linear regression modeling) predicted driver probability by similarity-based classification. *In PDF file page 117.*

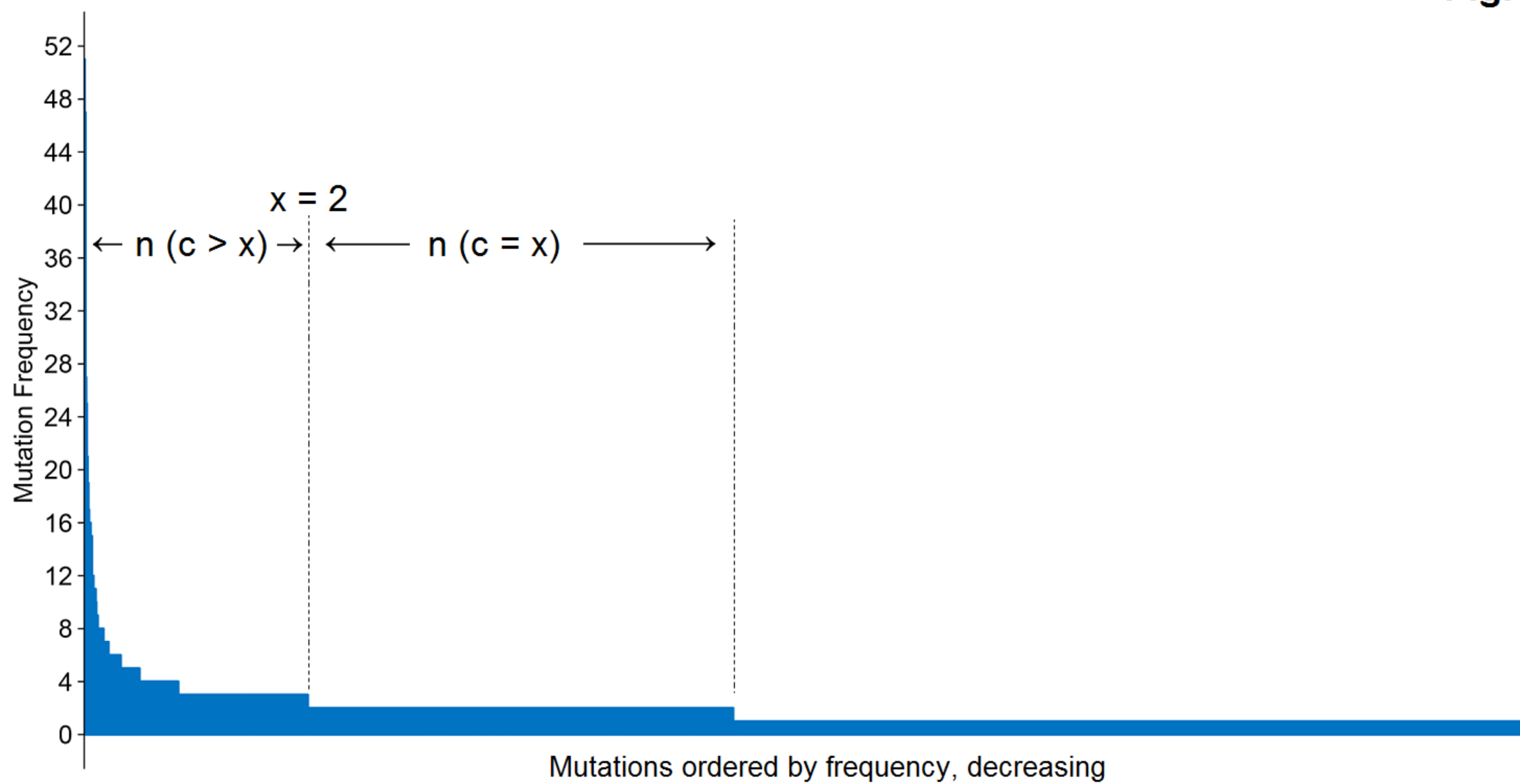
A



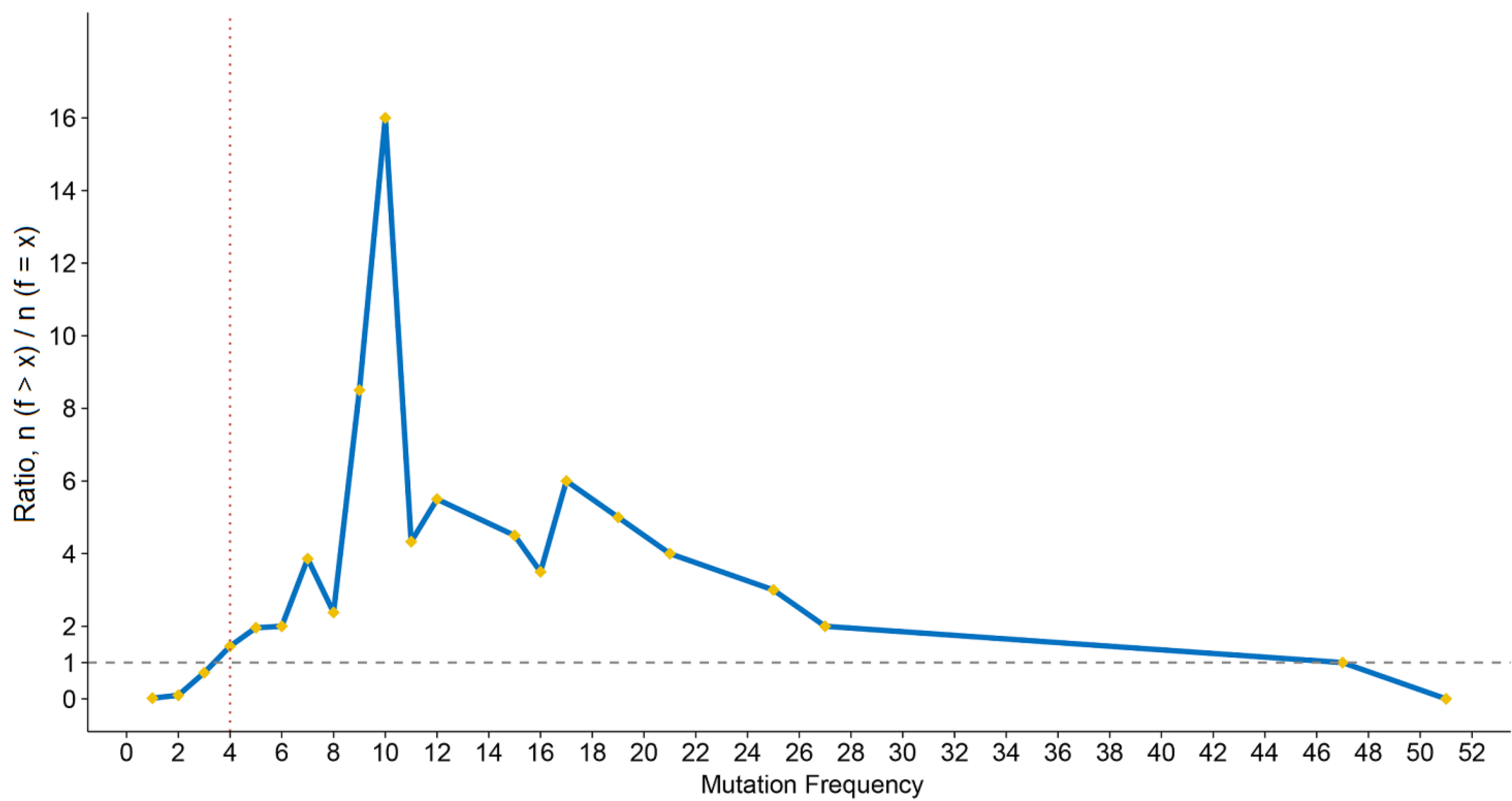
B

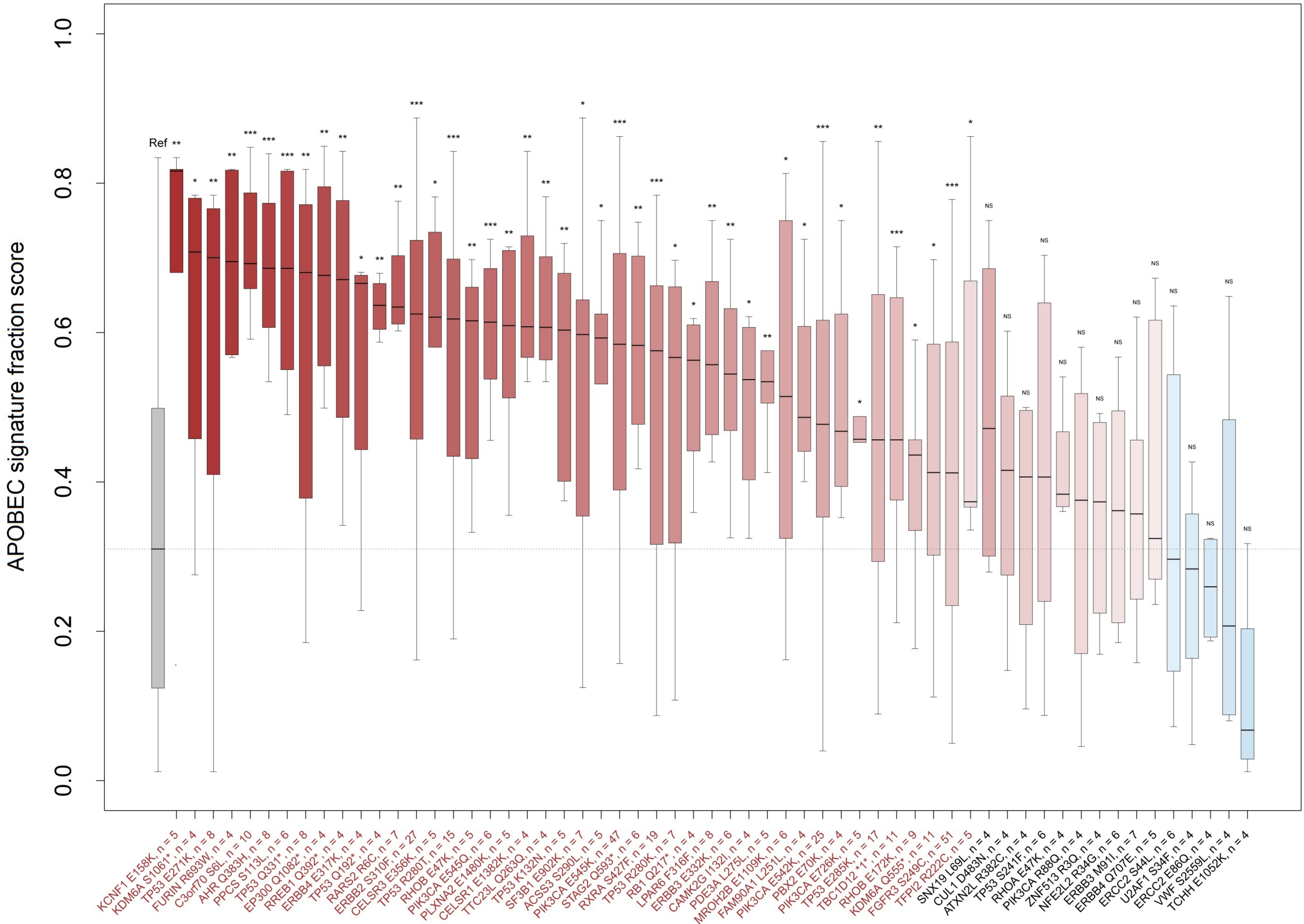


A



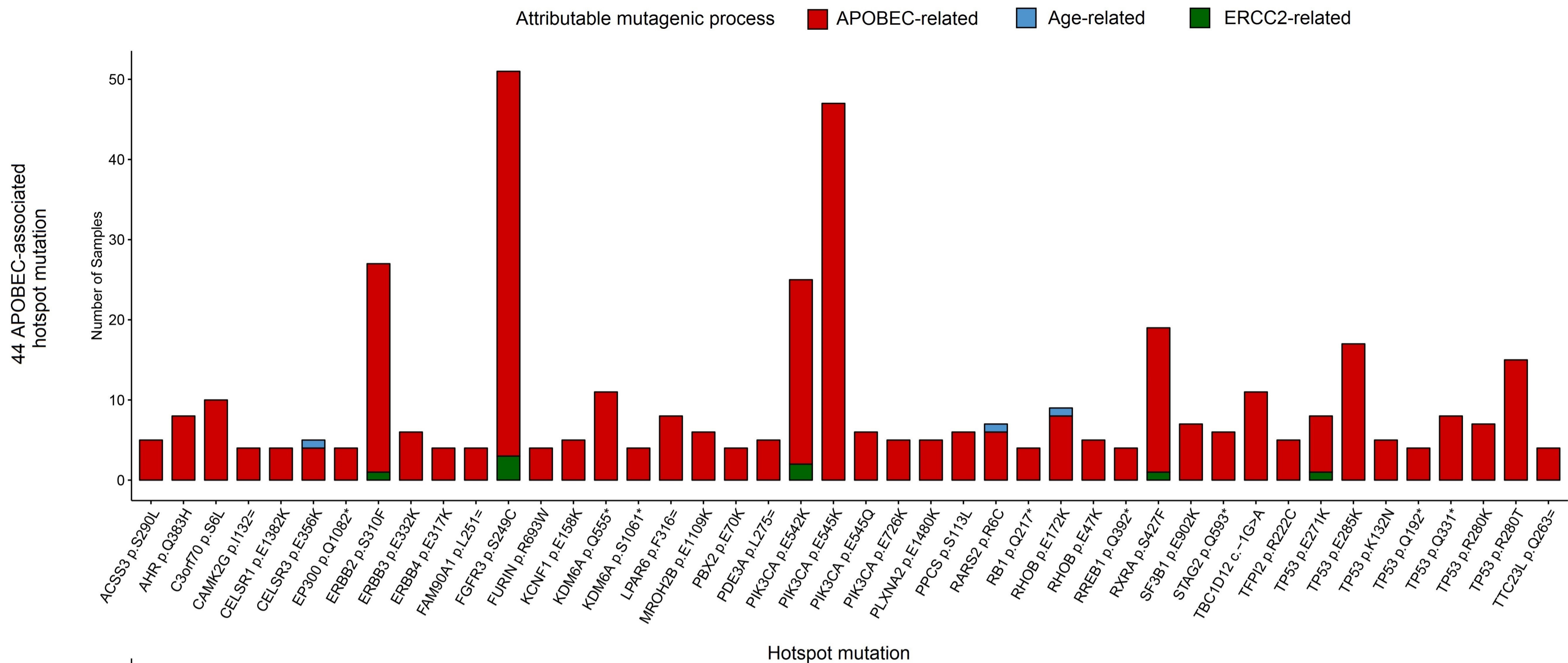
B



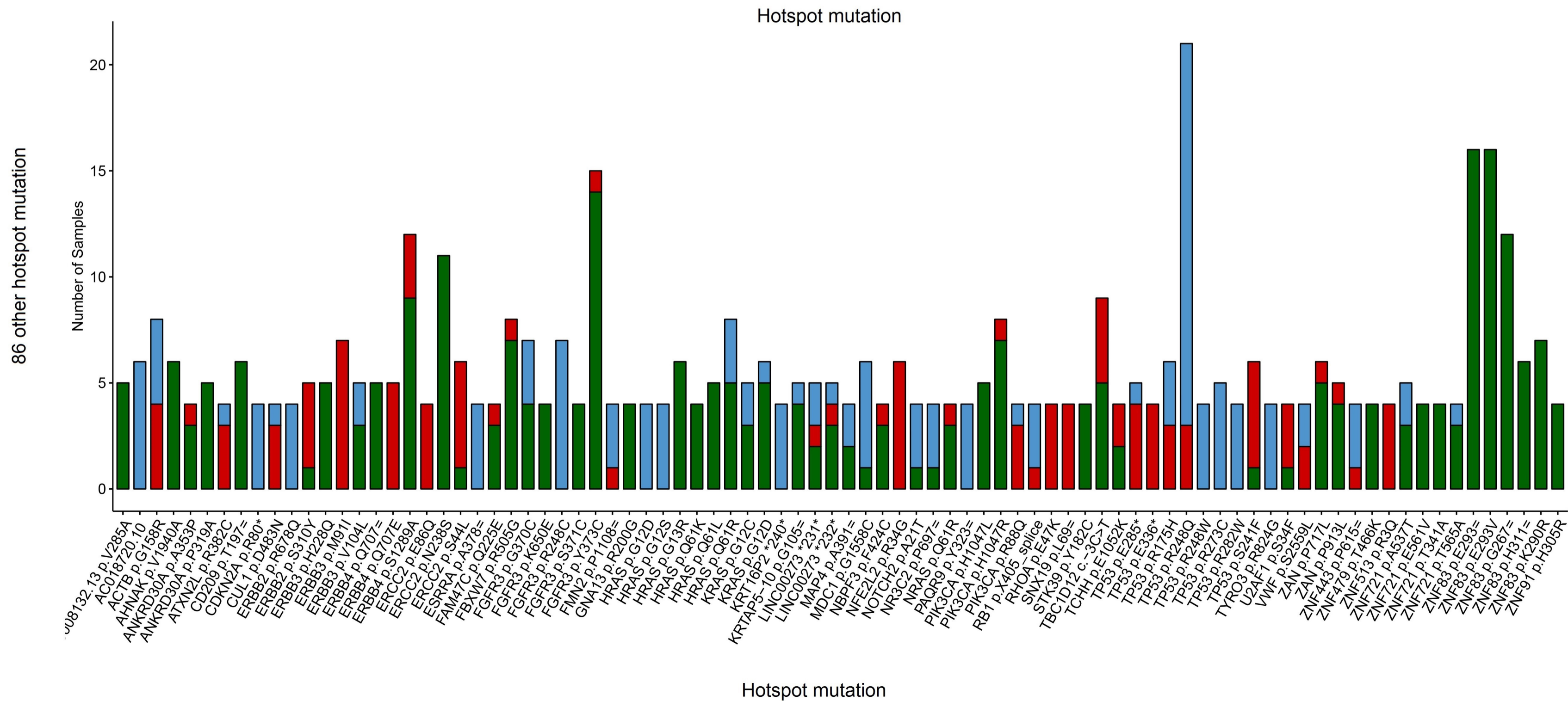


Candidate APOBEC-associated hotspot mutations, $n = 59$

A



B



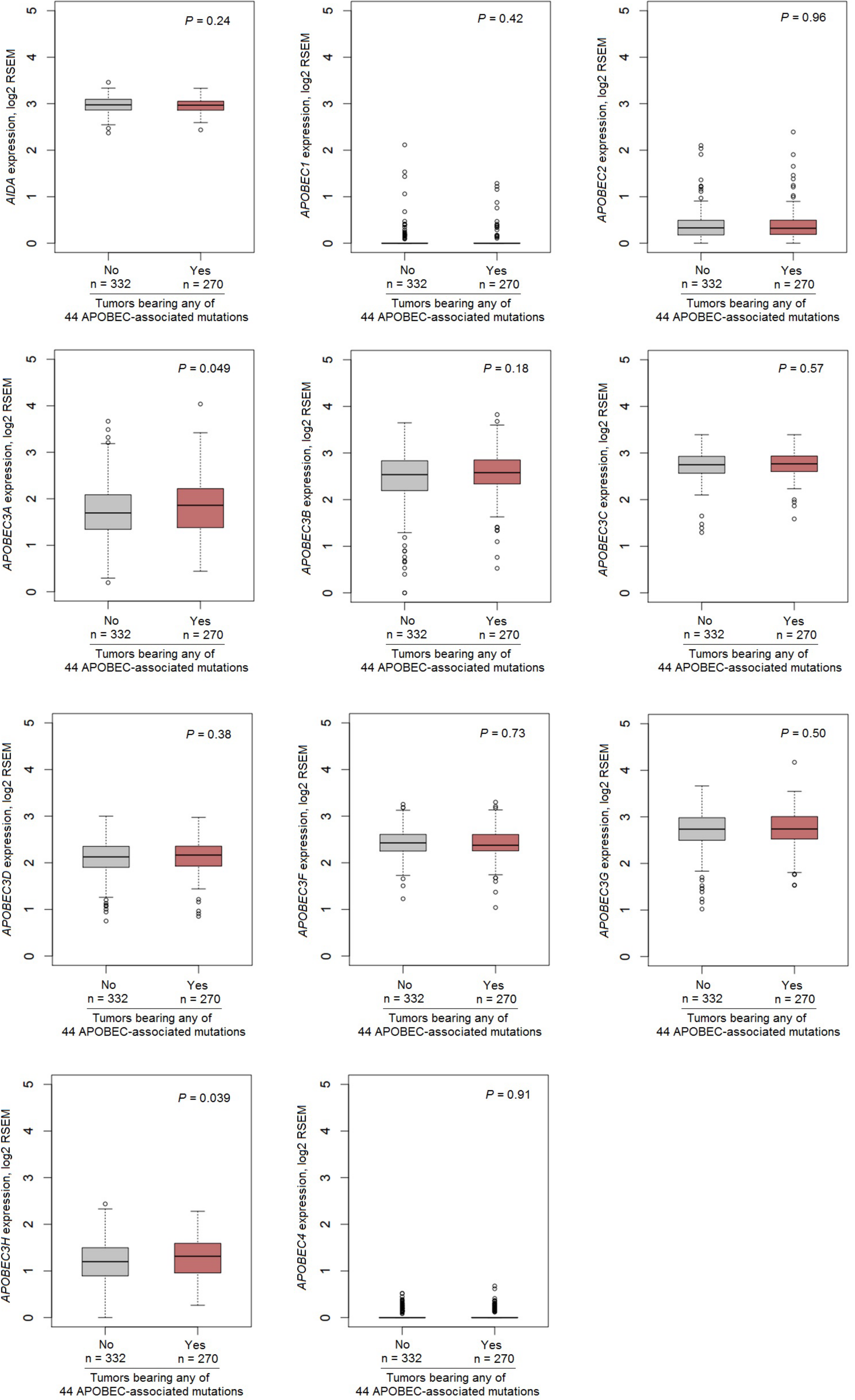
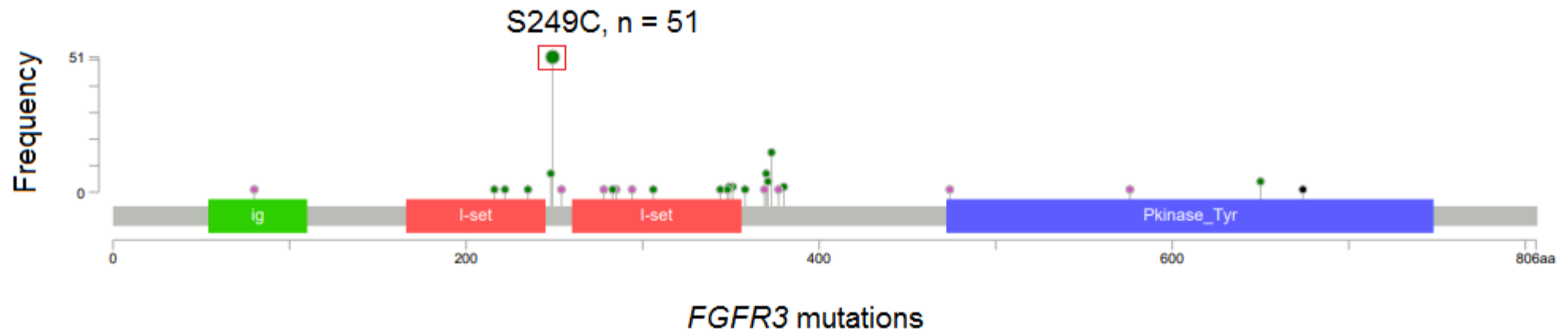
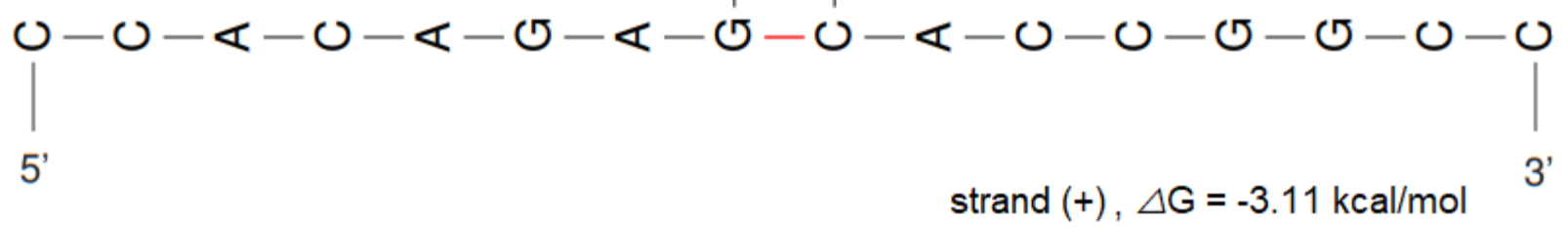
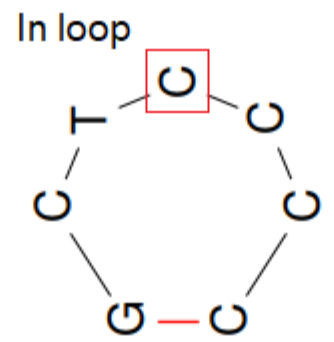
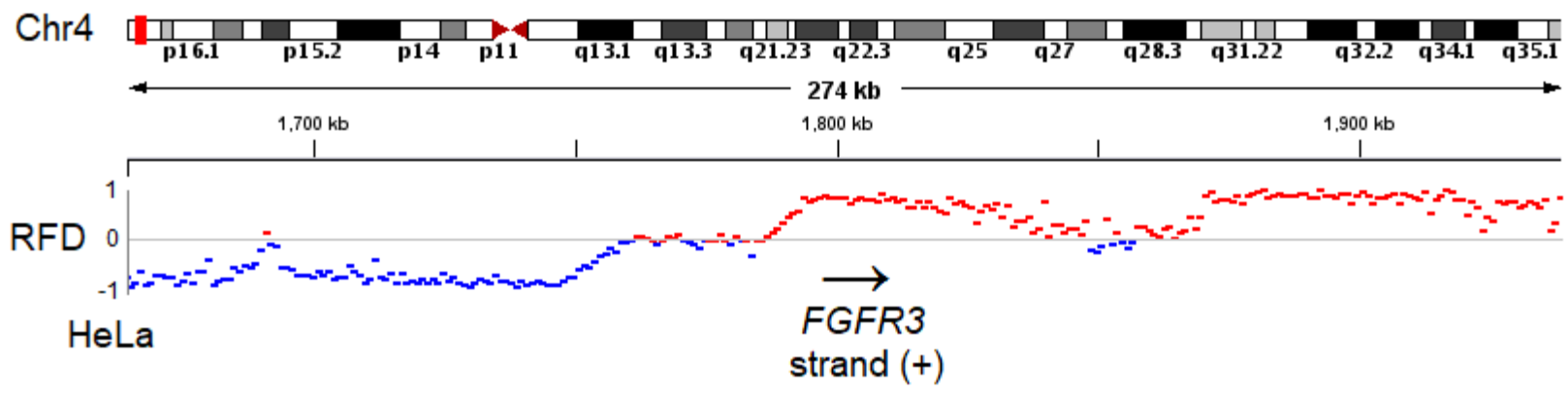
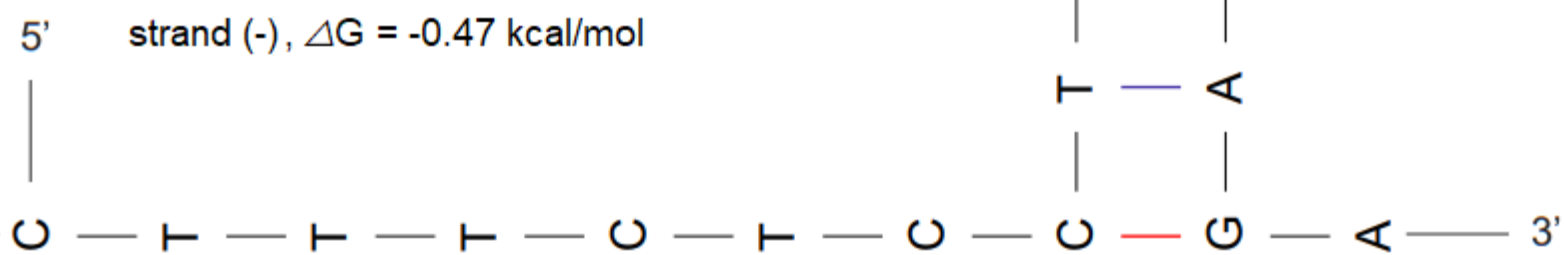
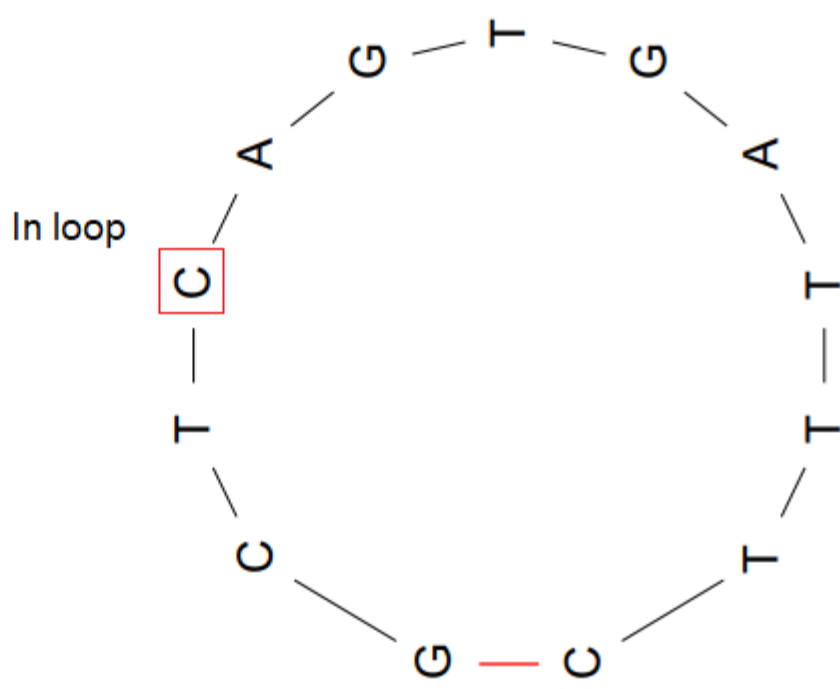
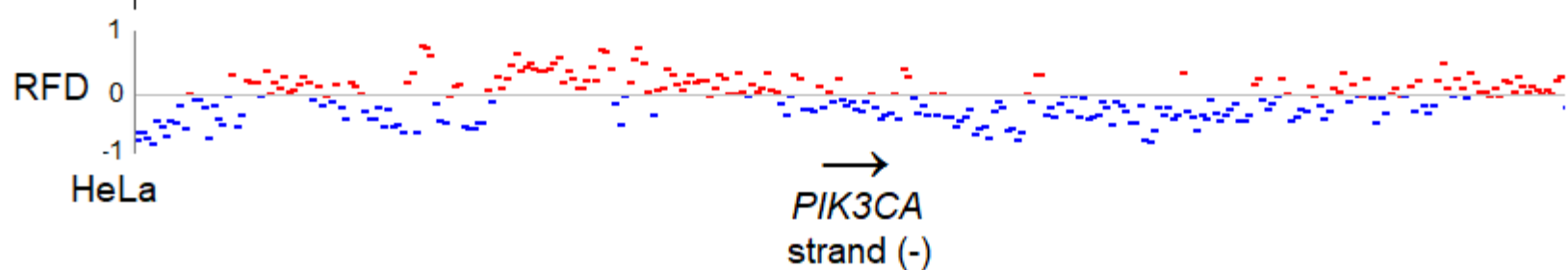
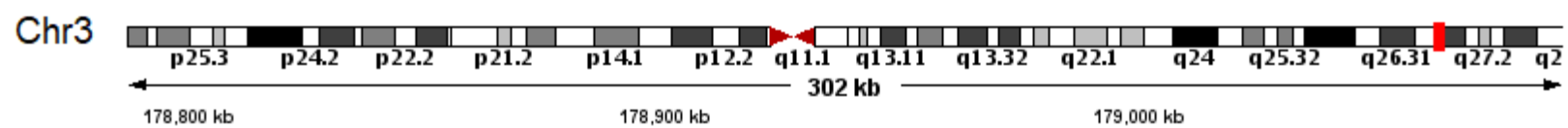
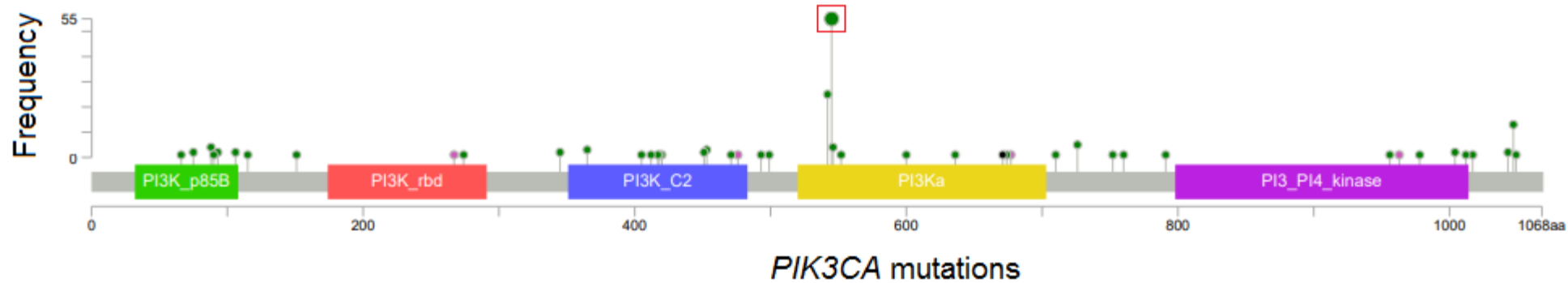


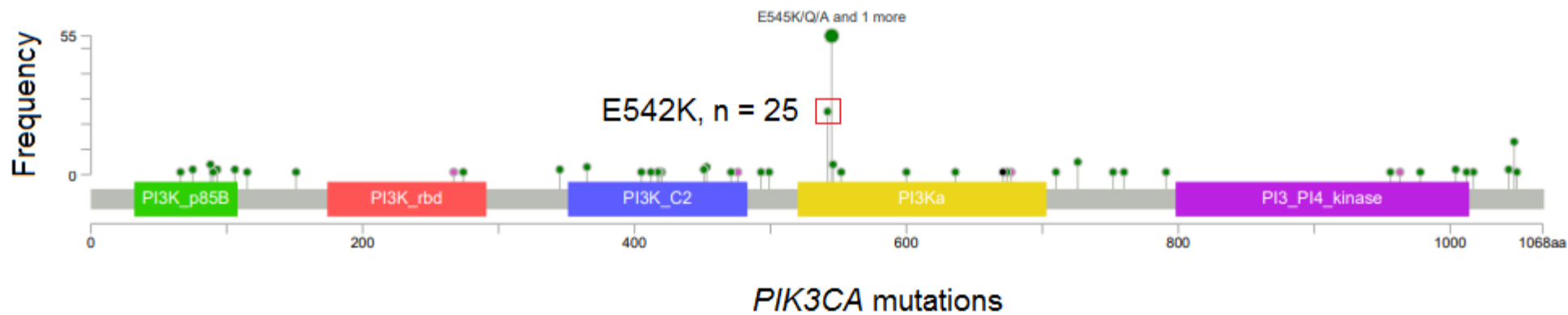
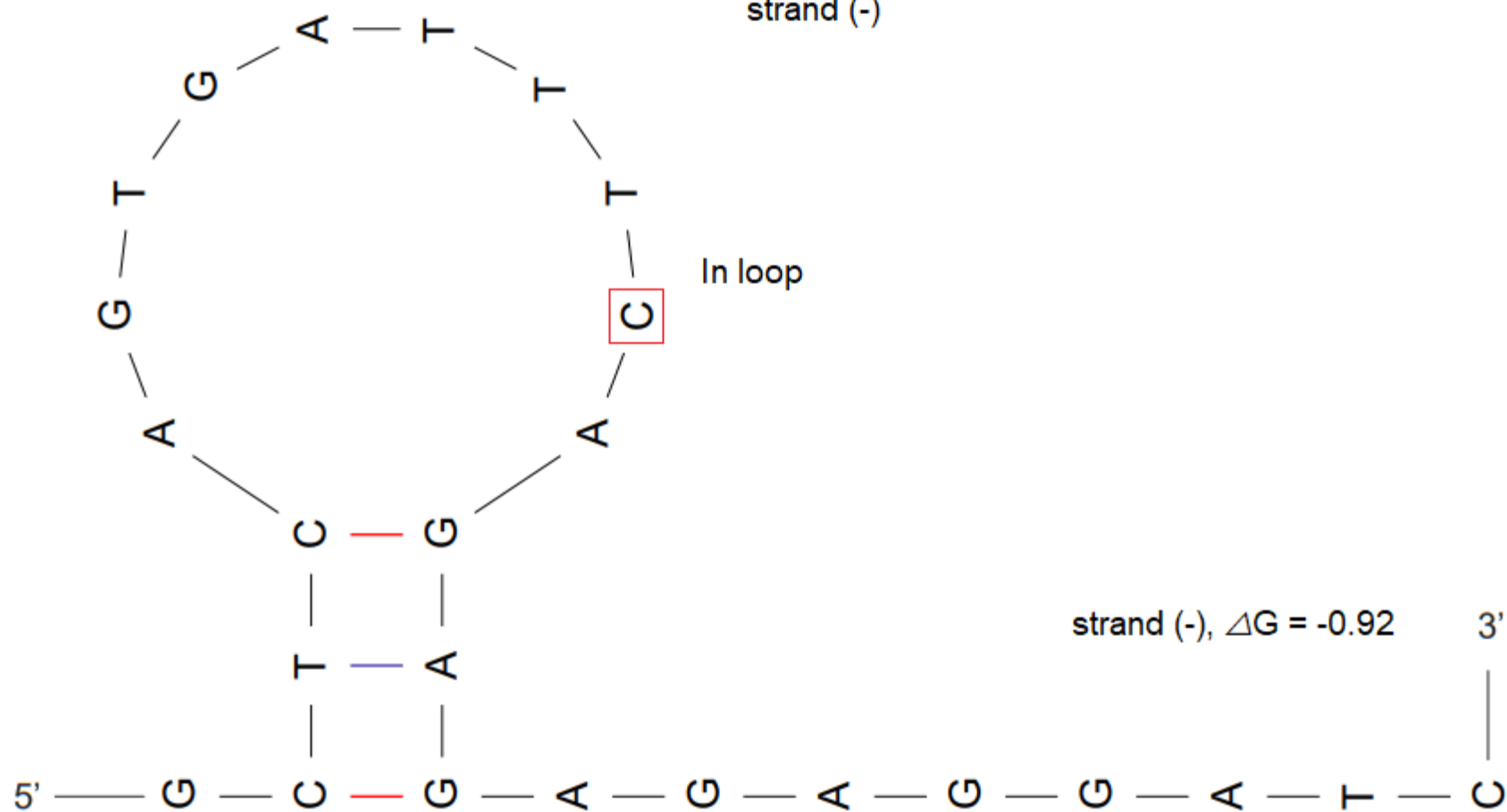
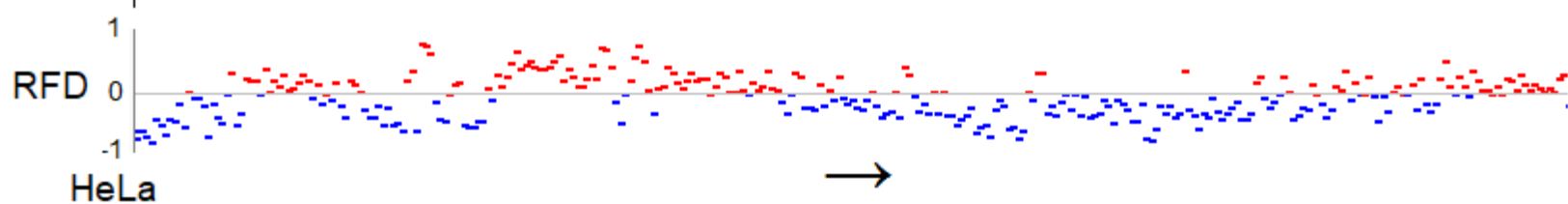
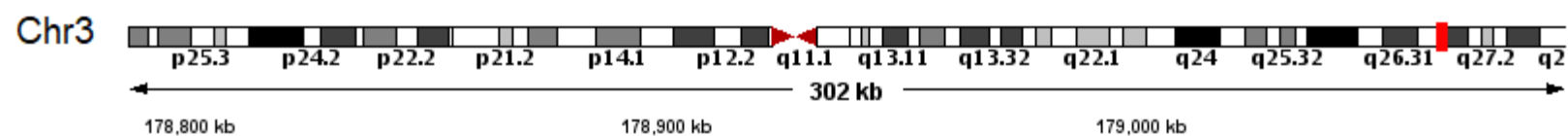
Fig. S6
(Including 43 subfigures)

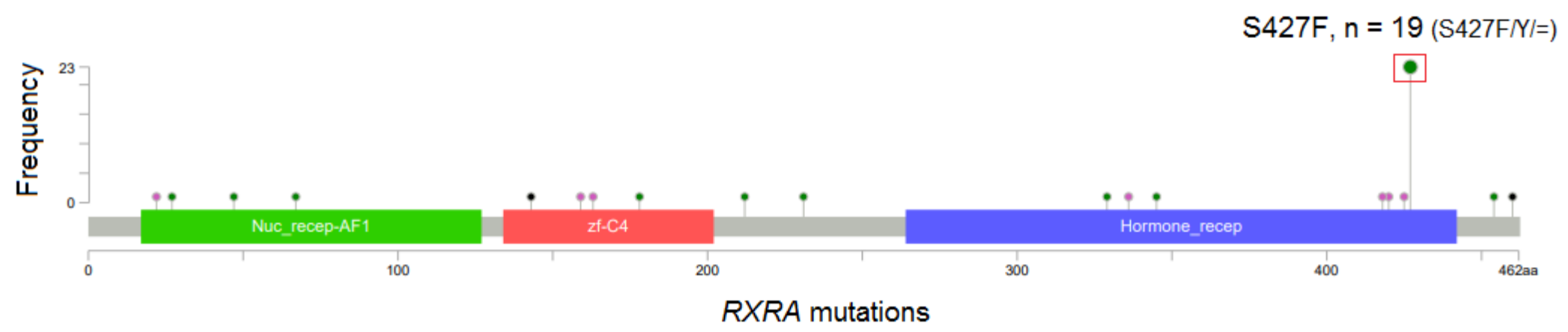
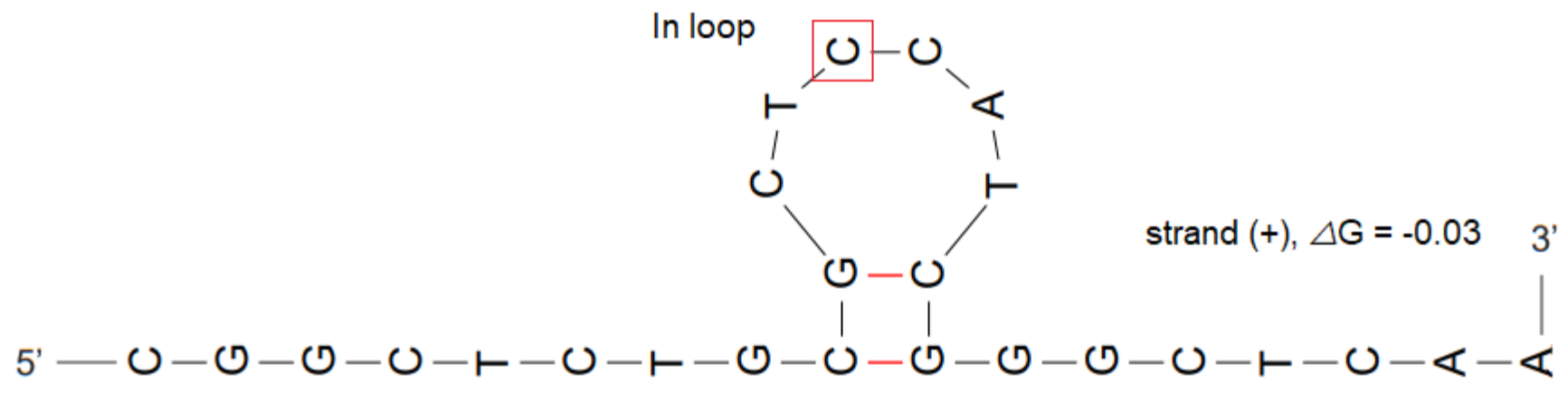
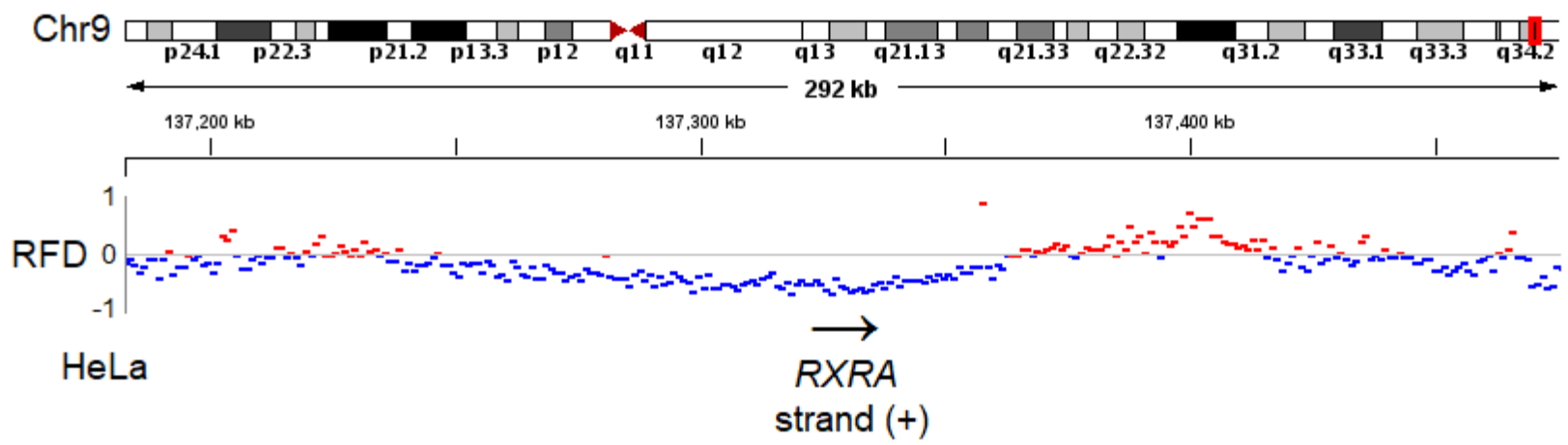
A*FGFR3* S249C, TCC → TGC

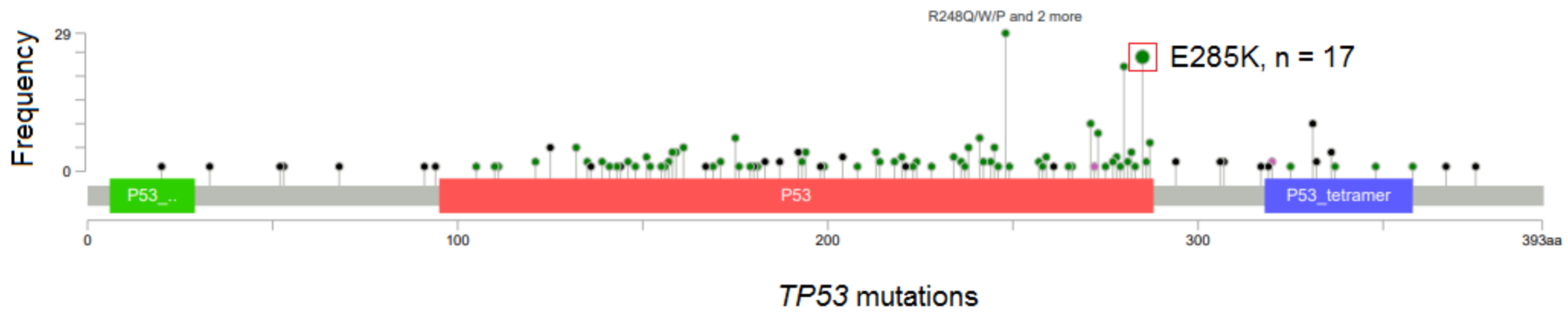
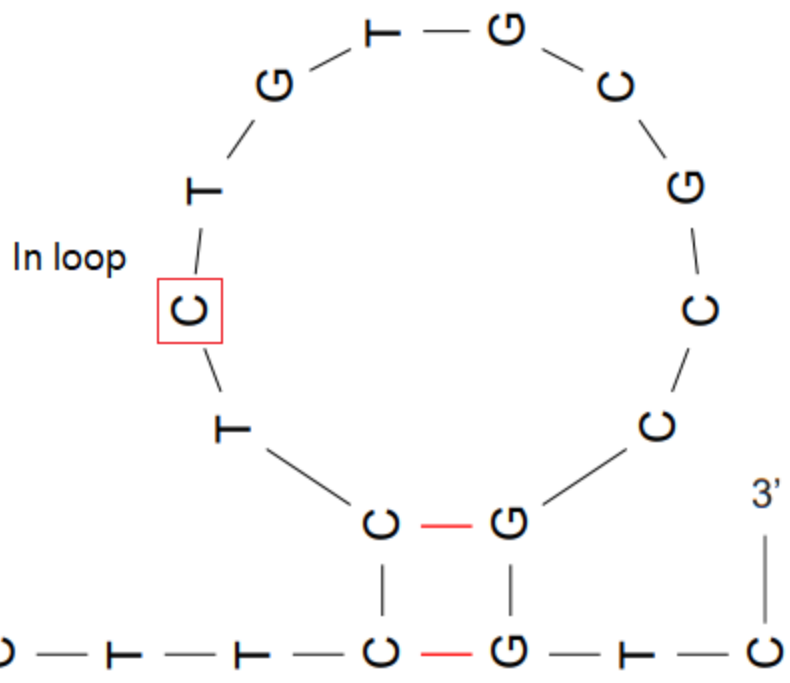
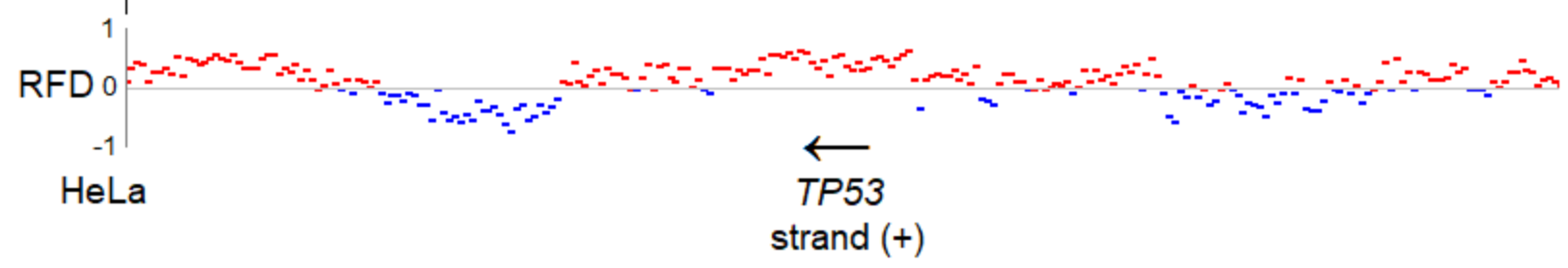
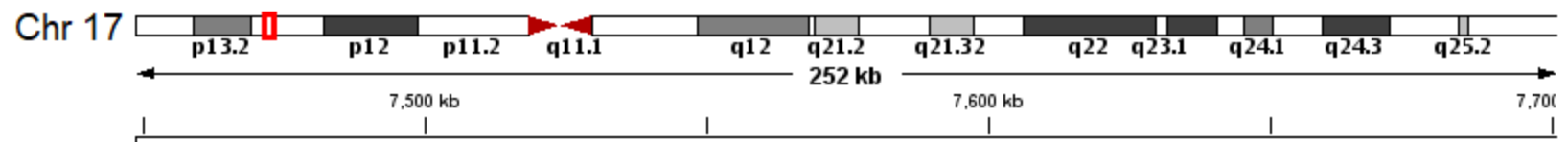
B*PIK3CA* E545K, TGA → TAA

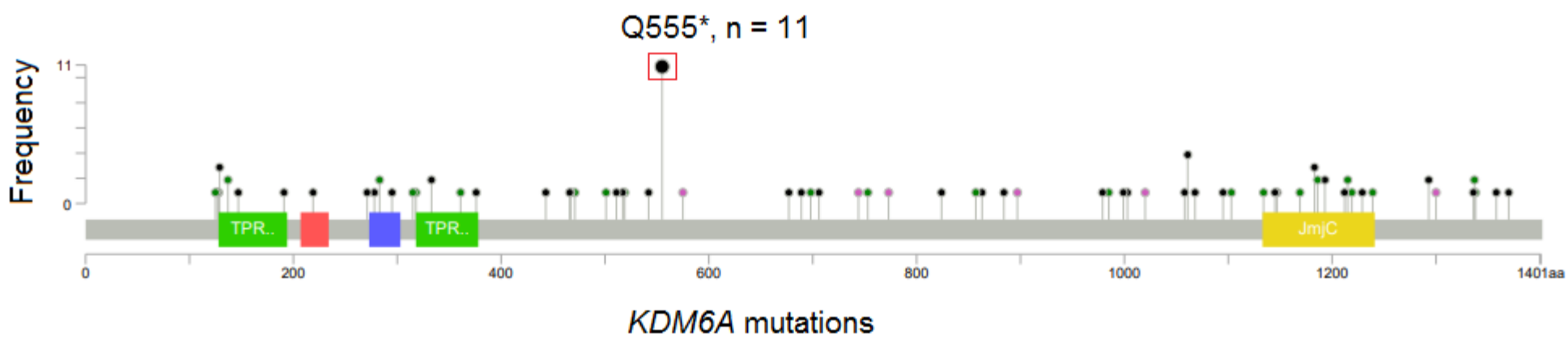
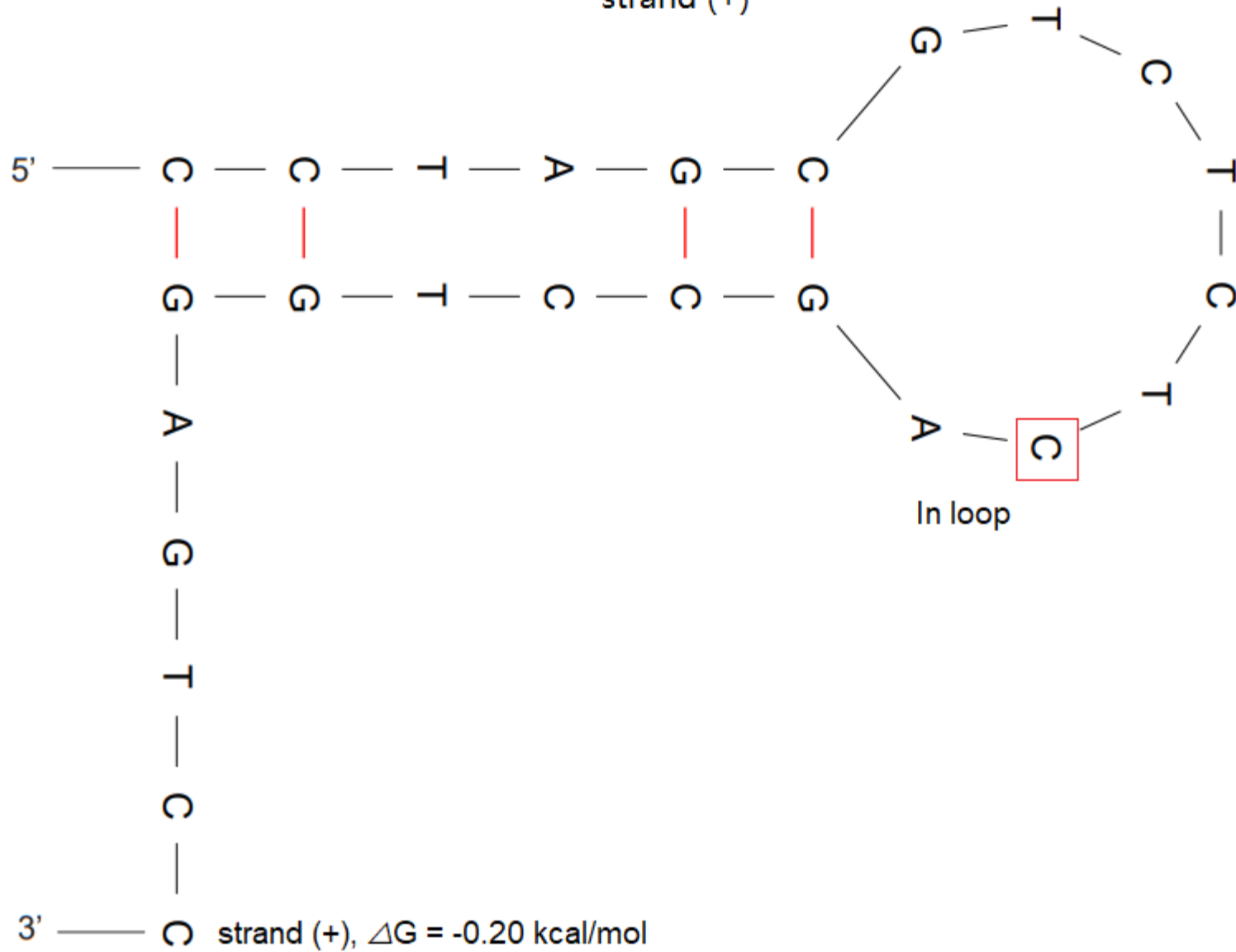
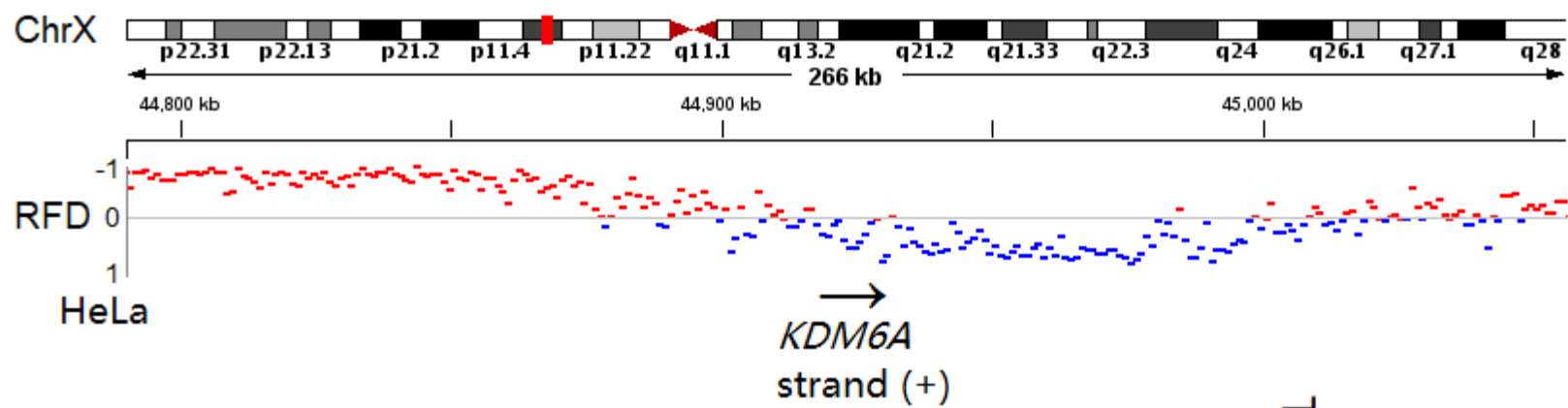
E545K, n = 47 (E545K/Q/A)

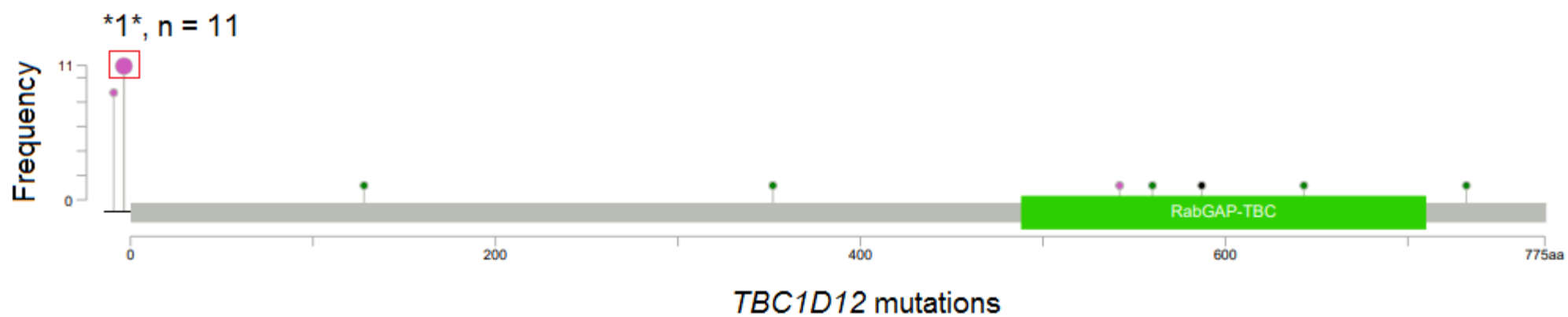
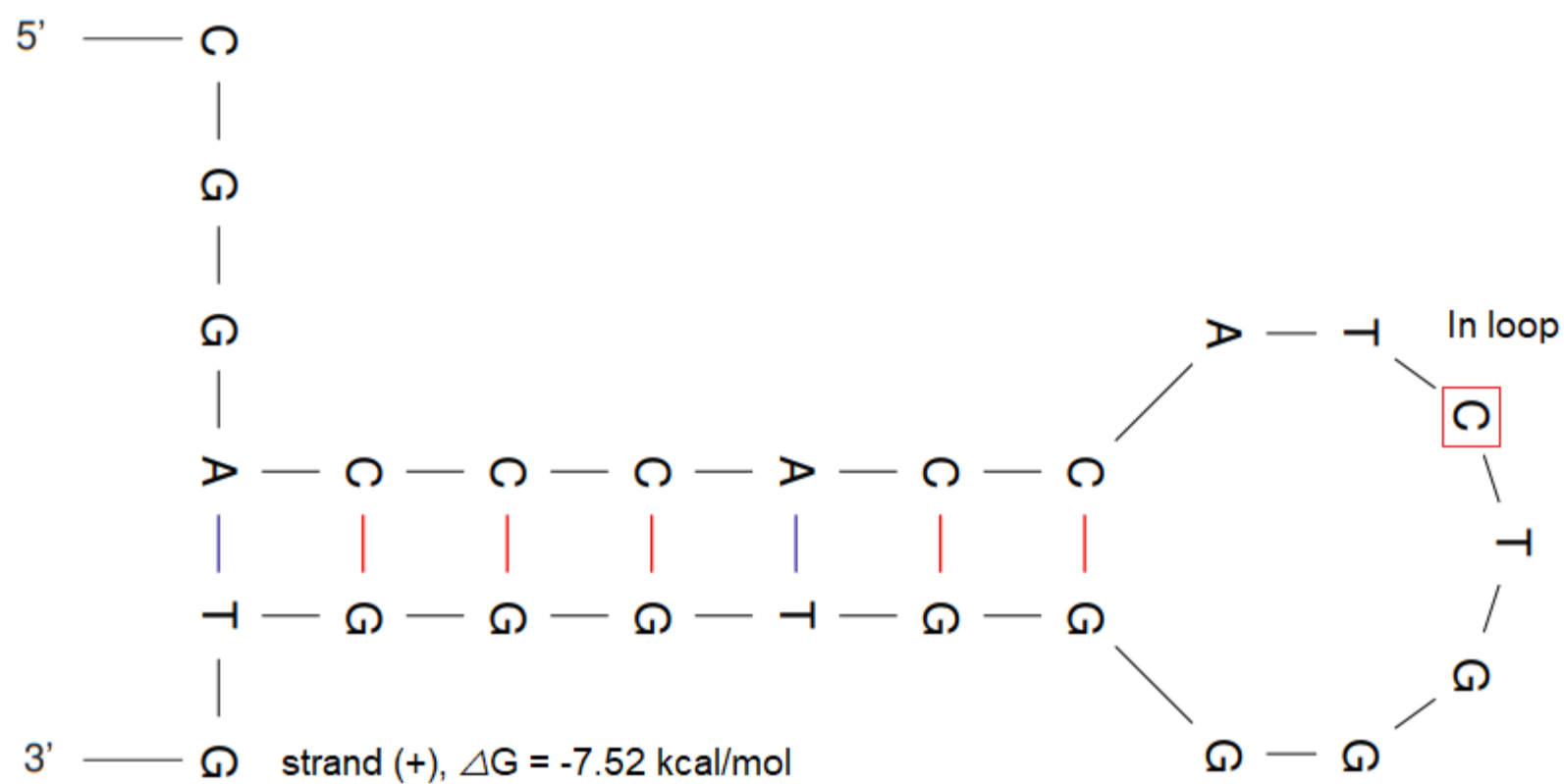
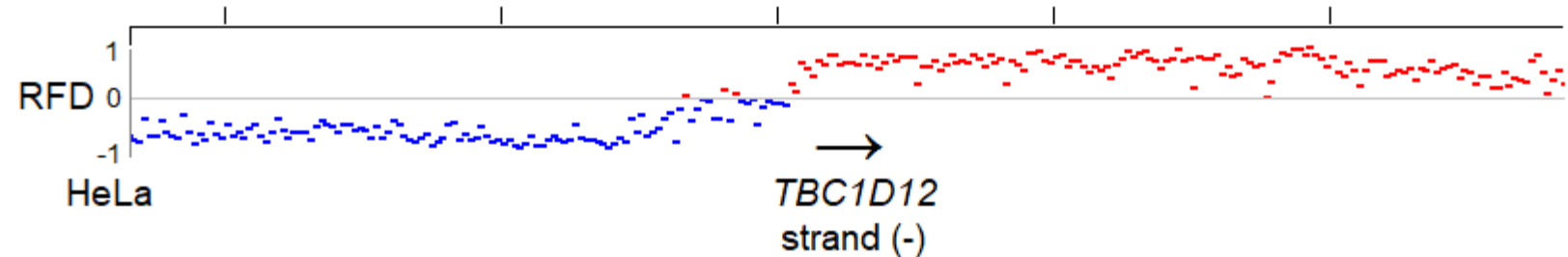
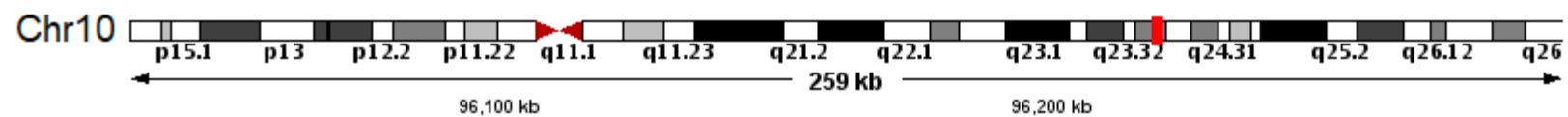


C**PIK3CA E542K, TGA → TAA**

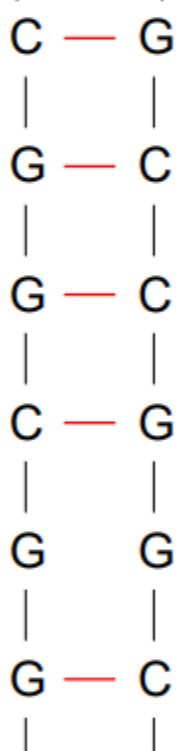
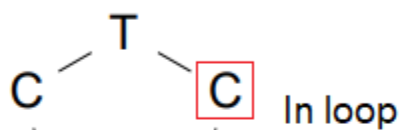
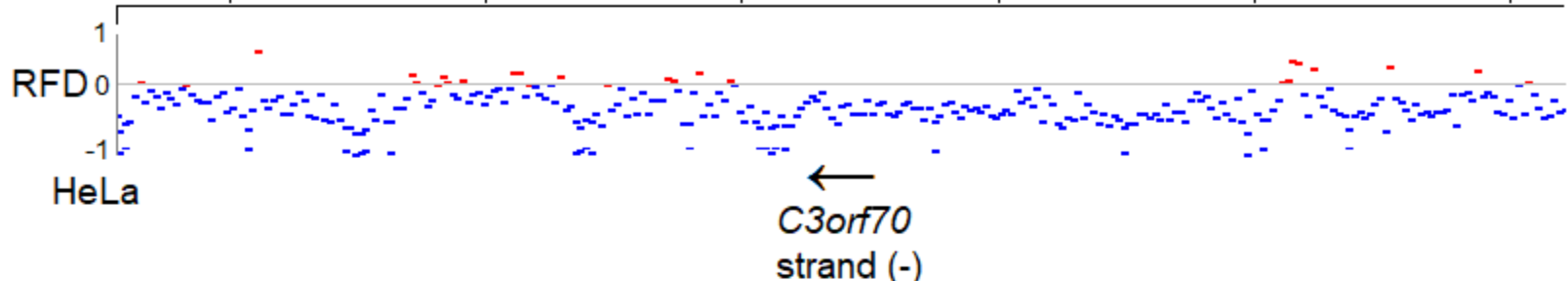
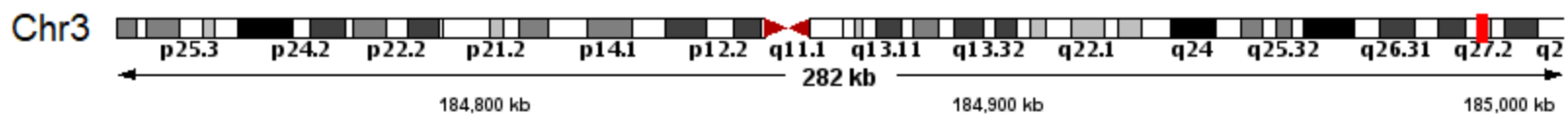
D*RXRA* S427F, TCC → TIC

E**TP53 E285K, TCT → TTT**

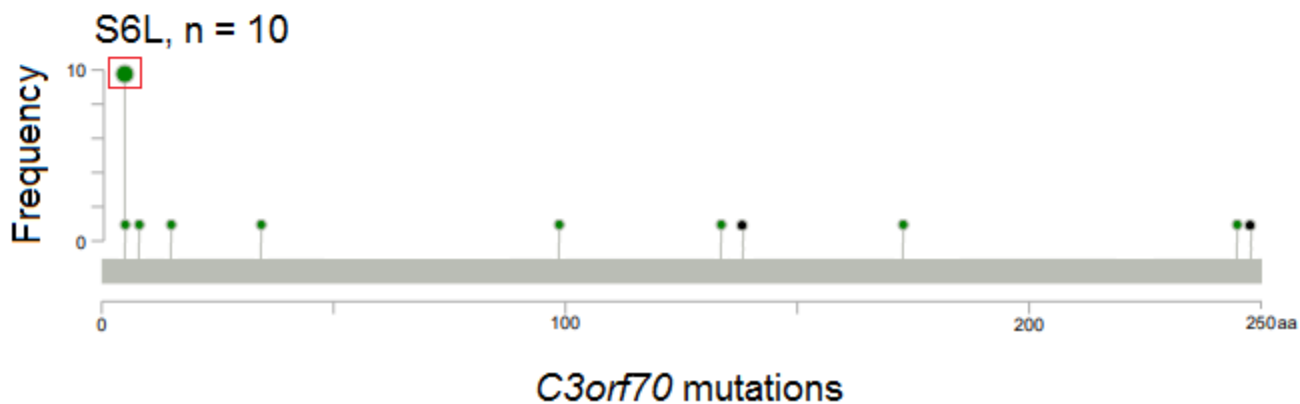
G*KDM6A* Q555*, TCA → TIA

H*TBC1D12* *1*, AGA → AAA

C3orf70 S6L, CGA → CAA

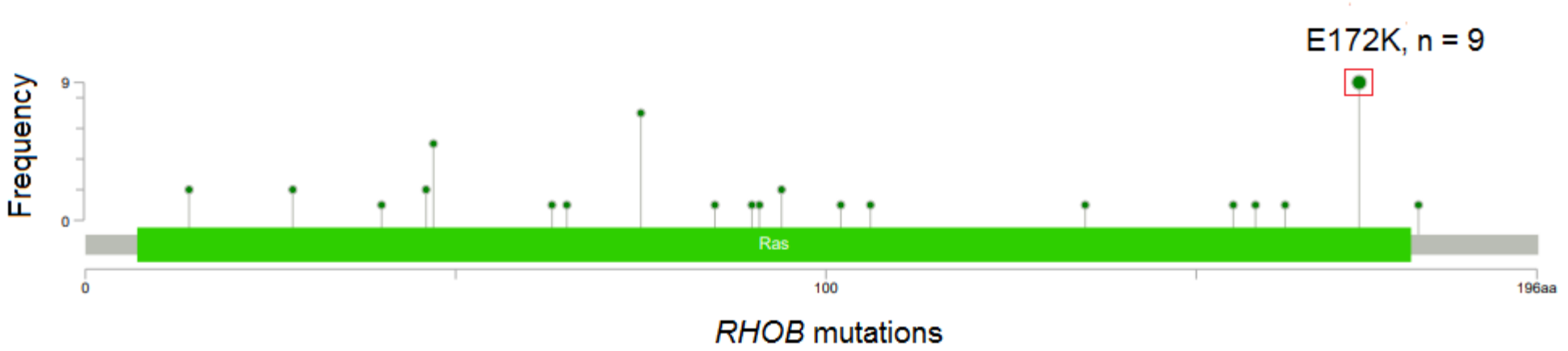
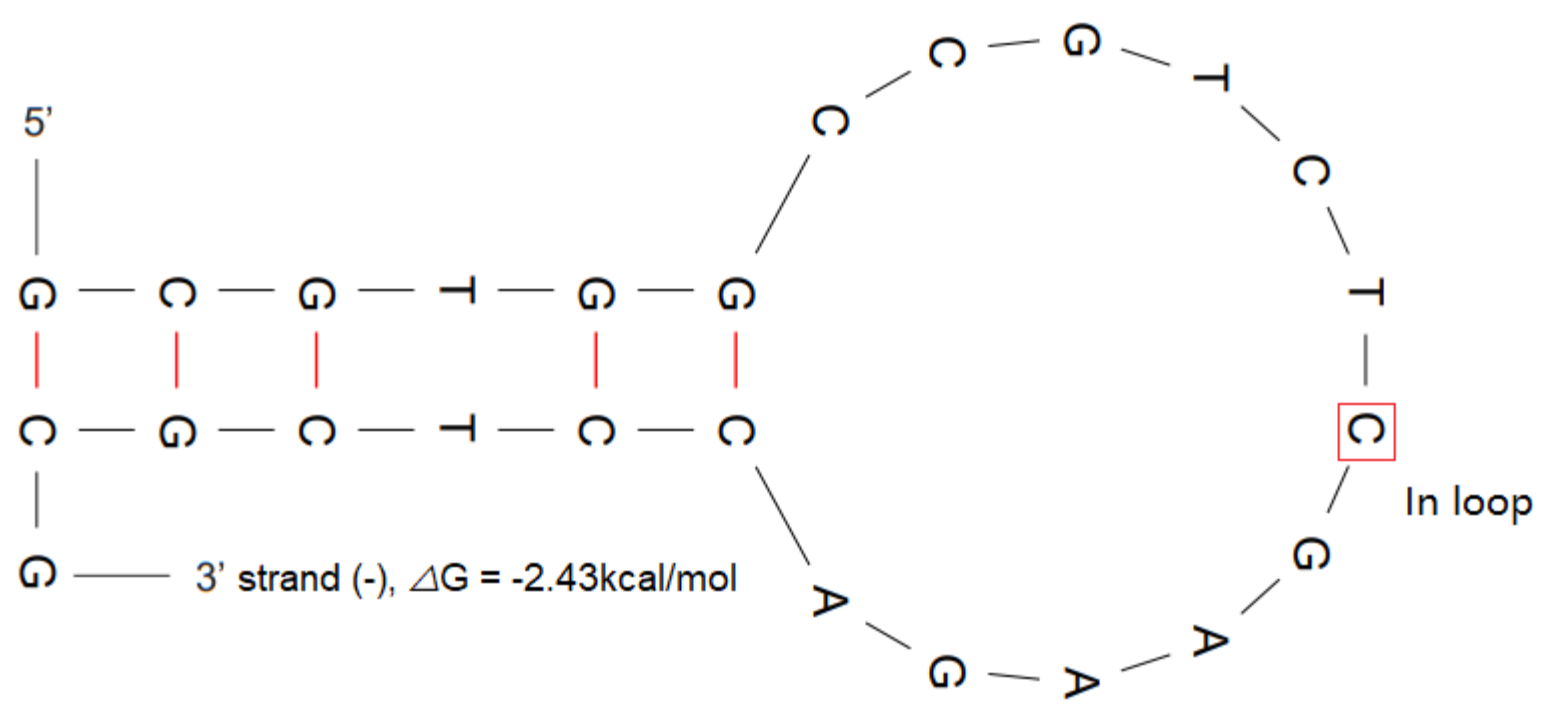
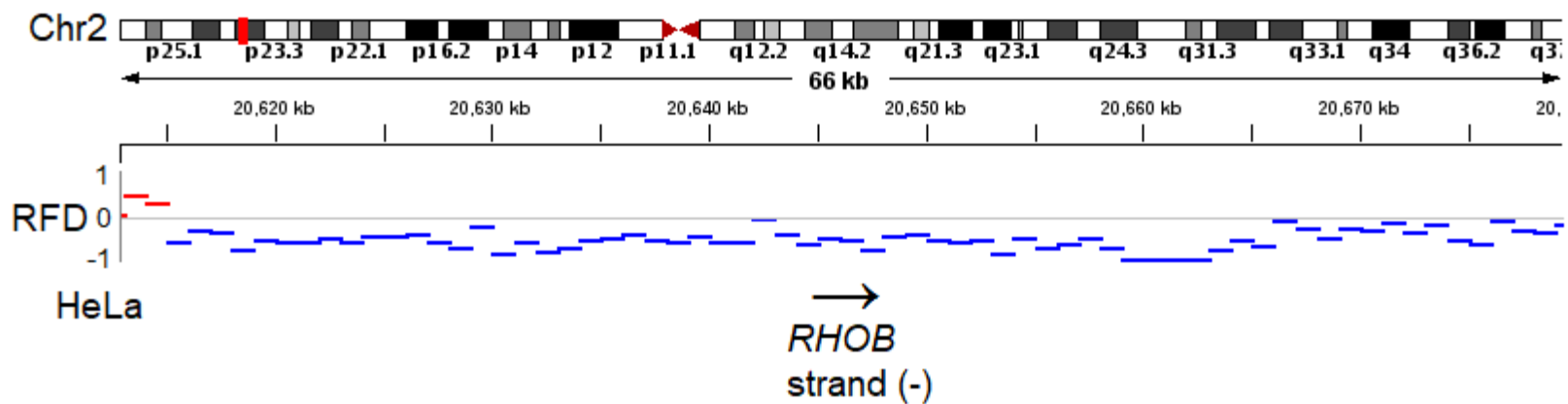


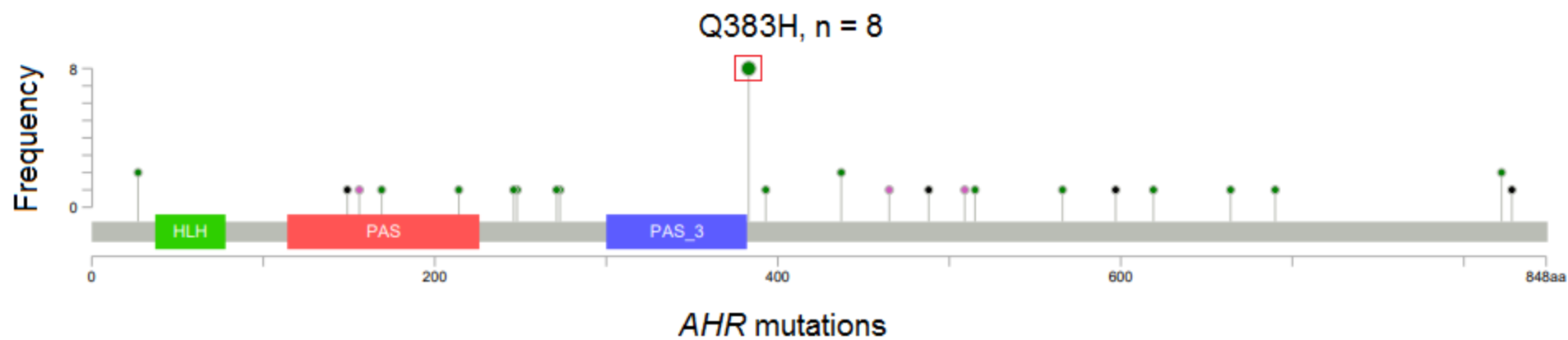
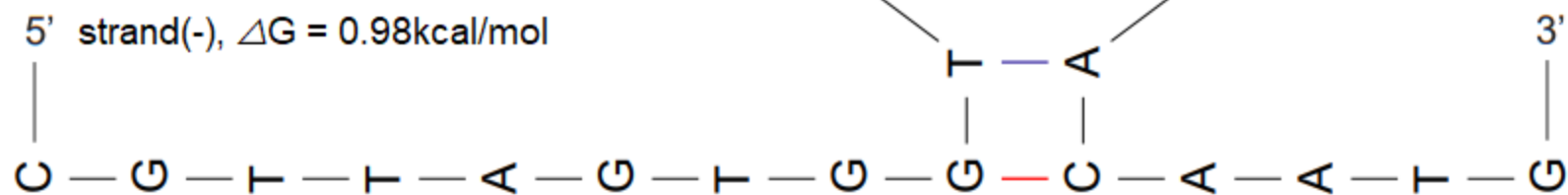
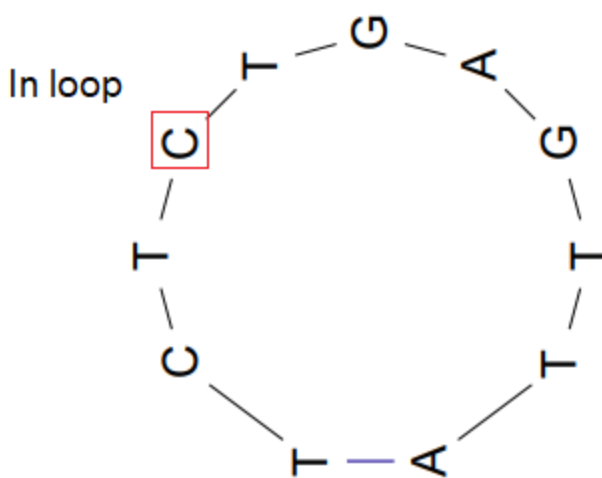
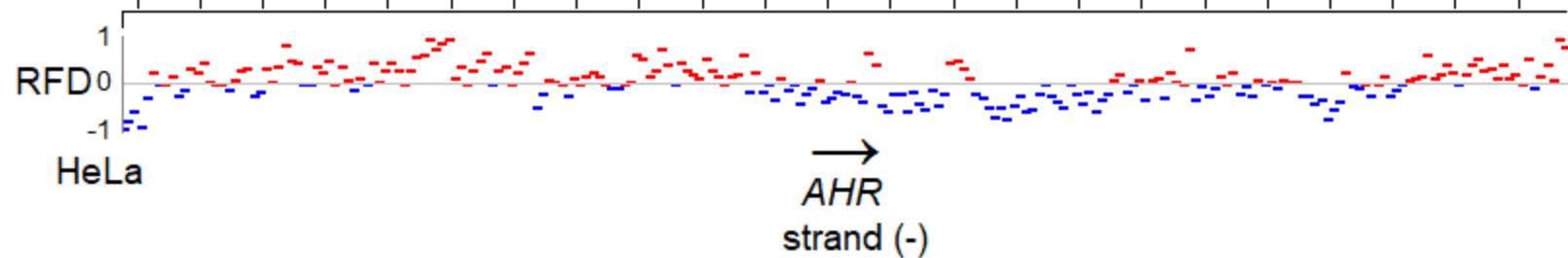
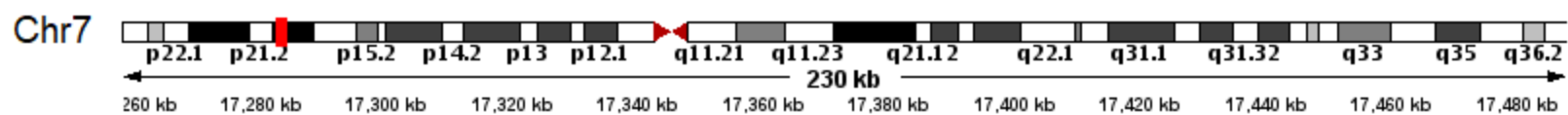
strand (-), $\Delta G = -8.21$ kcal/mol



J

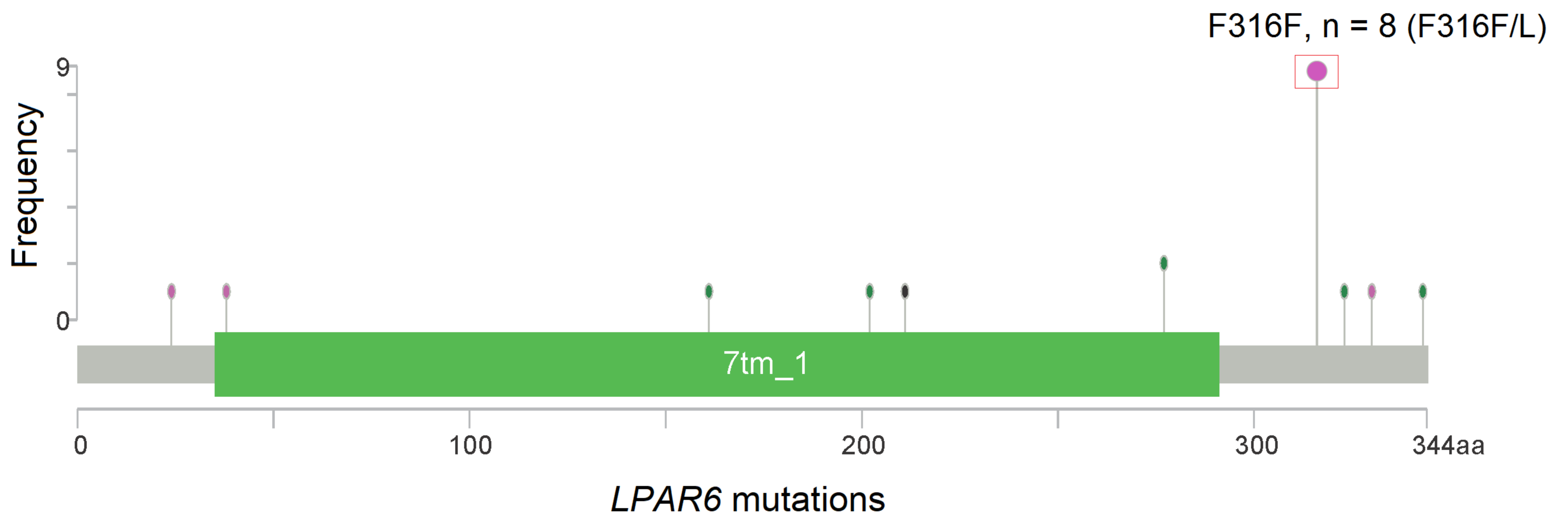
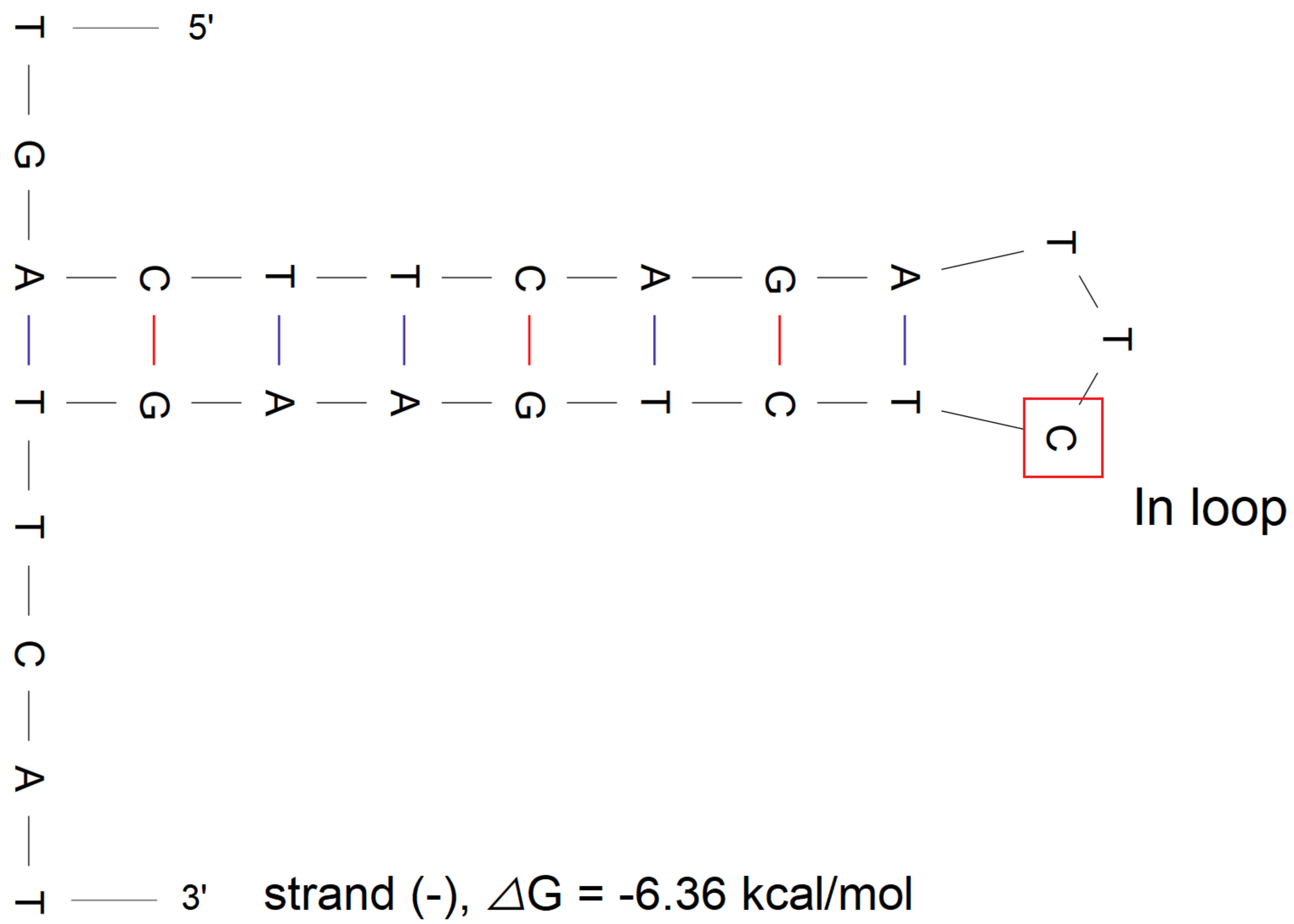
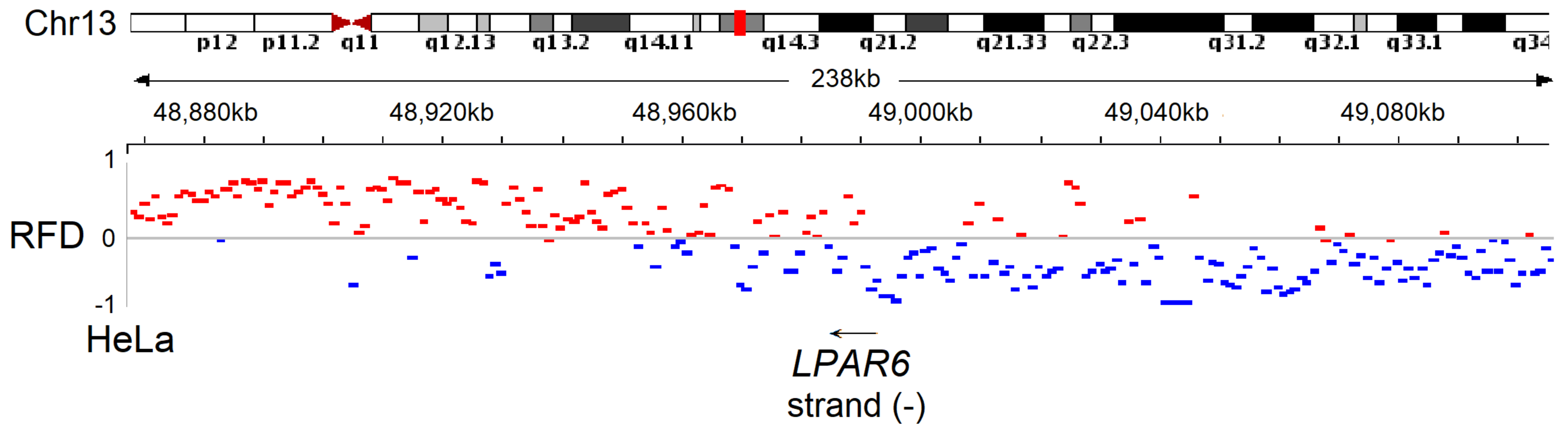
RHOB E172K, CGA → CAA

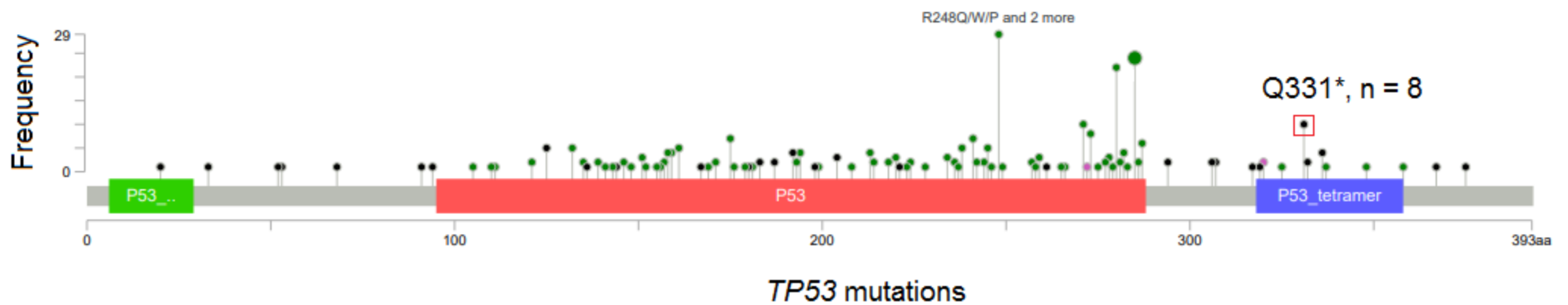
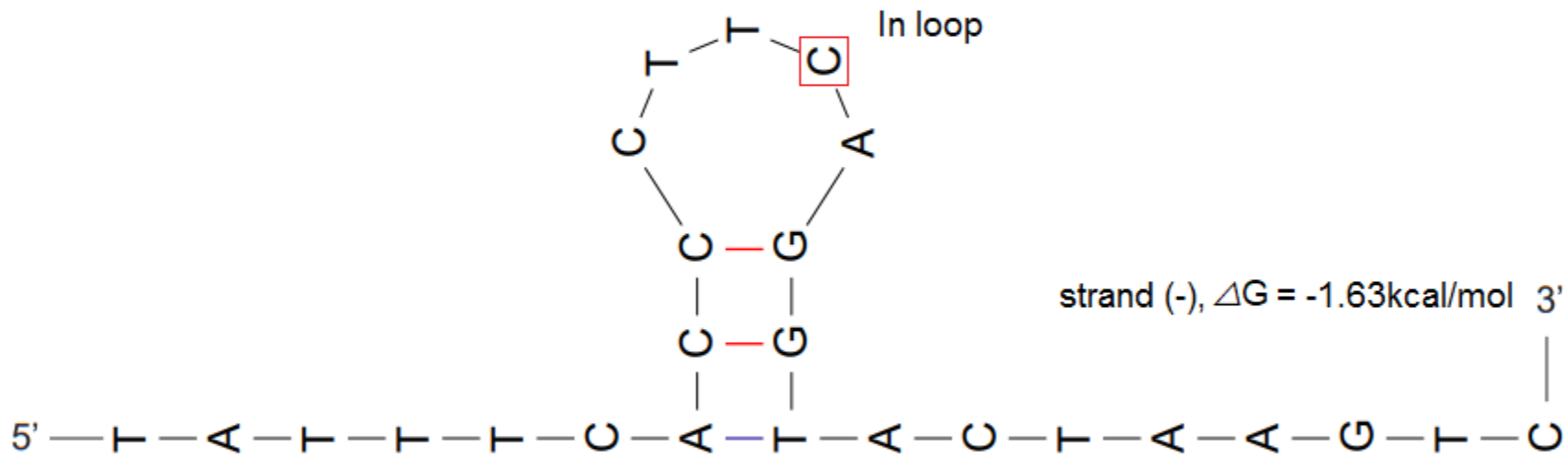
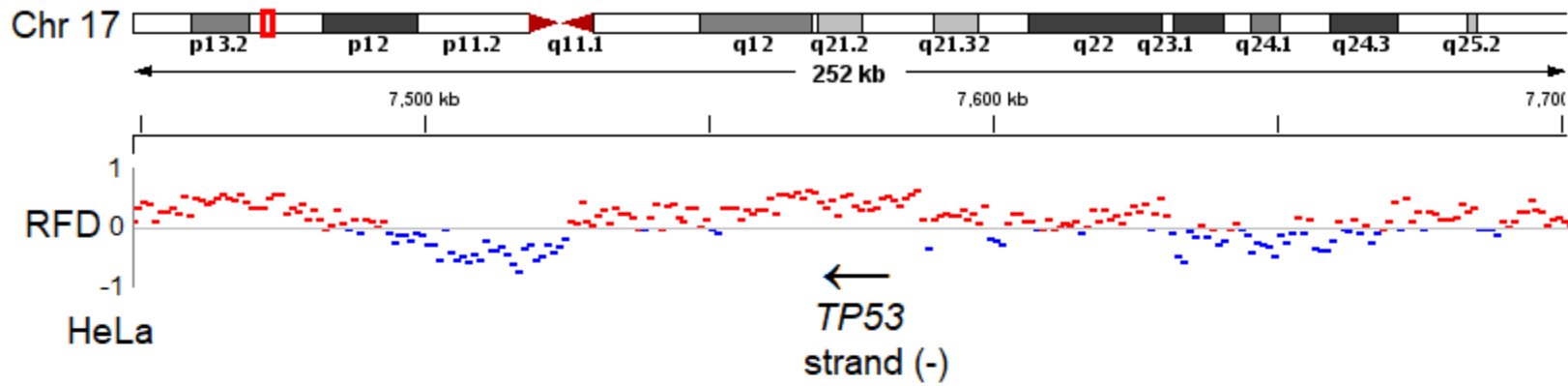


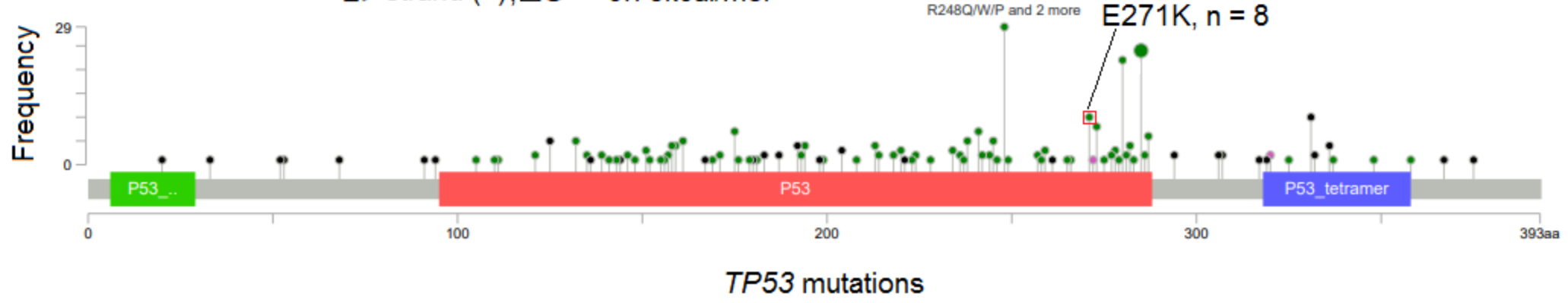
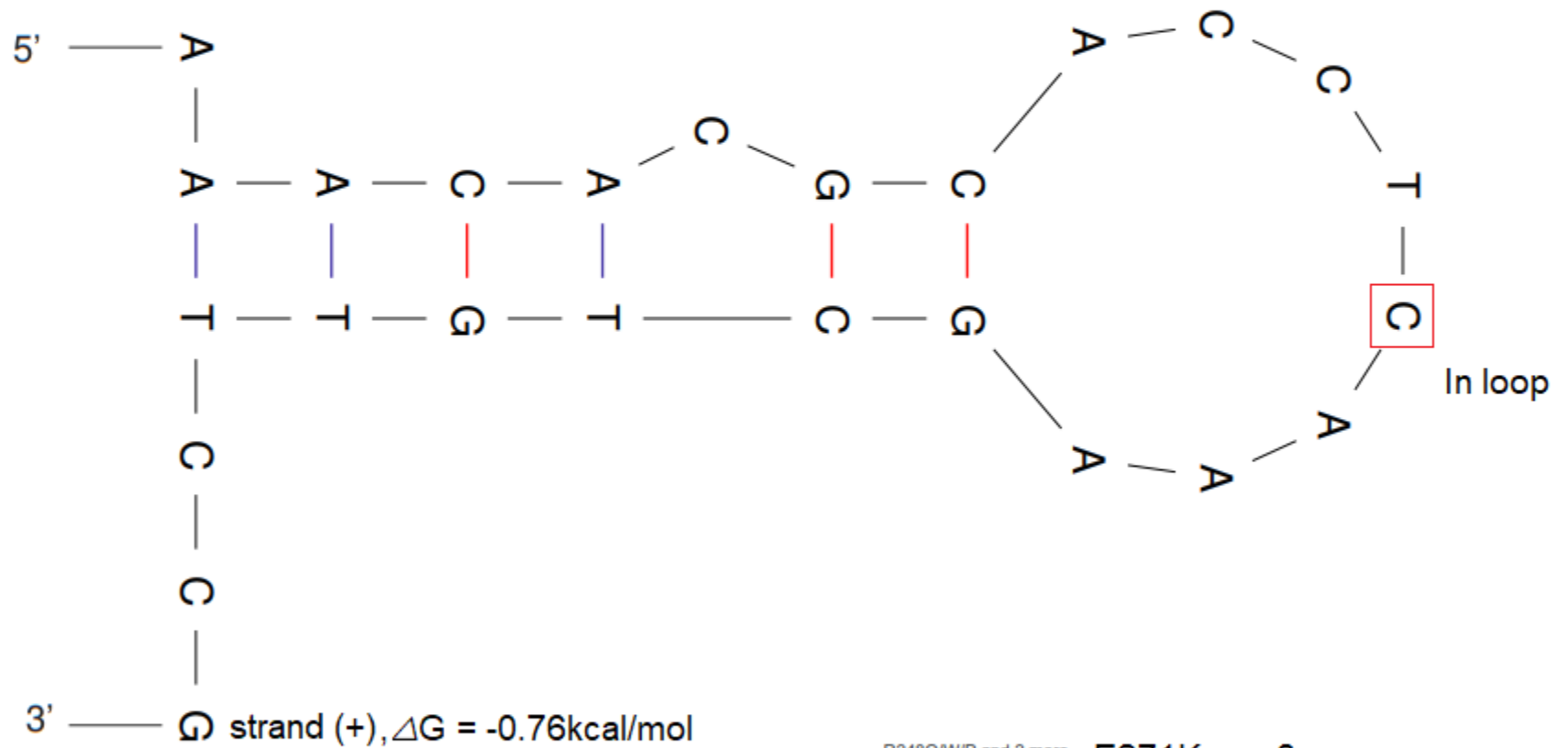
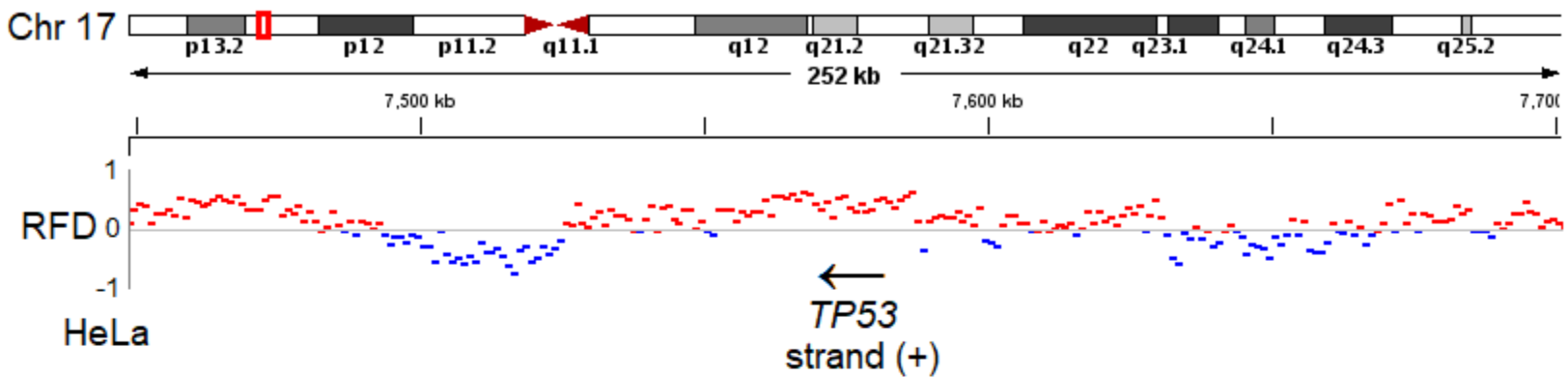
K*AHR* Q383H, AGA → ACA

L

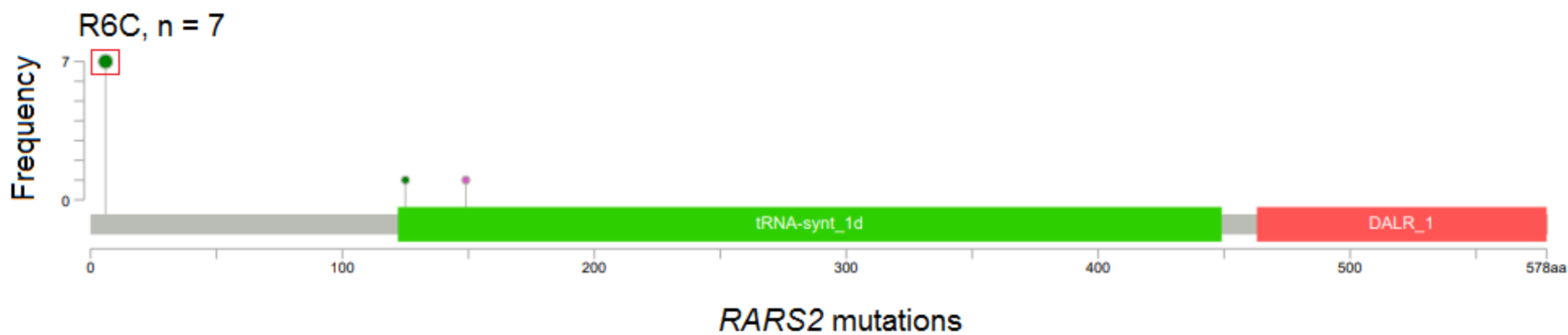
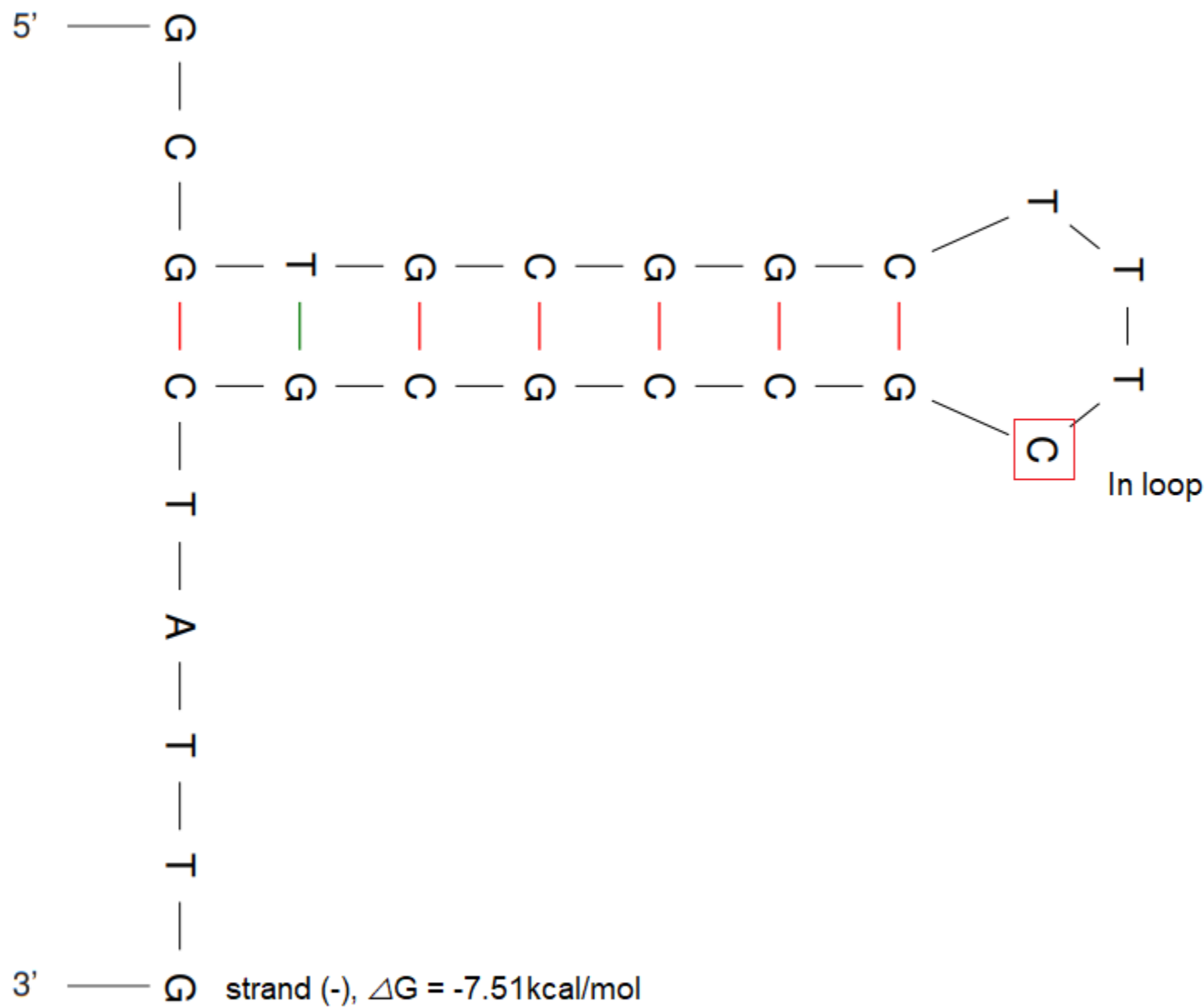
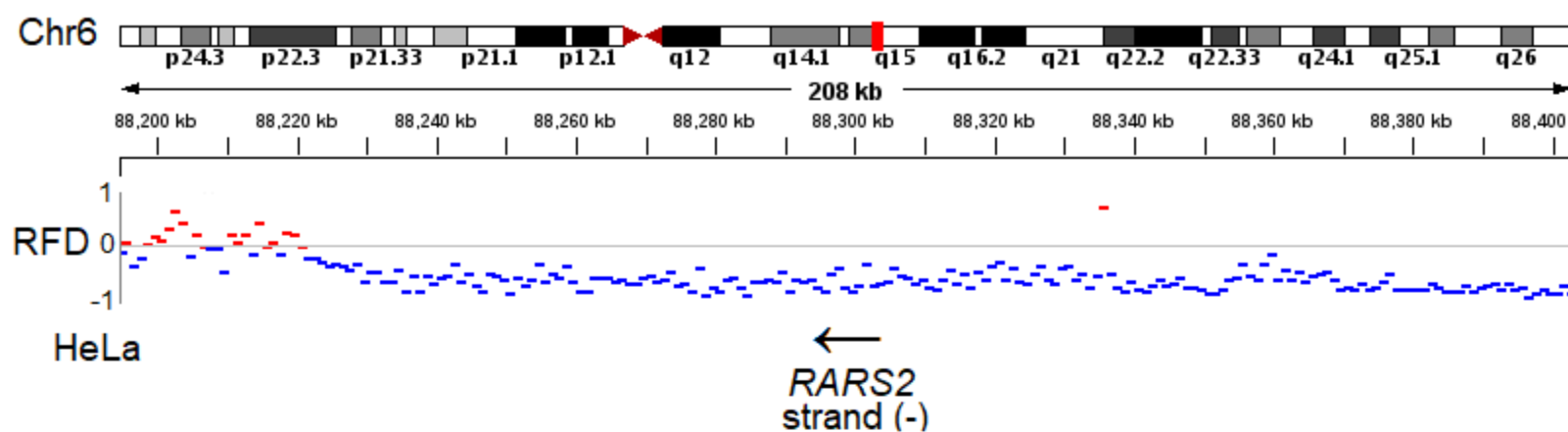
LPAR6 F316F, AGA → AAA

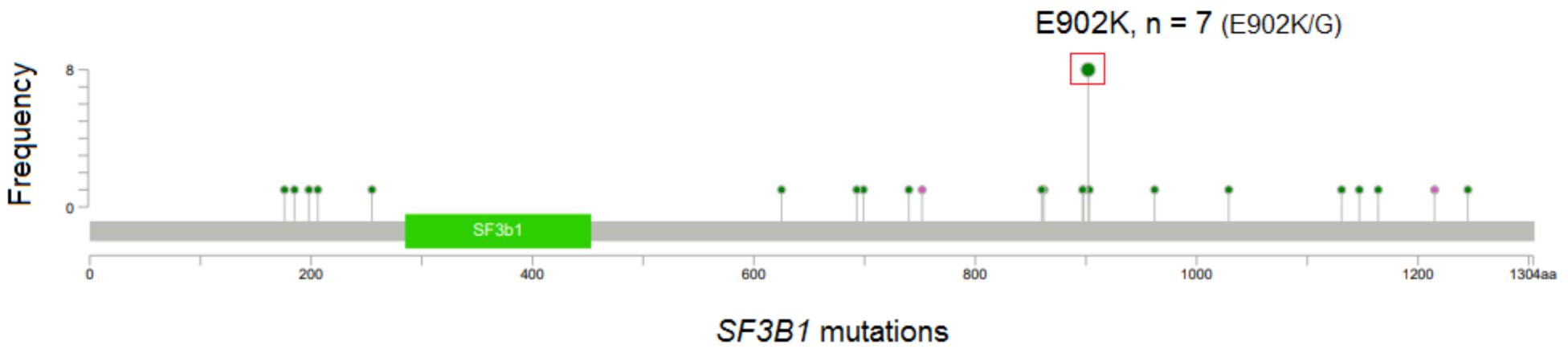
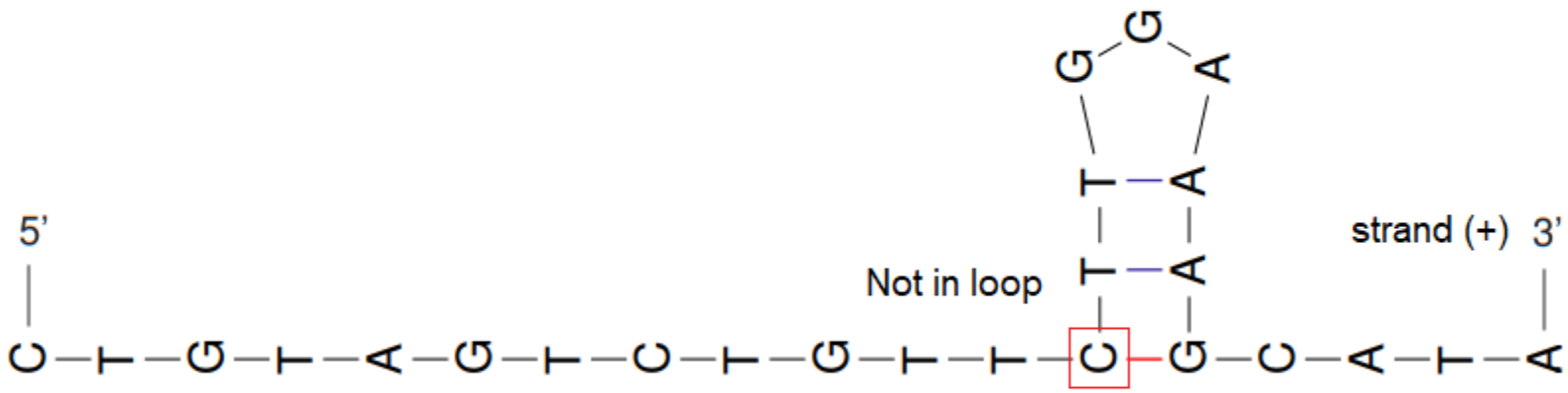
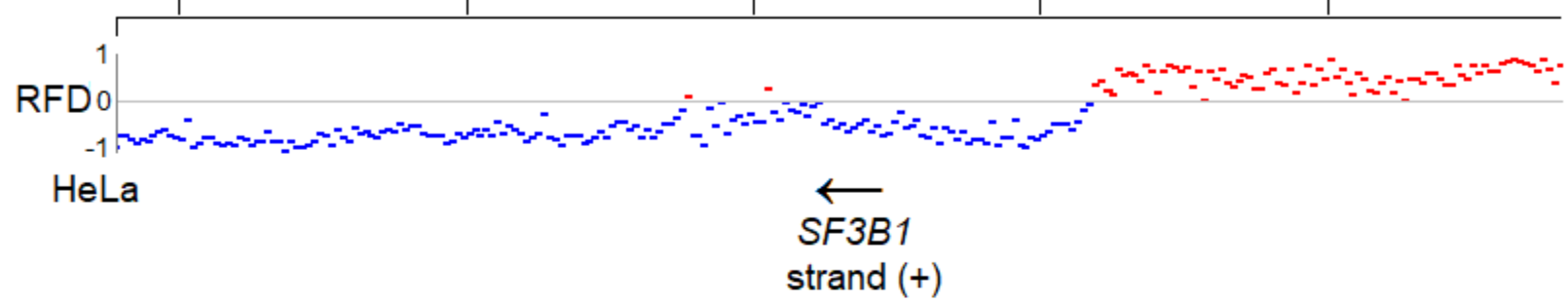
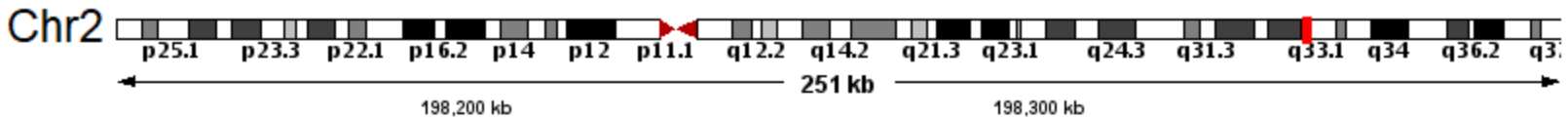


M*TP53* Q331*, TGA → TAA

N*TP53* E271K, TCA → TTA

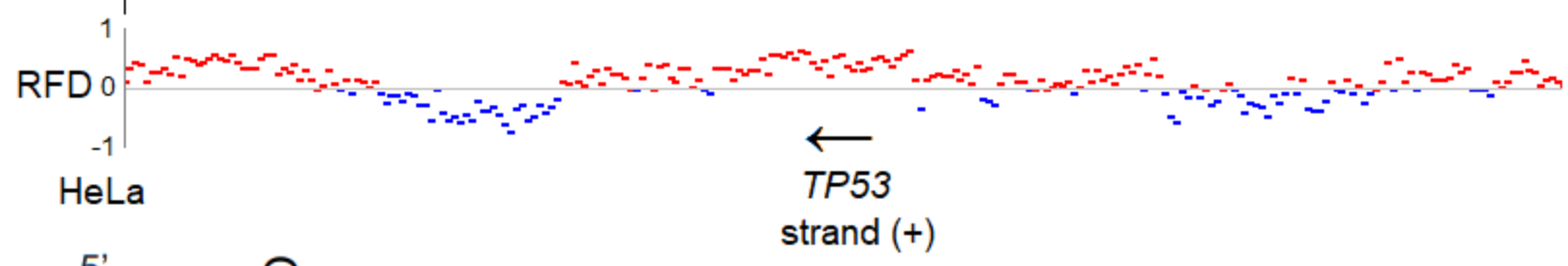
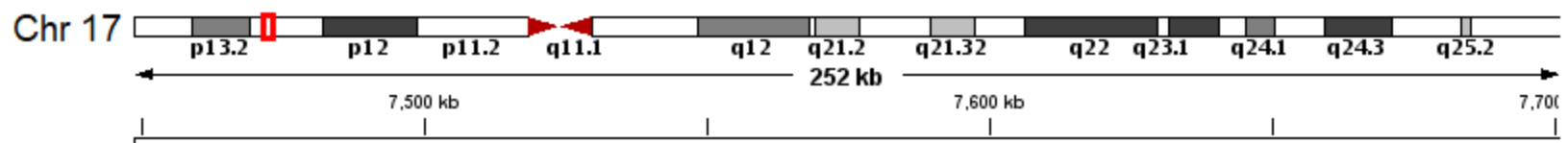
RARS2 R6C, CGA → CAA



P*SF3B1* E902K, TCT → TTT

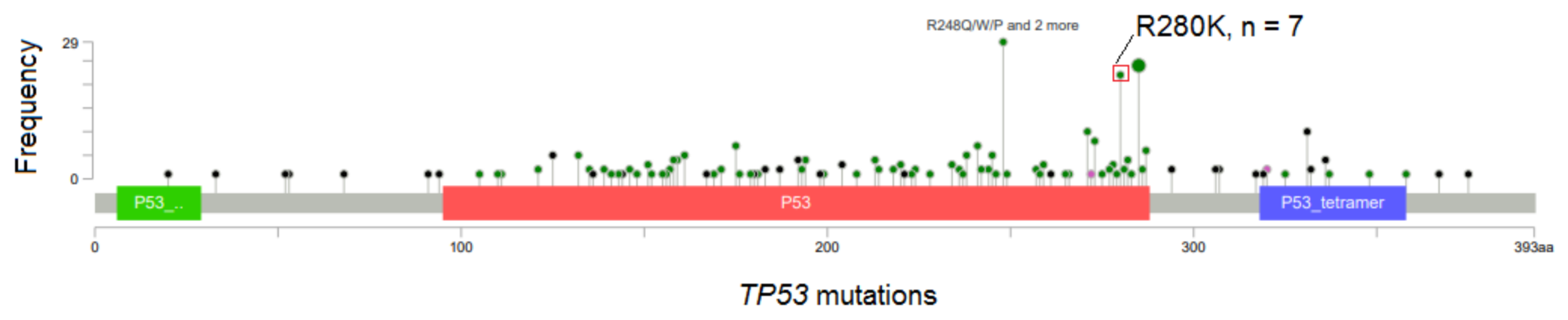
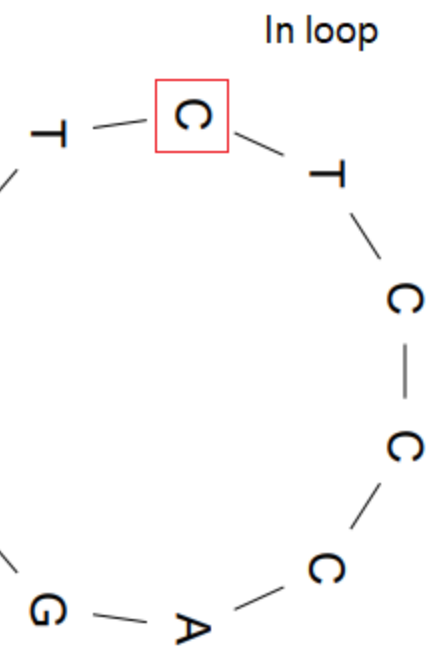
Q

TP53 R280K, TCT → TTT



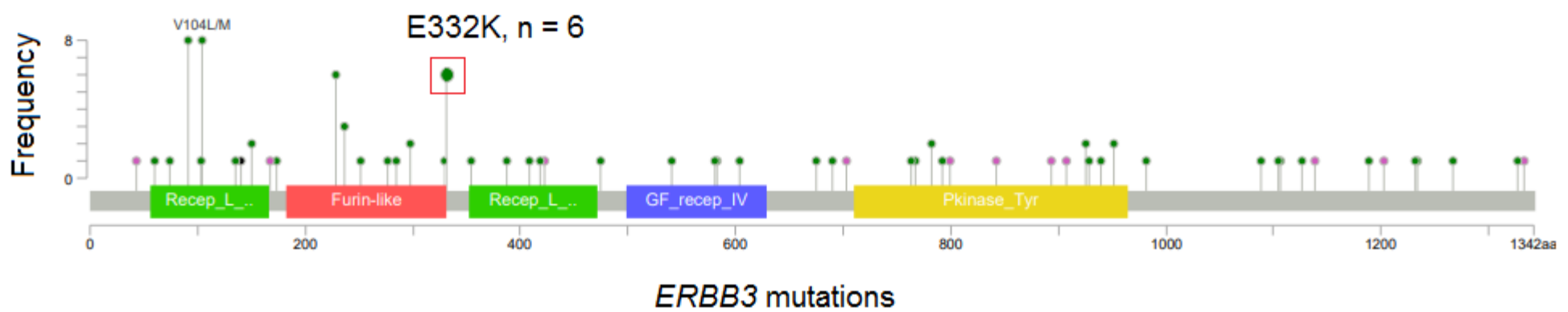
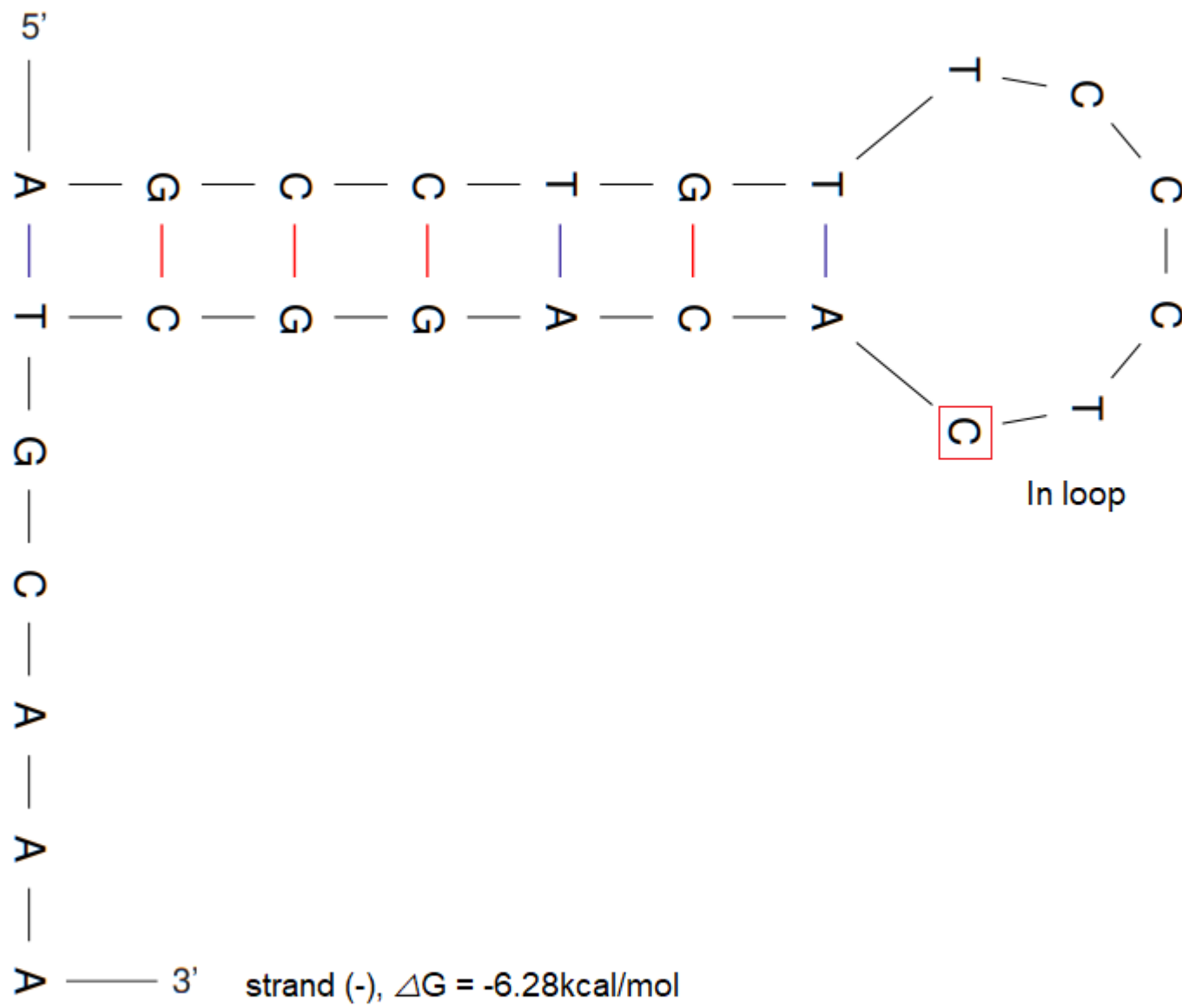
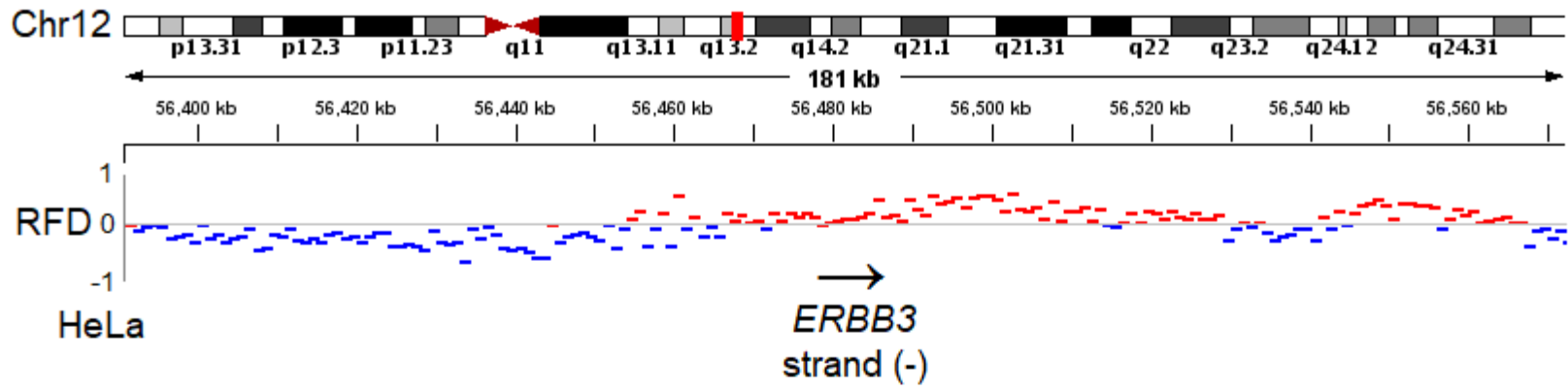
5' — G
— T
— G
— C
— G
— C — C — G — G — T — C
— G — G — A — C — A — G
3'

strand (+), $\Delta G = -1.76 \text{ kcal/mol}$



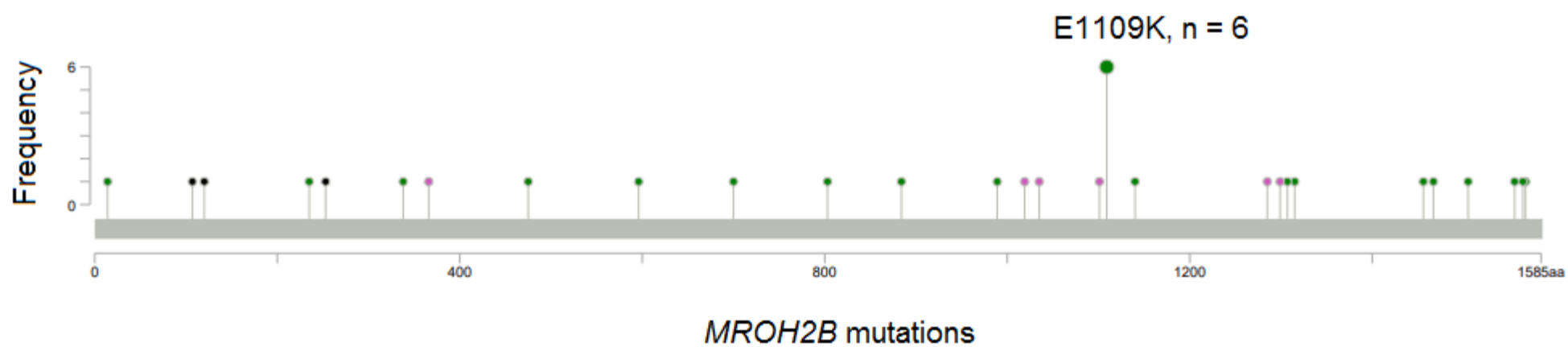
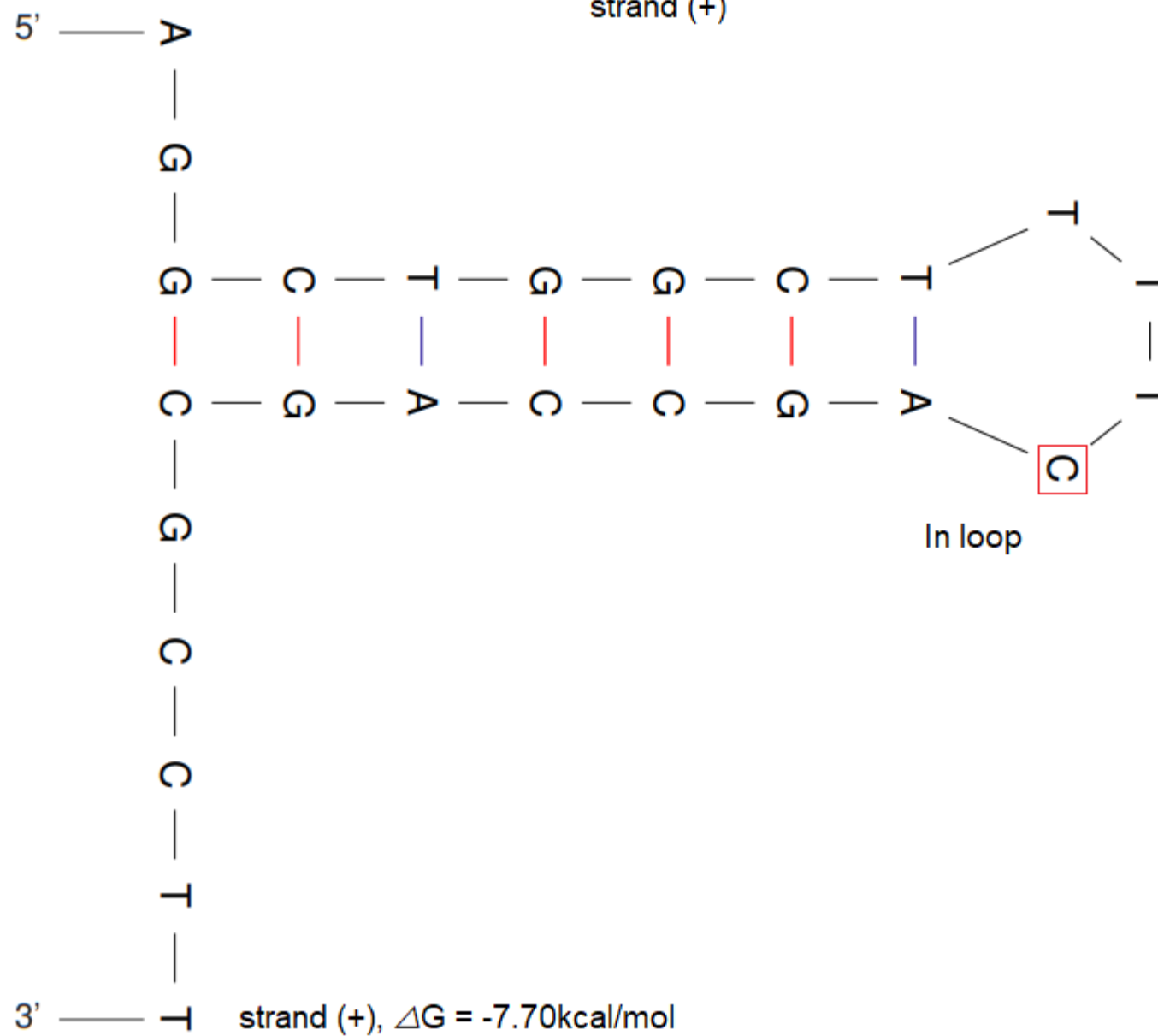
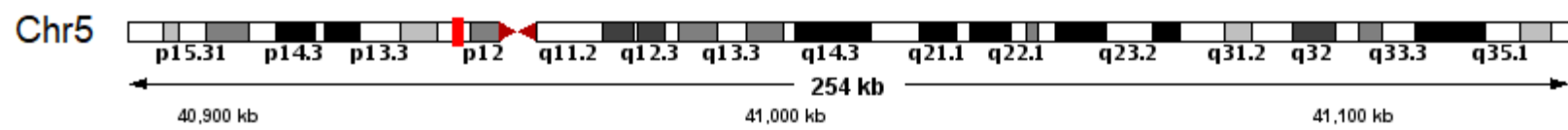
R

ERBB3 E332K, TGA → TAA



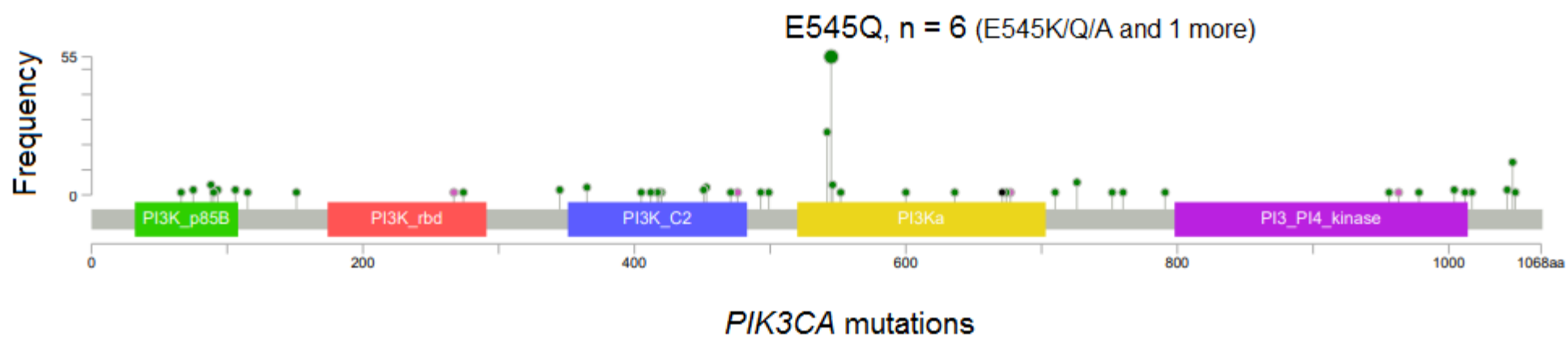
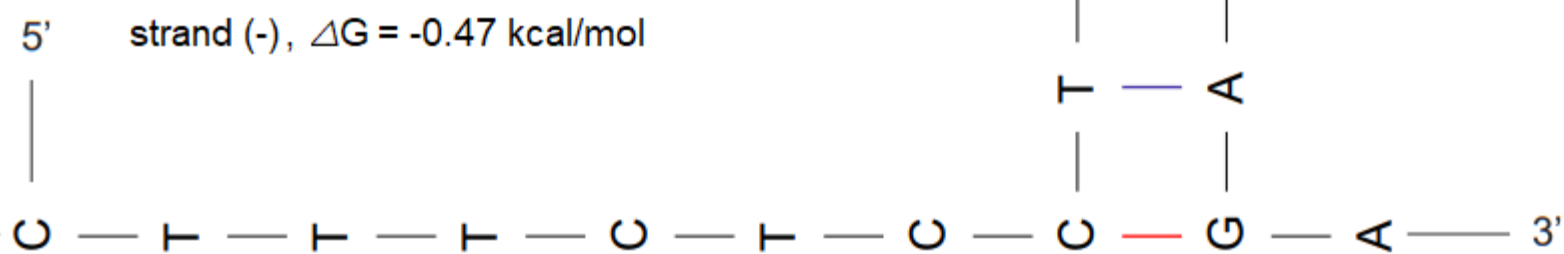
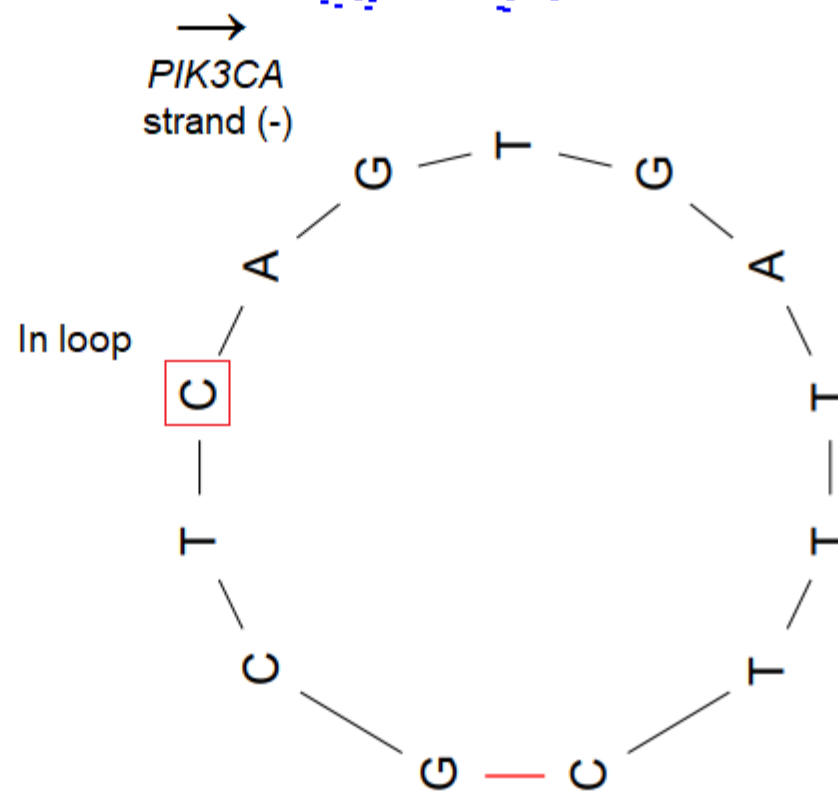
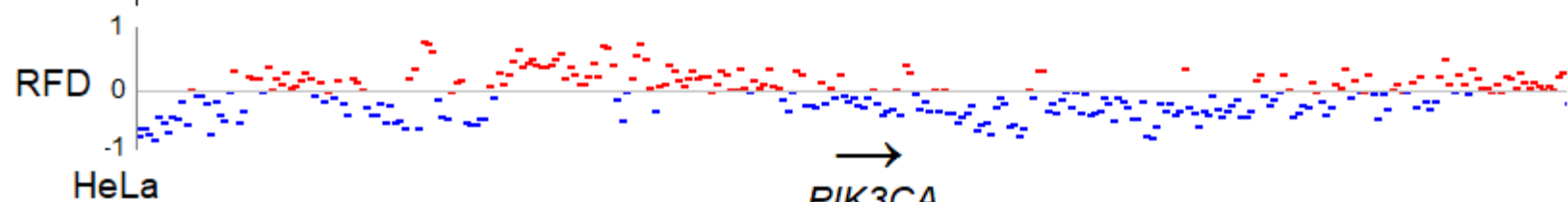
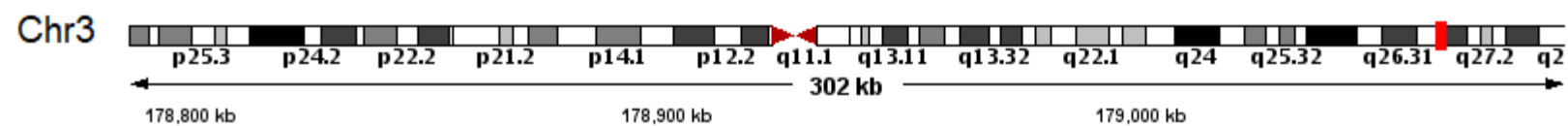
S

MROH2B E1109K, TCA → TTA

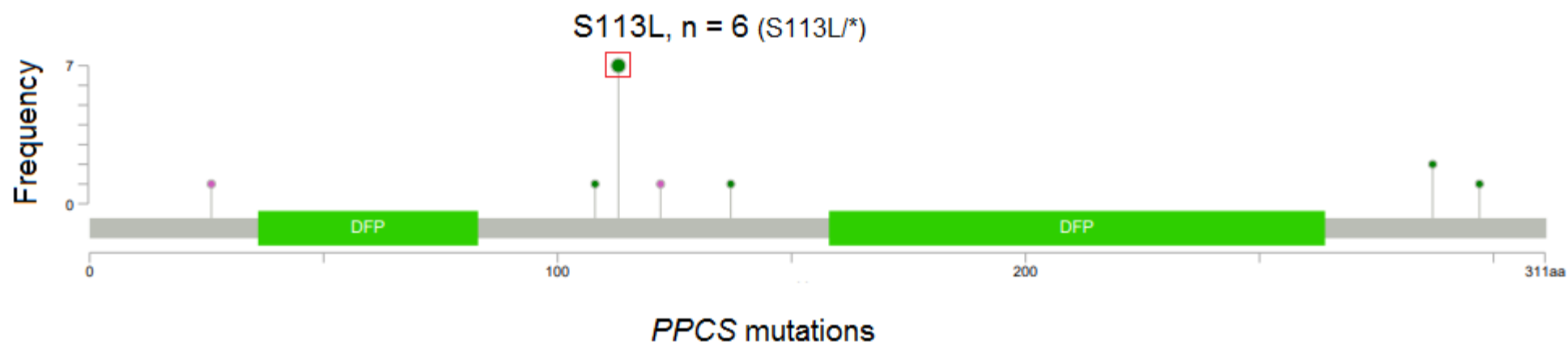
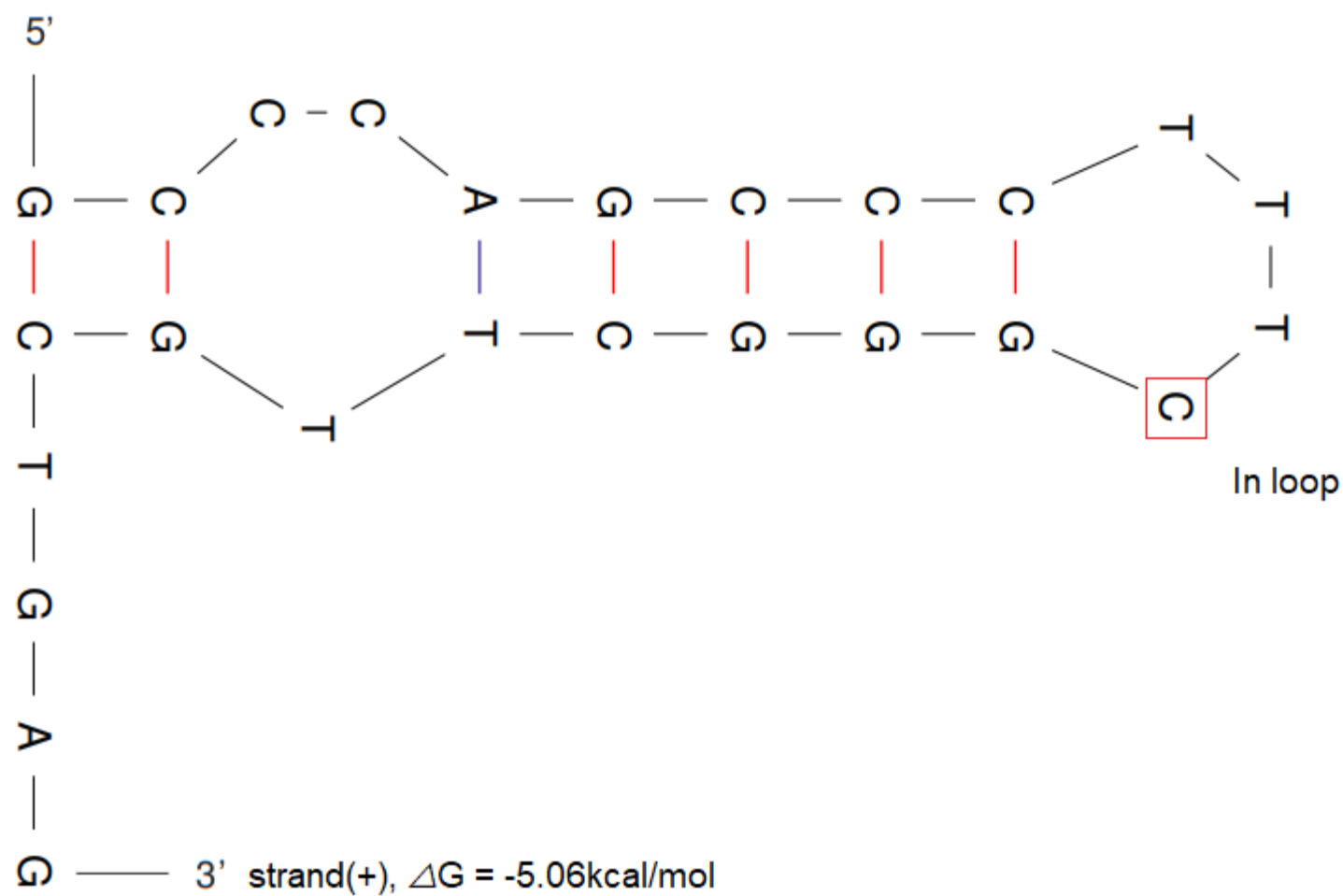
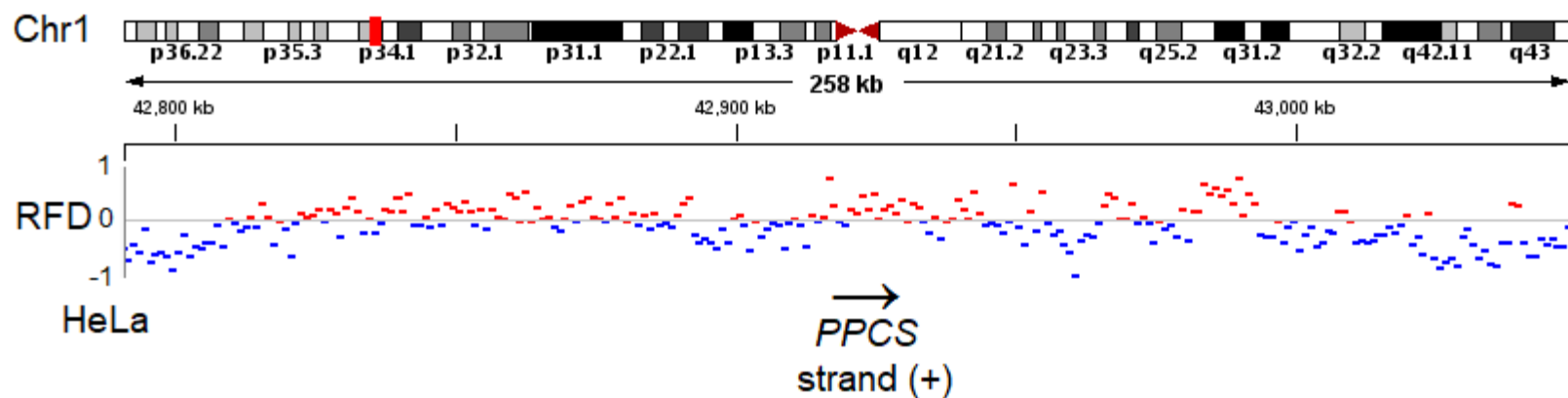


T

PIK3CA E545Q, TGA → TCA

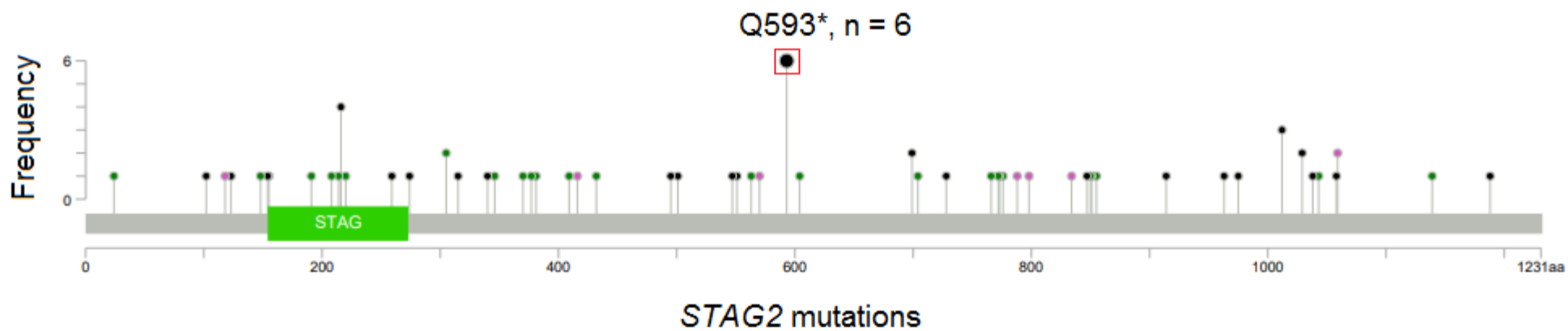
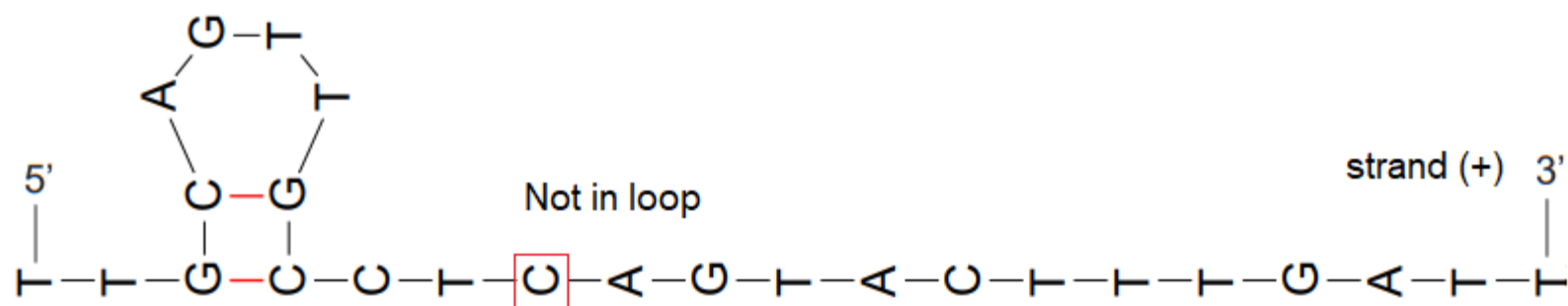
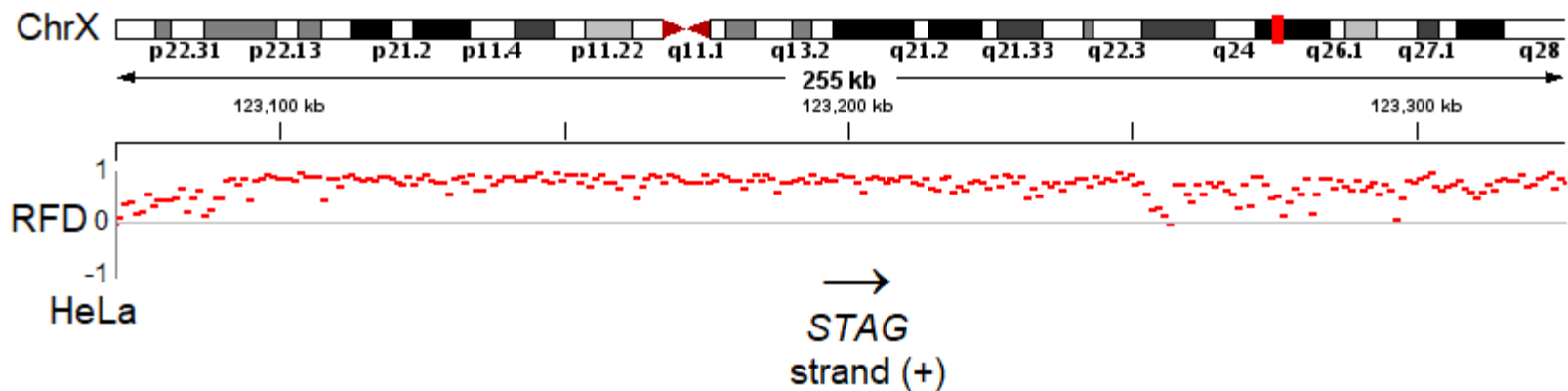


PPCS S113L, TCG → TTG



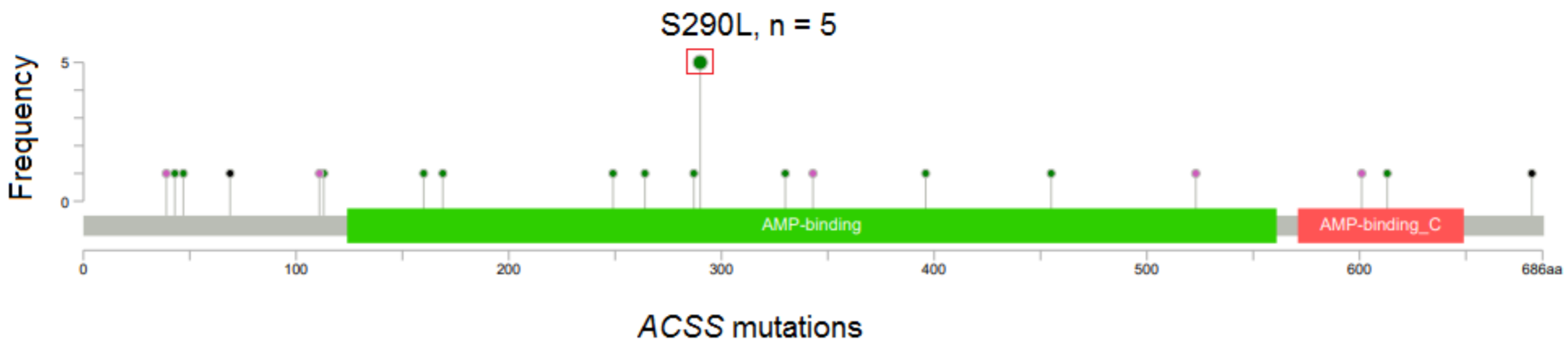
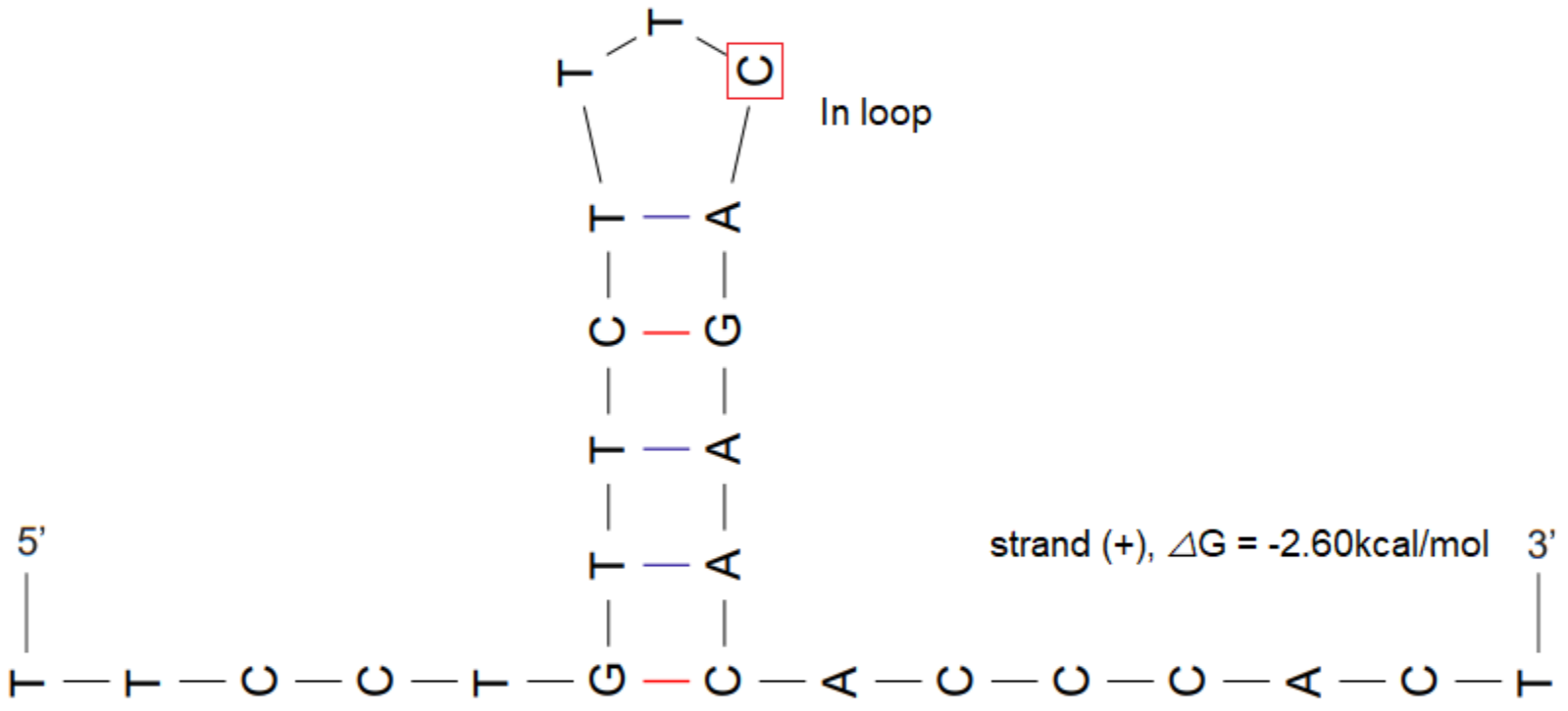
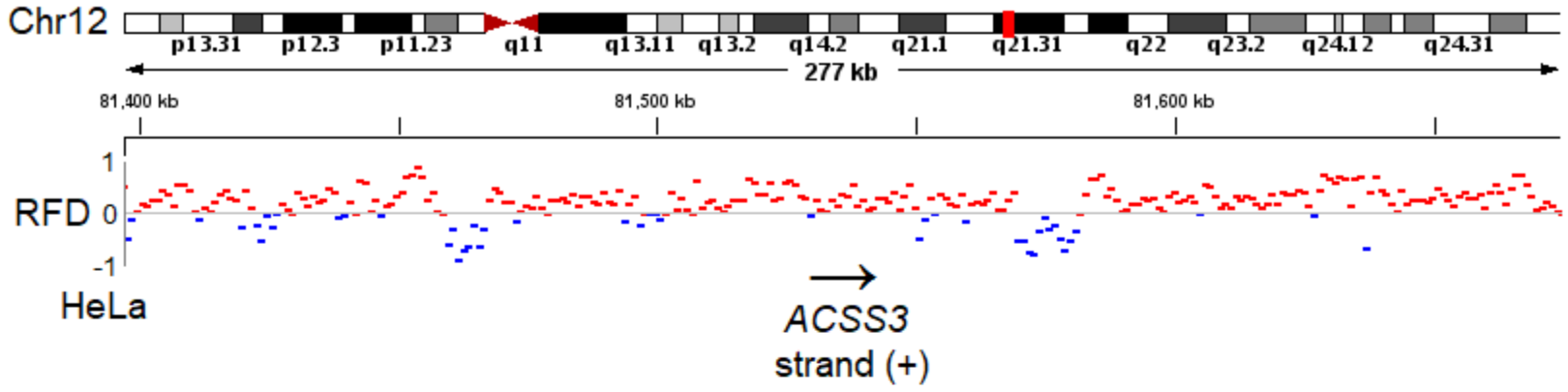
V

STAG2 Q593*, TCA → TTA



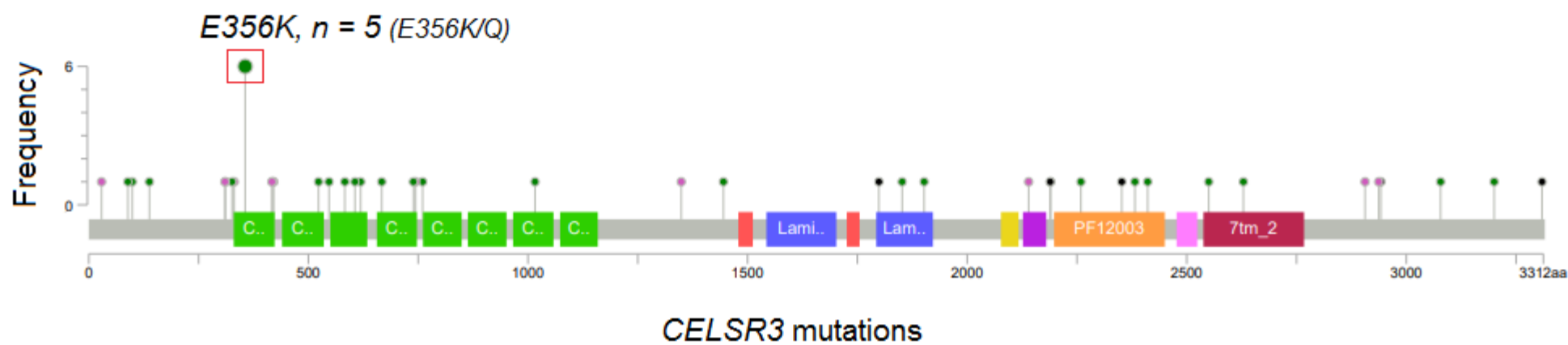
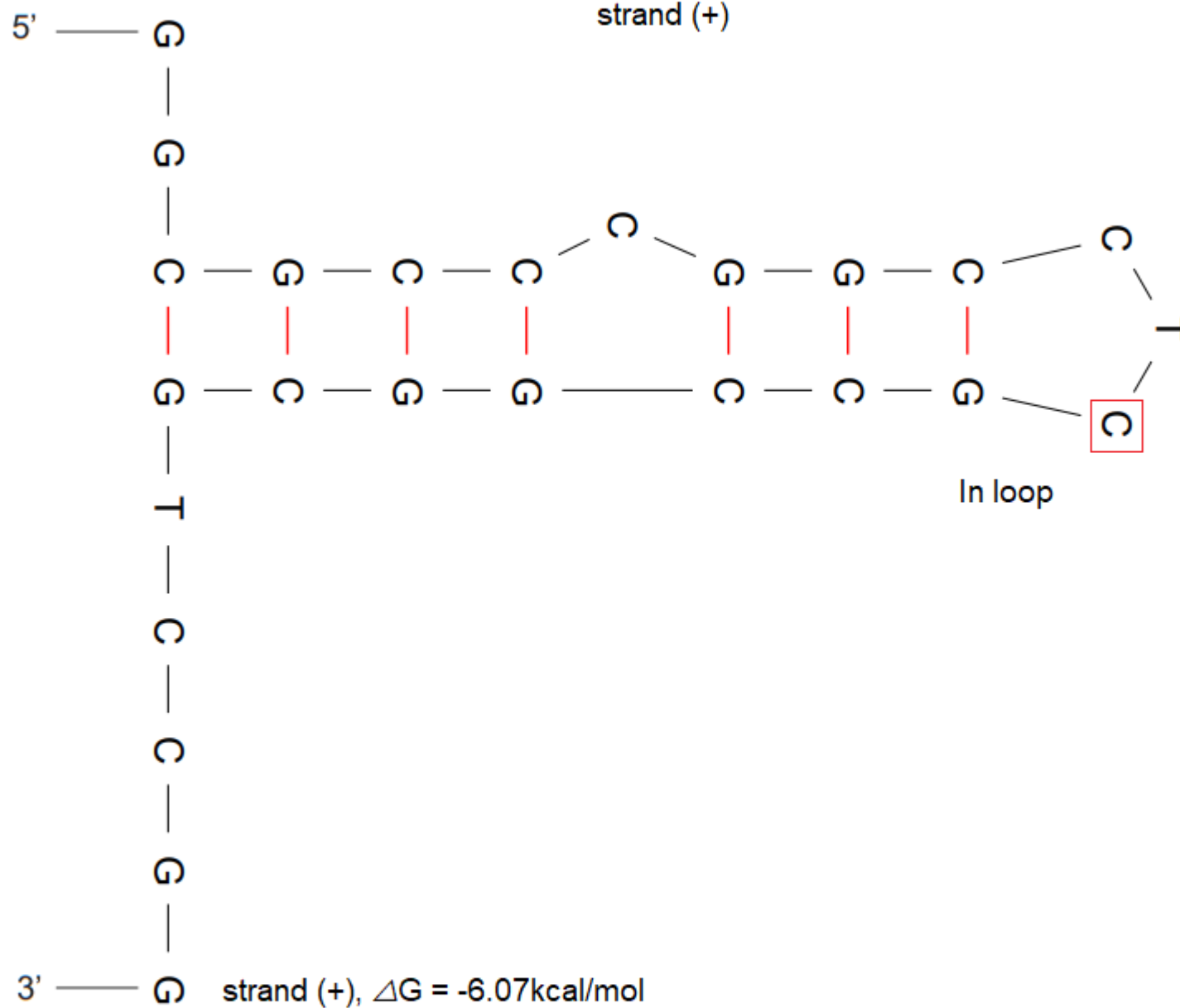
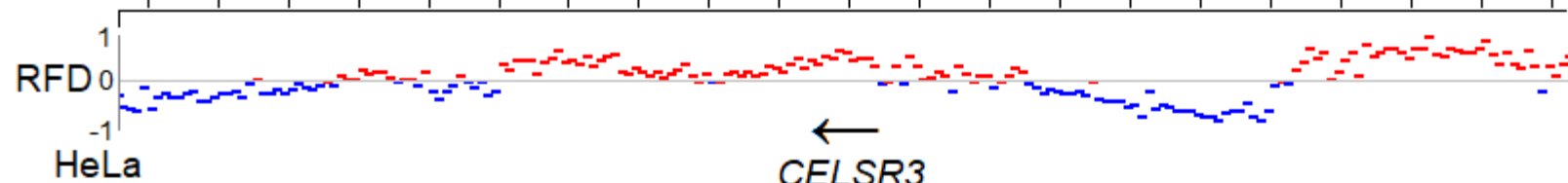
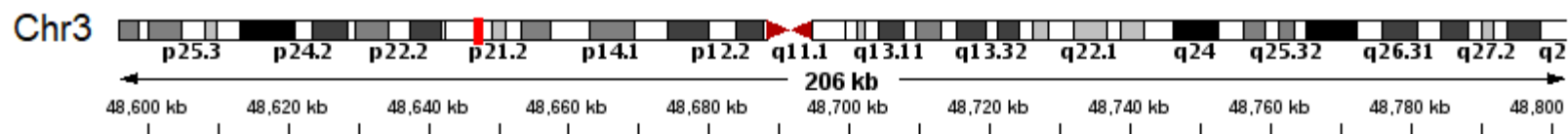
W

ACSS3 S290L, TCA → TIA



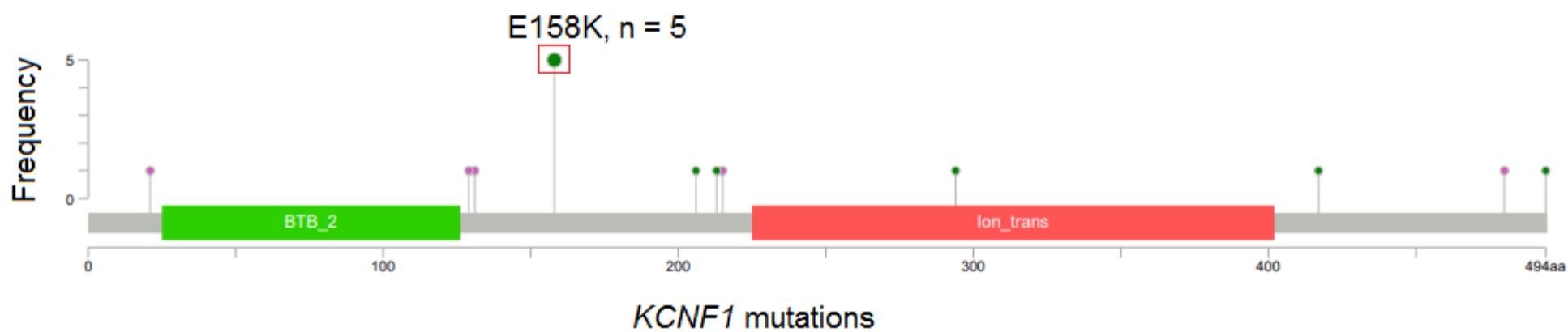
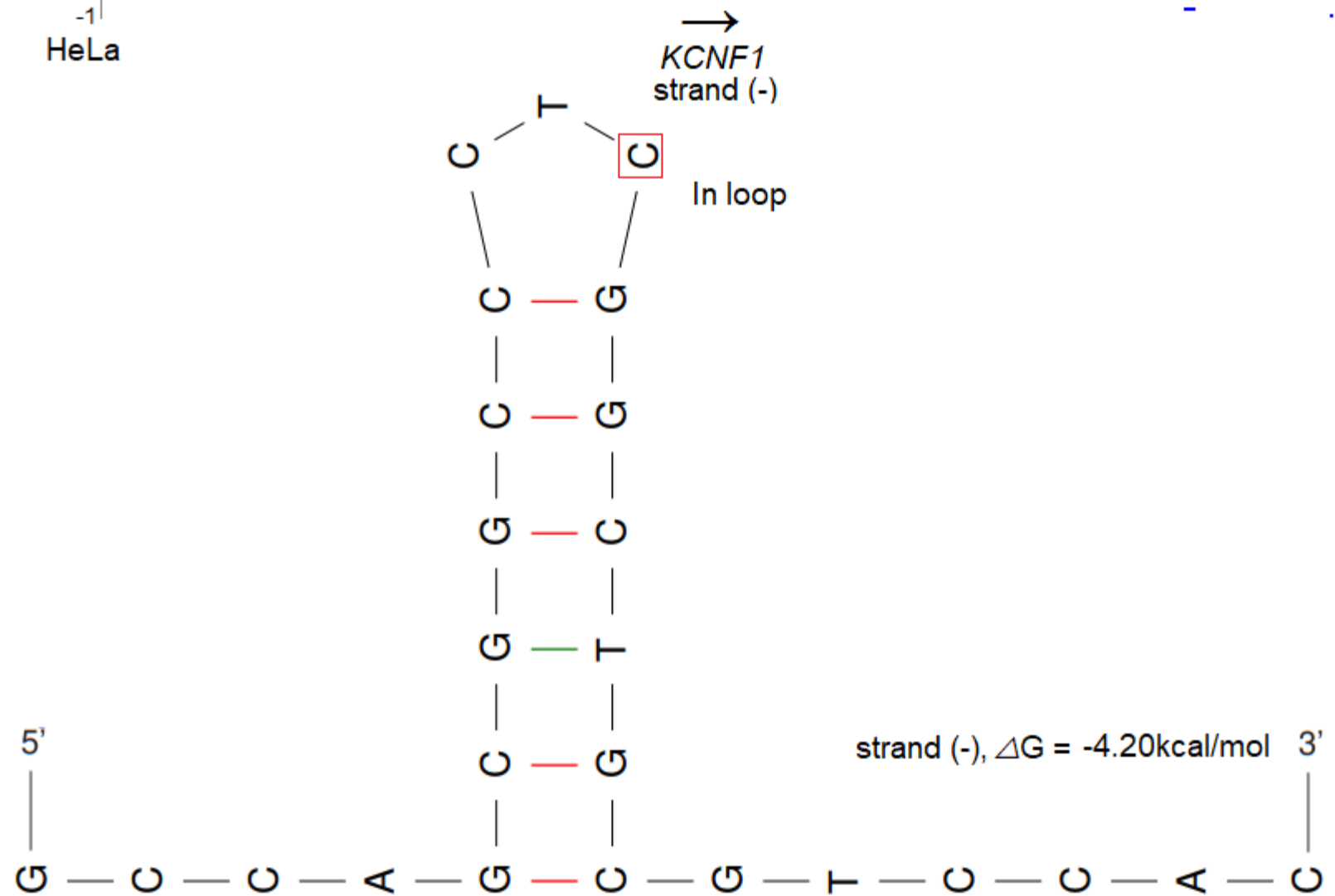
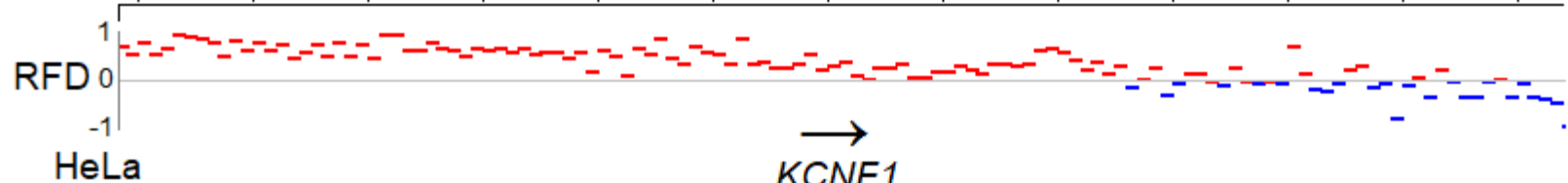
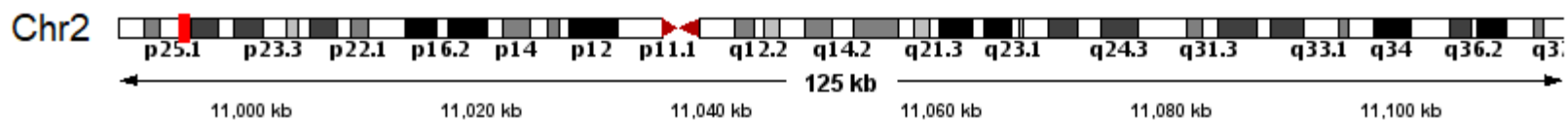
X

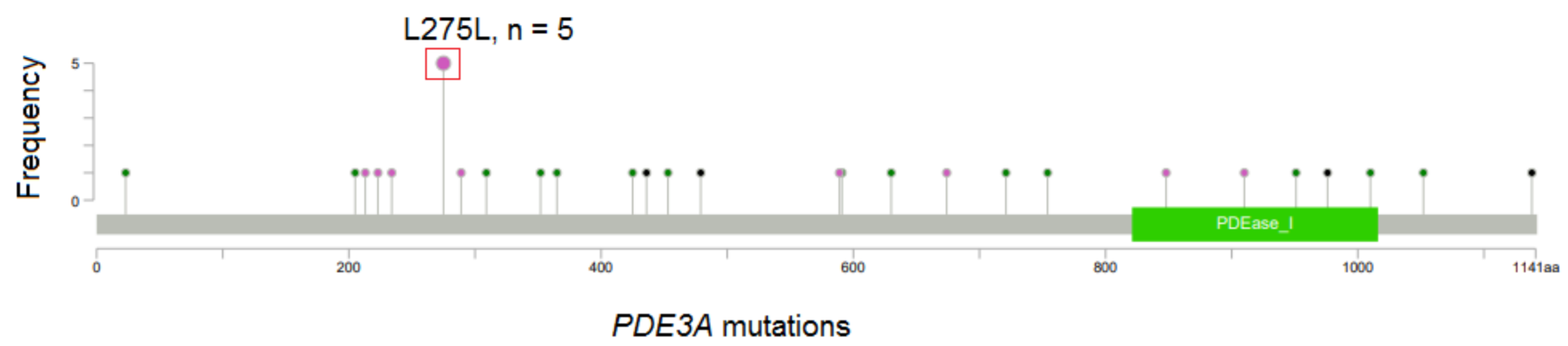
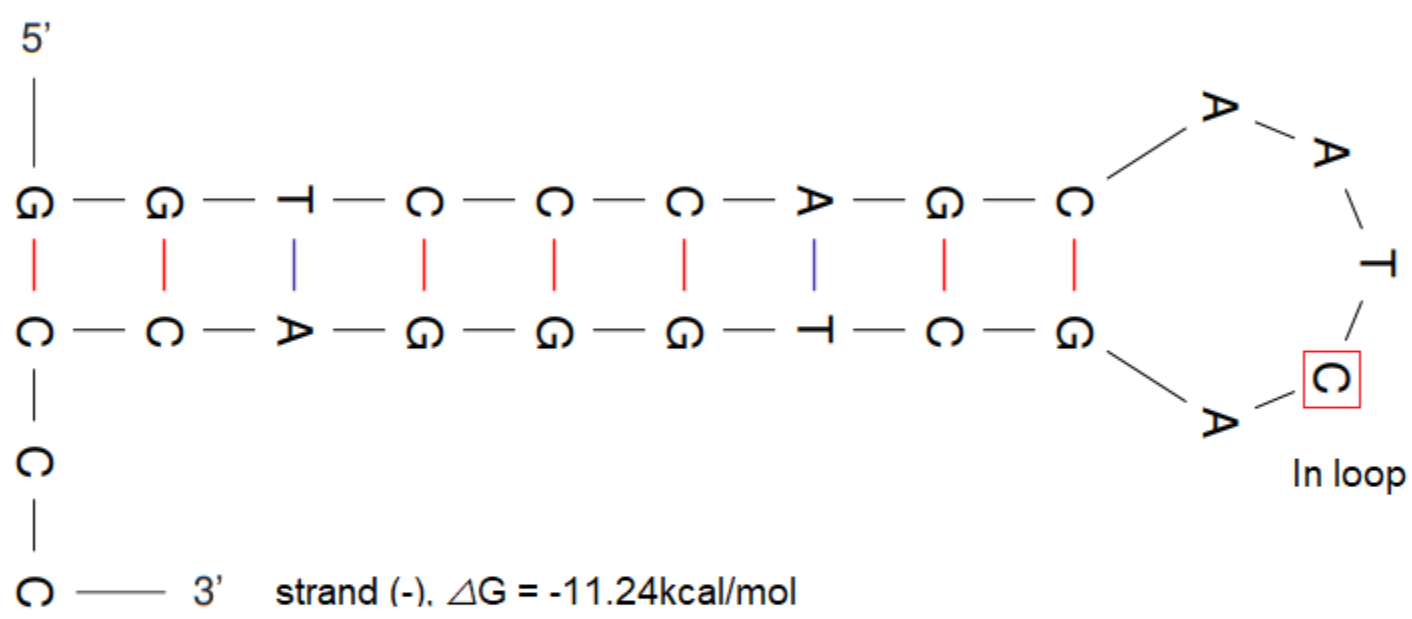
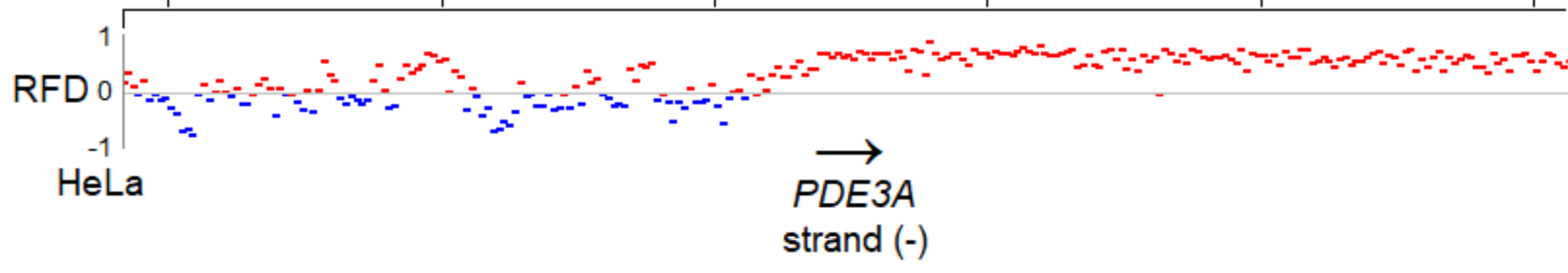
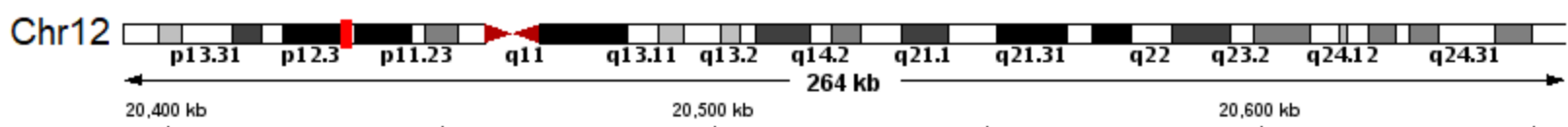
CELSR3 E356K, TCG → TIG



Y

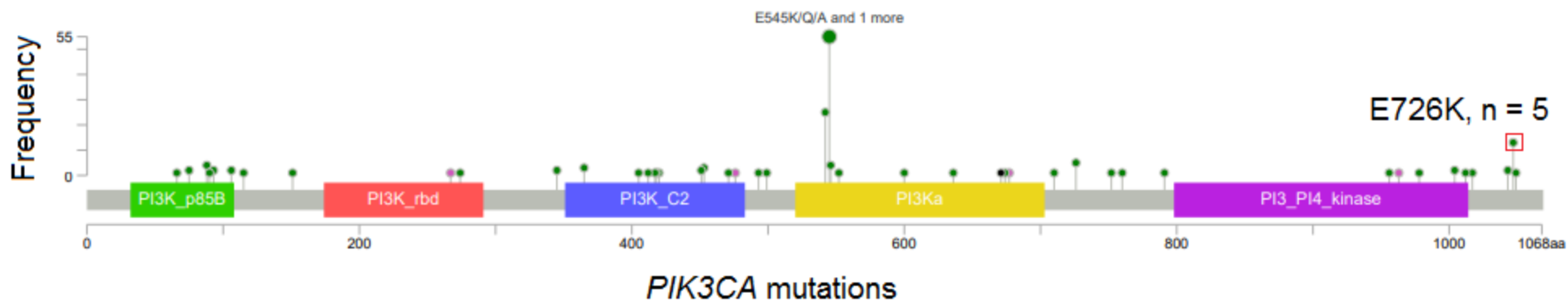
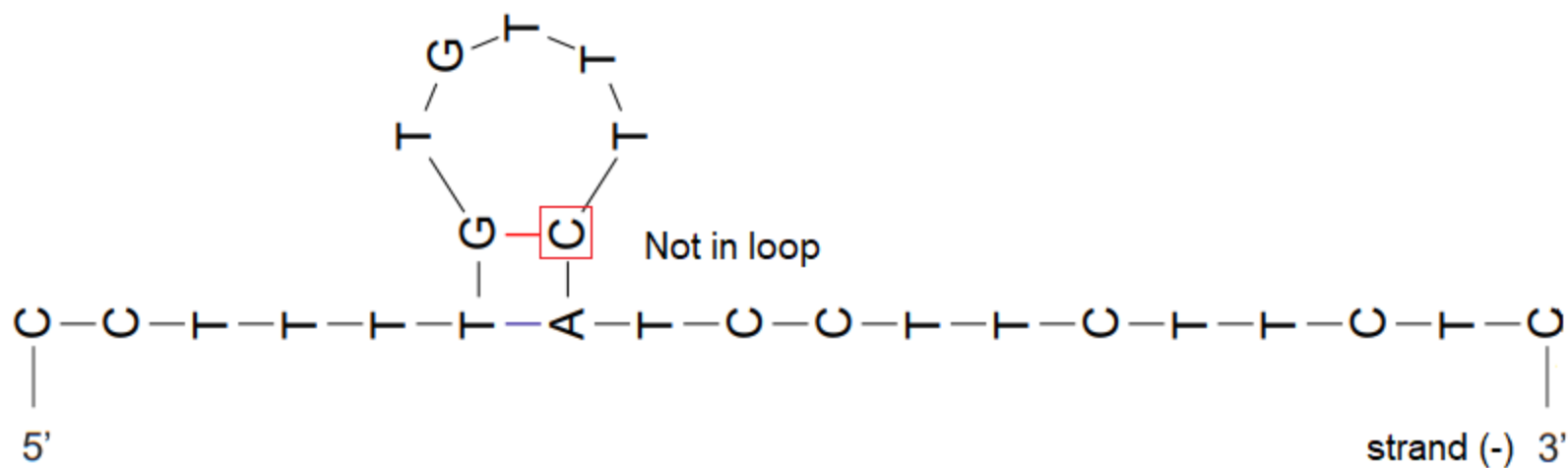
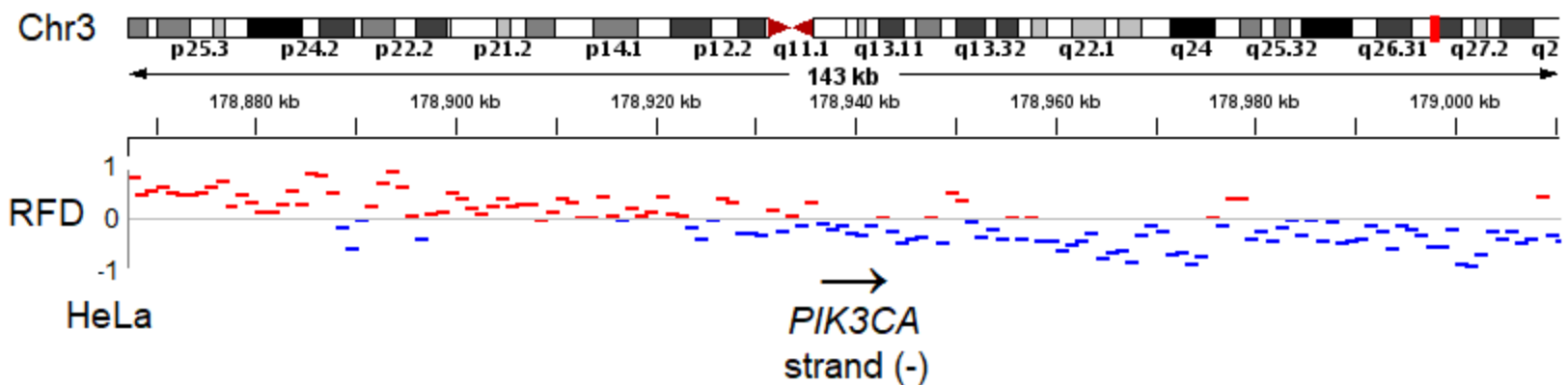
KCNF1 E158K, CGA → CAA

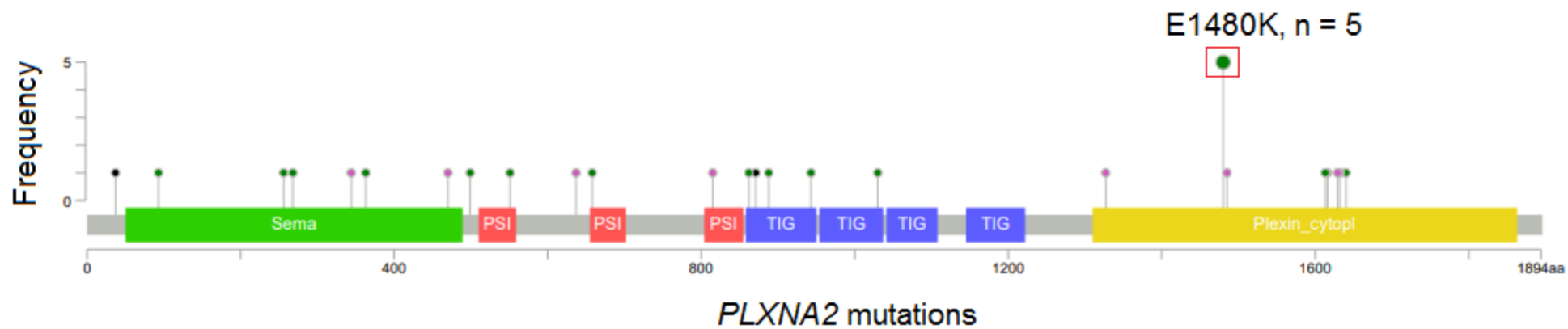
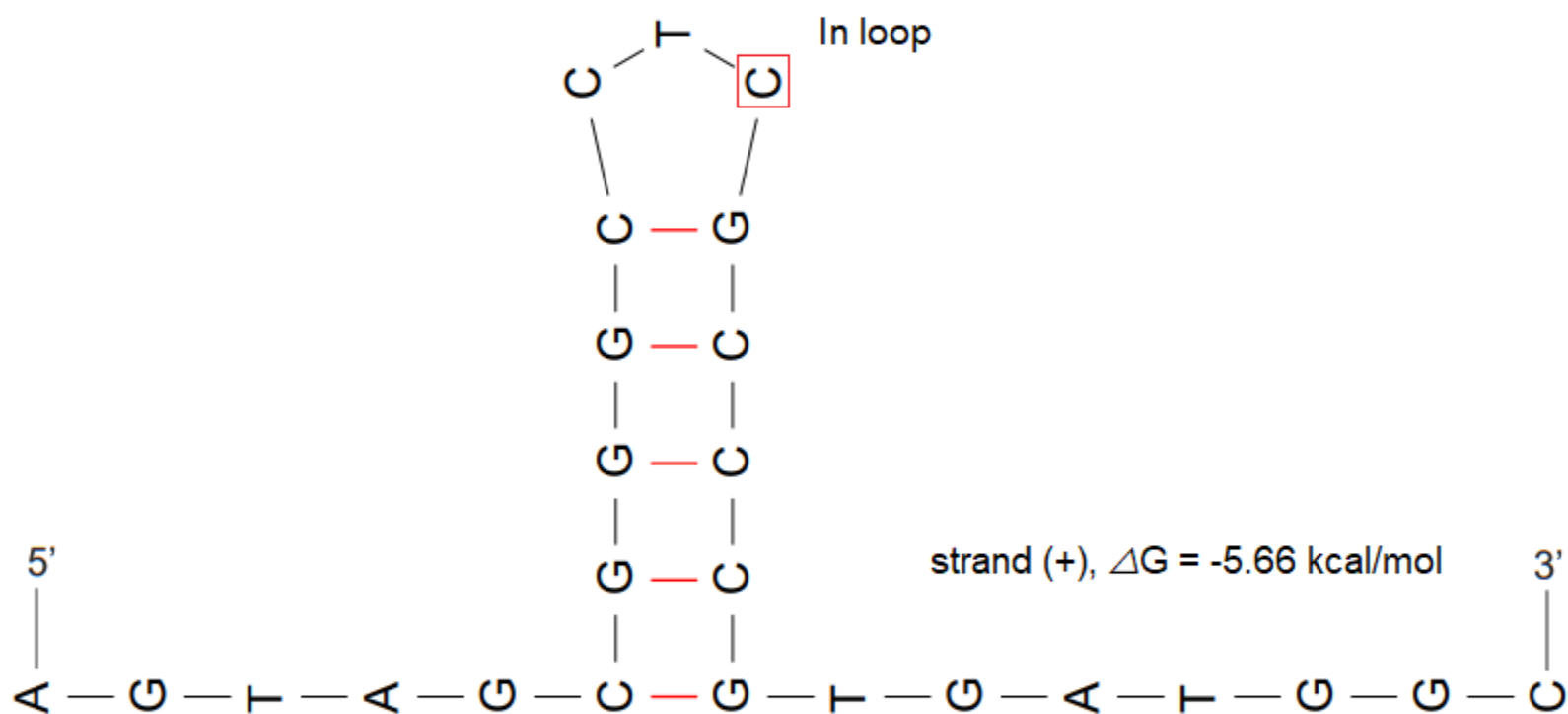
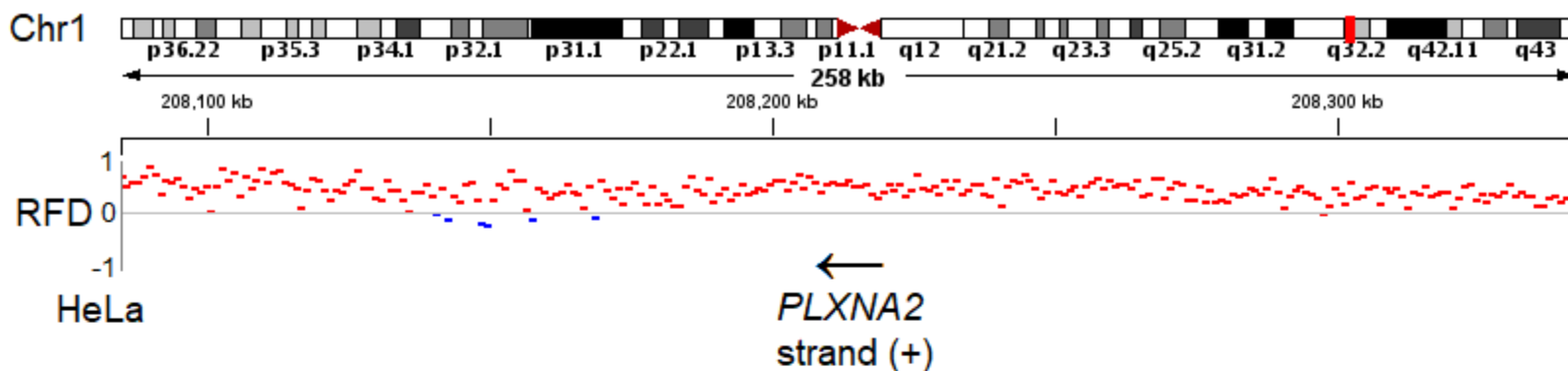


Z*PDE3A* L275L, TGA → TAA

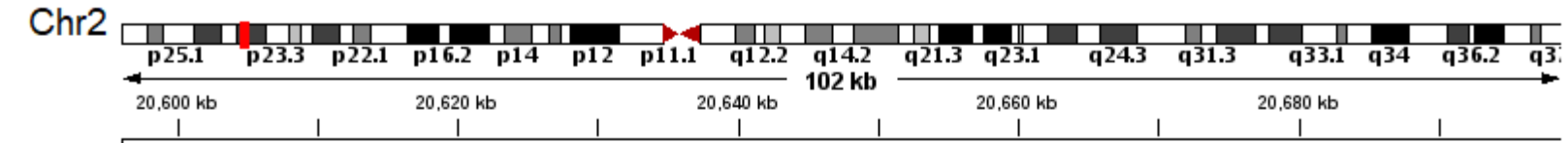
AA

PIK3CA E726K, TGA → TAA



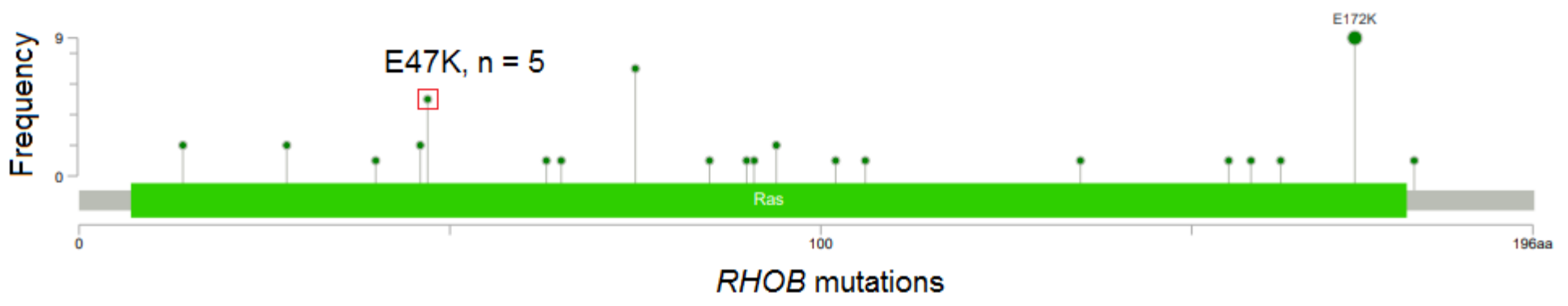
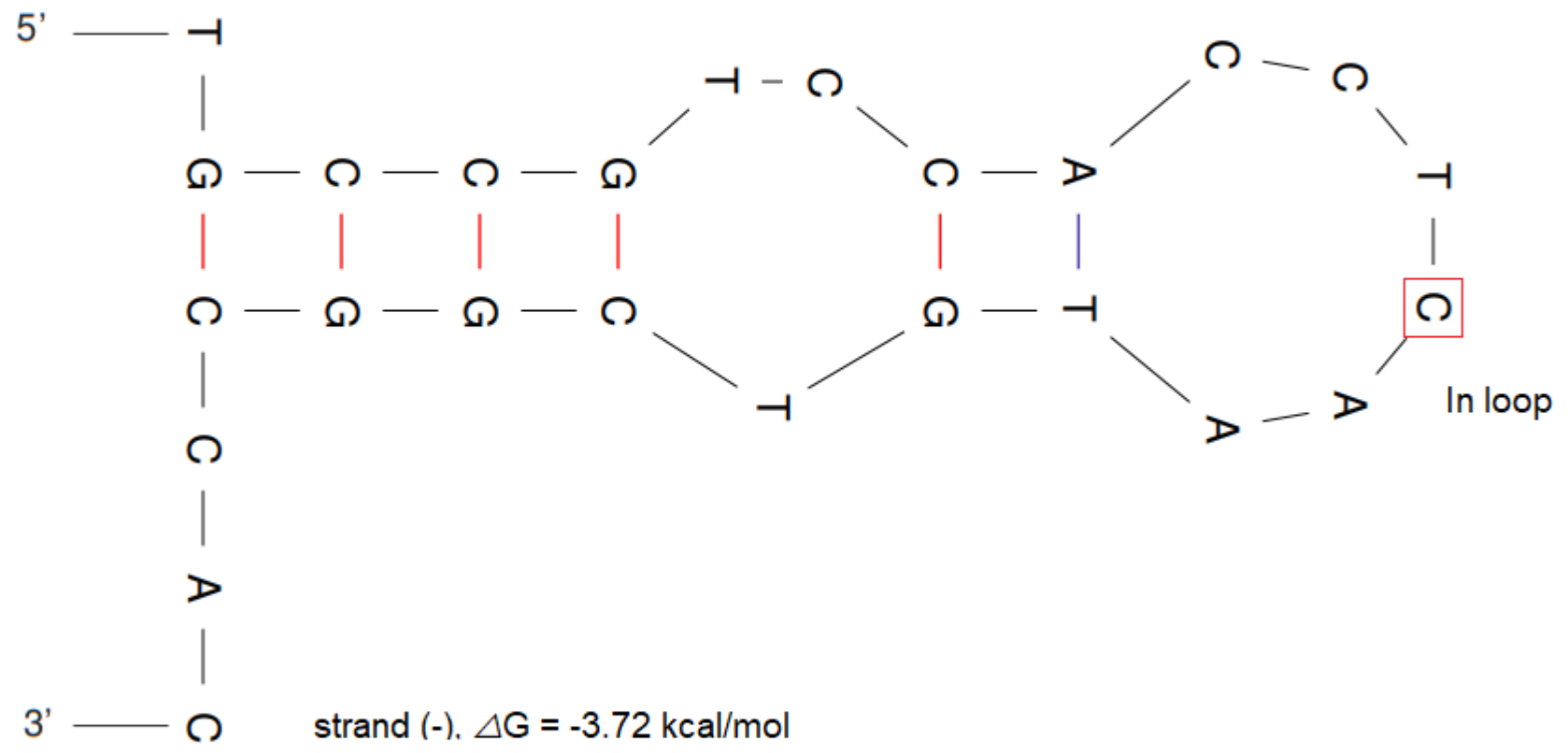
AB*PLXNA2* E1480K, TCG → TIG

RHOB E47K, TGA → TAA

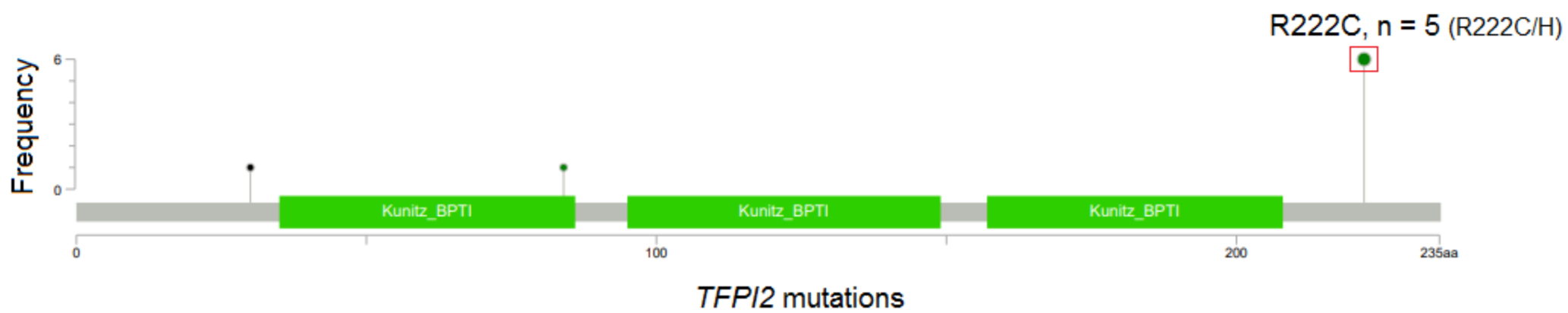
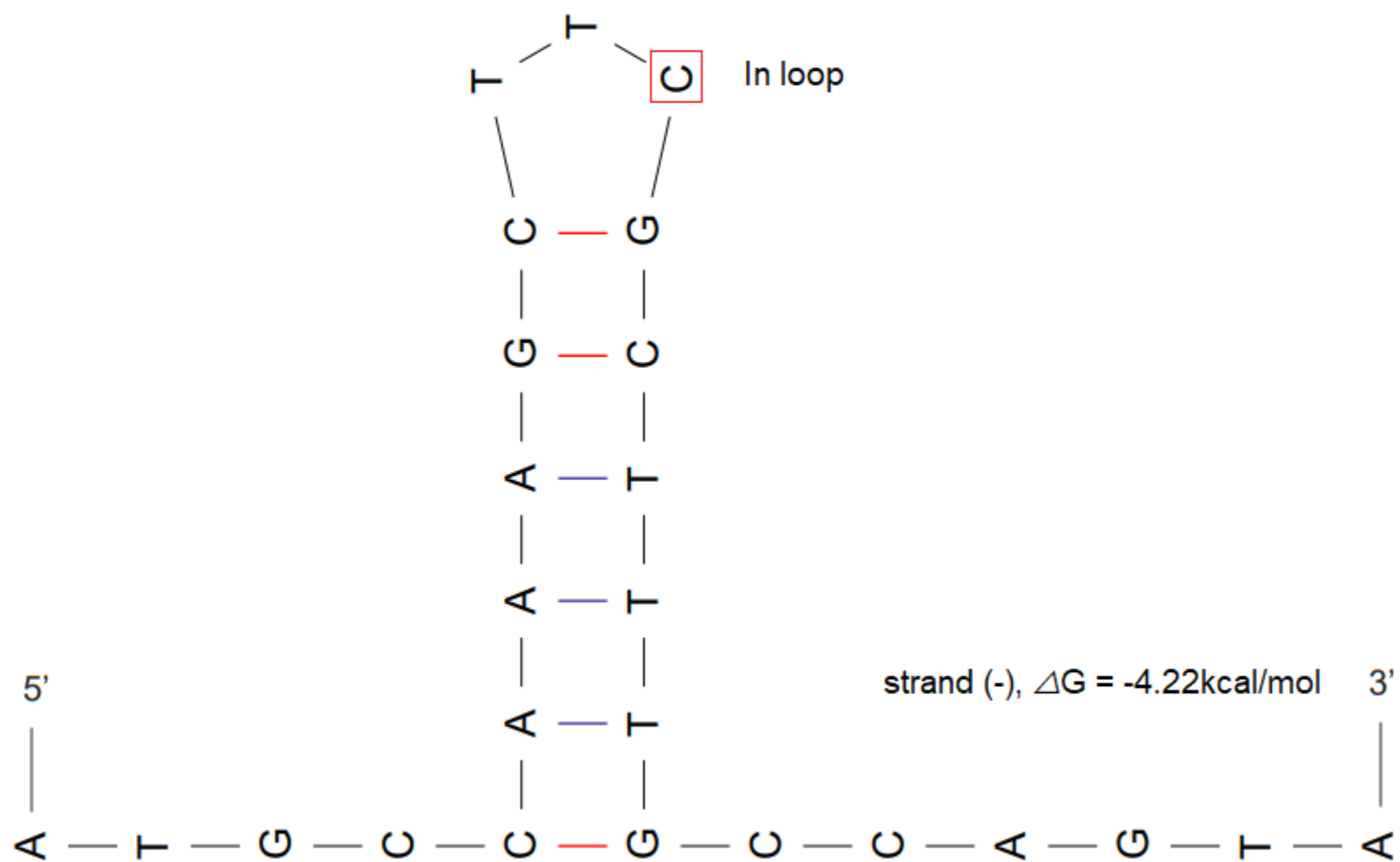
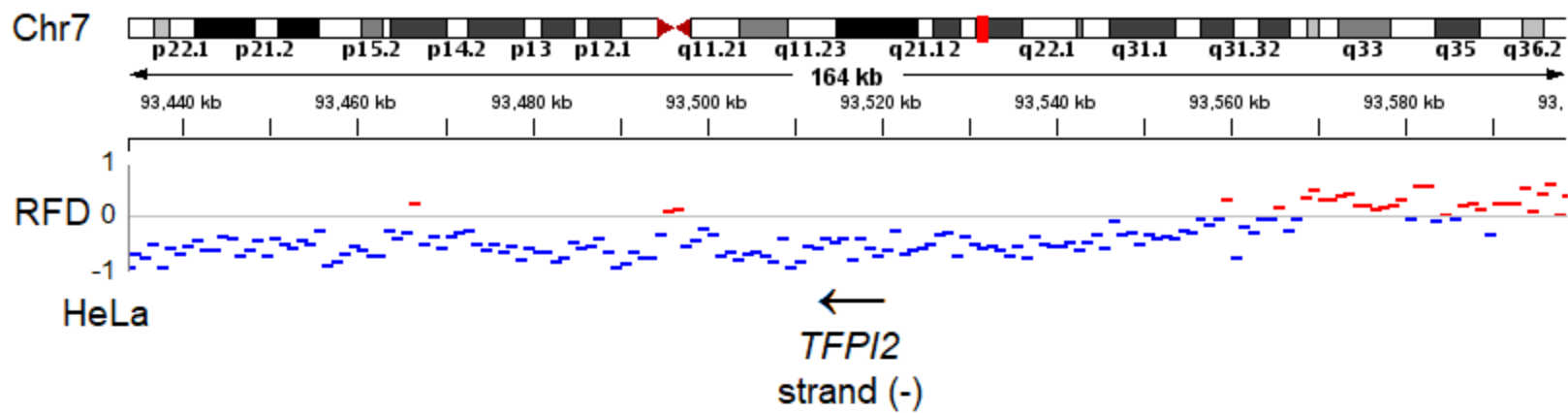


HeLa

→
RHOB
strand (-)

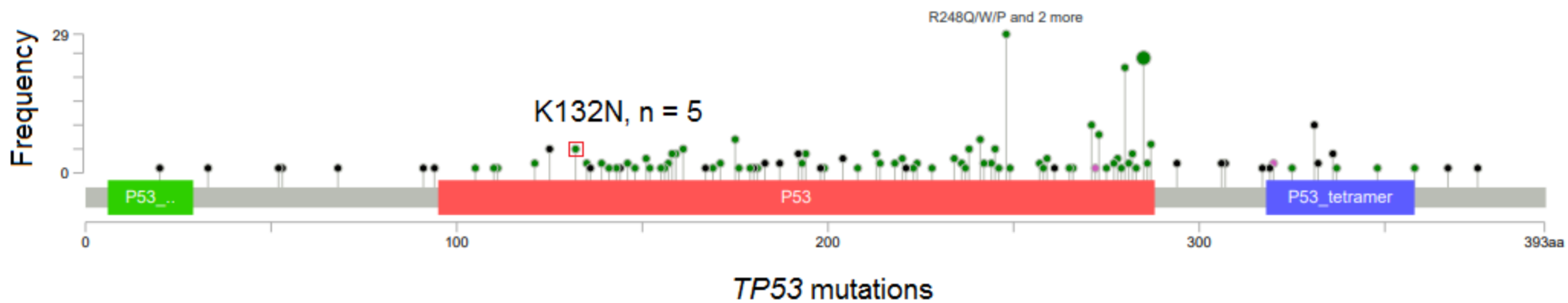
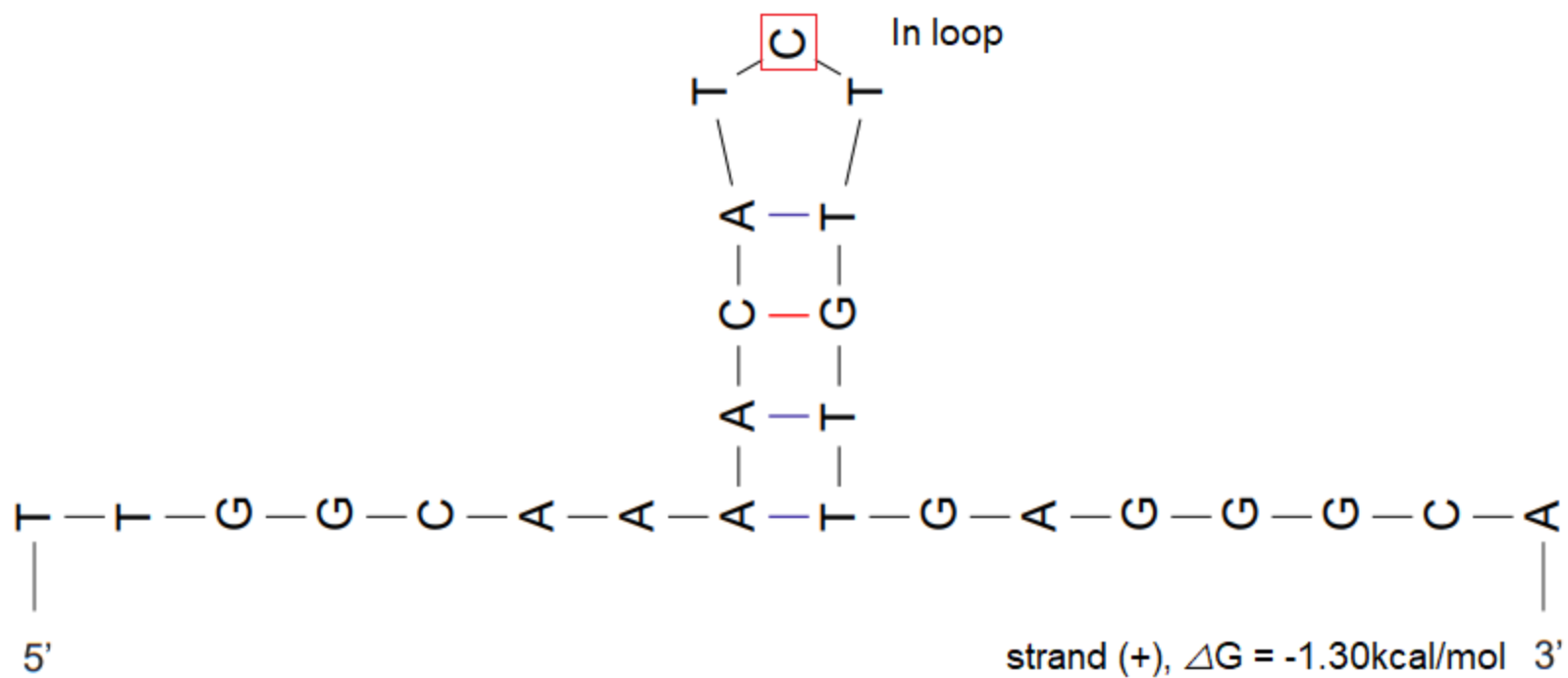
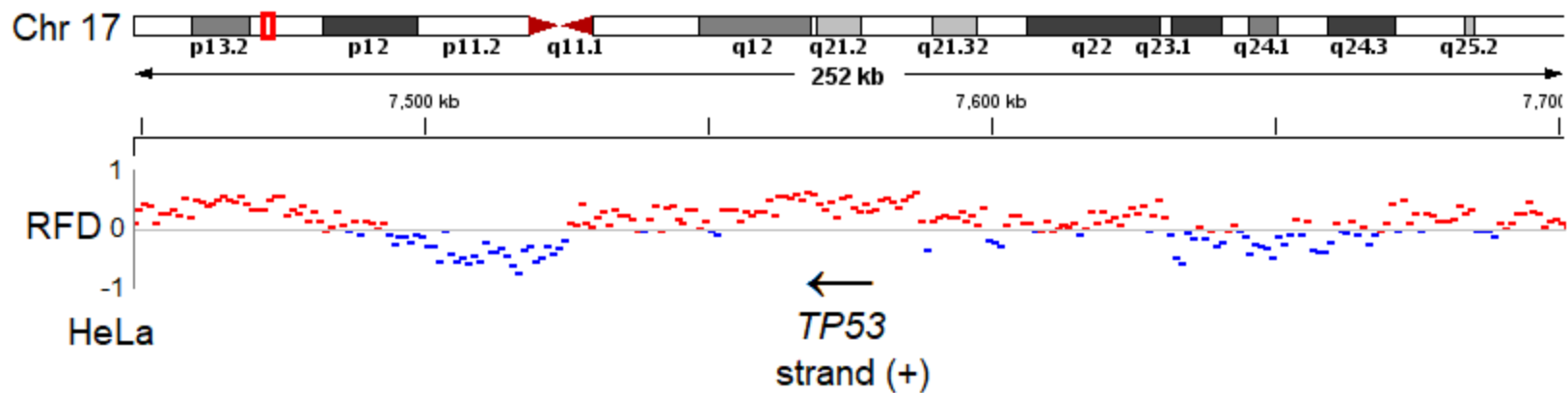


AD

TFPI2 R222C, CGA → CAA

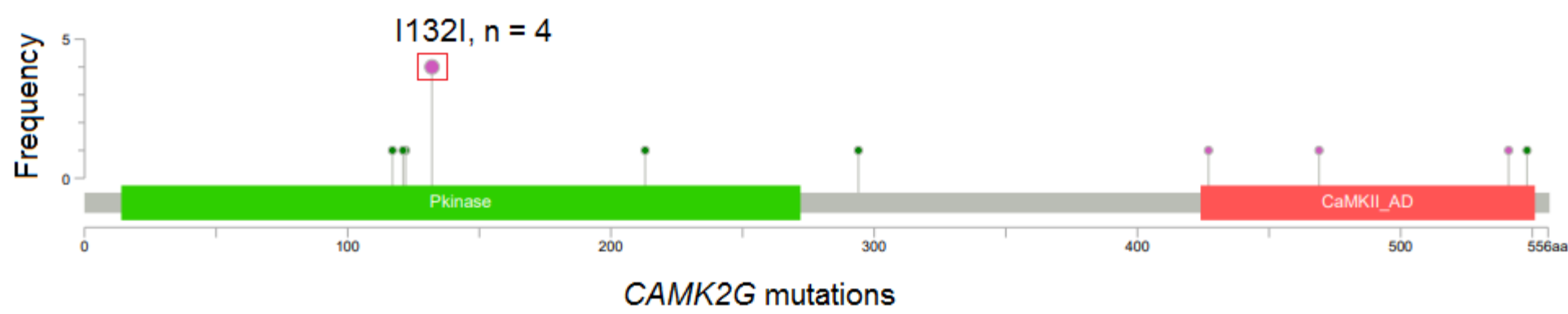
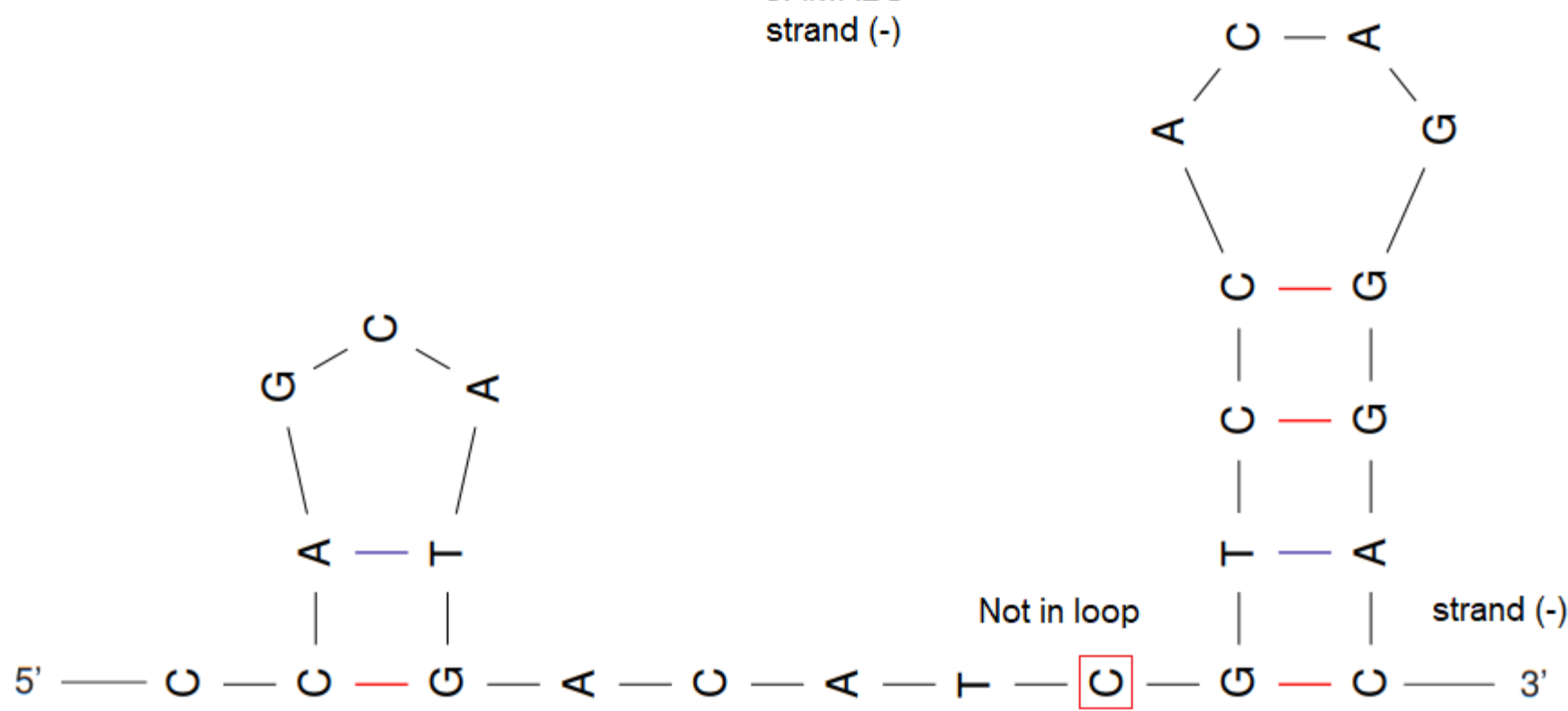
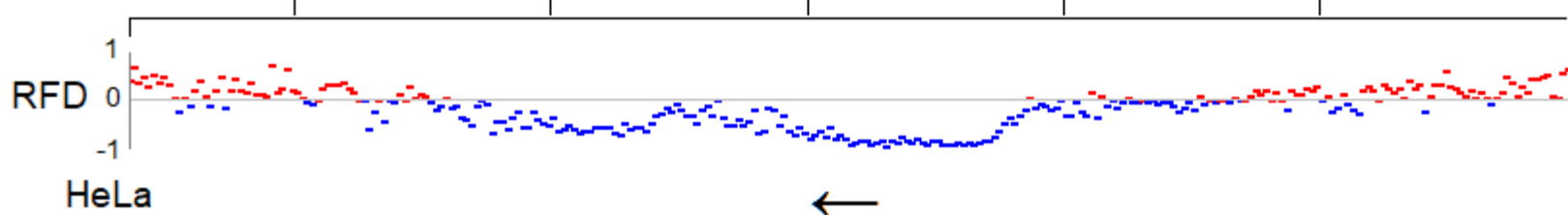
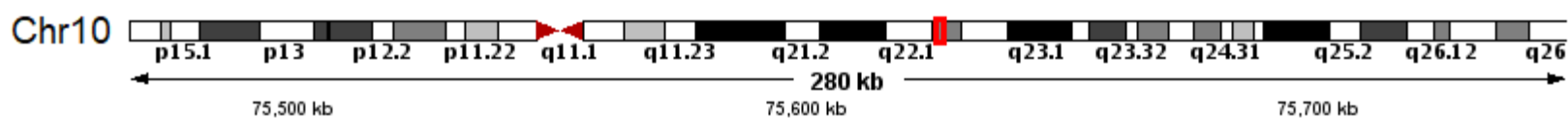
AE

TP53 K132N, TCT → TGT

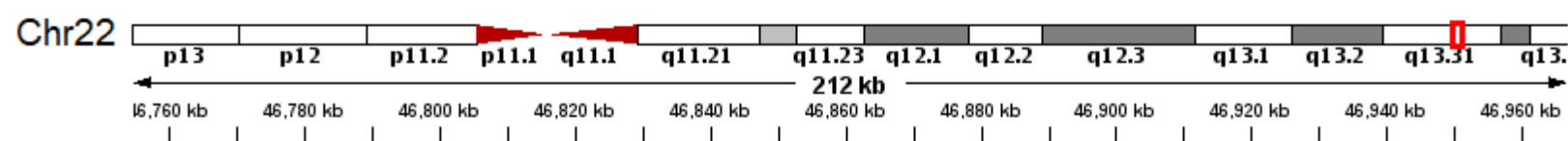


AF

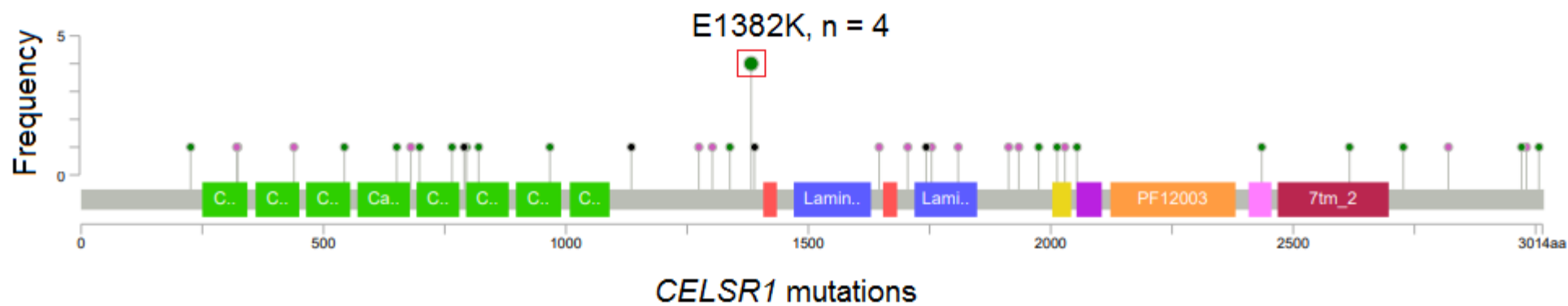
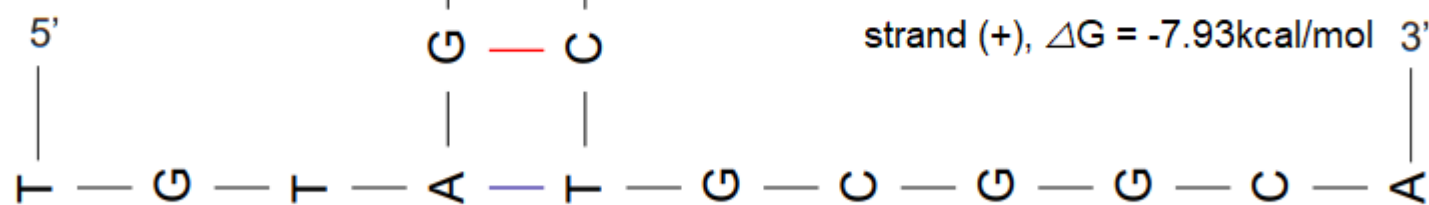
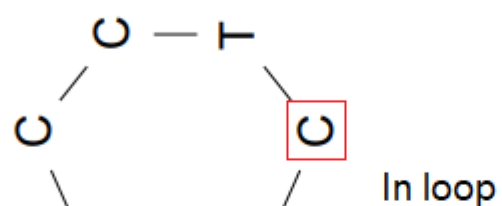
CAMK2G I132I, CGA → CAA



CELSR1 E1382K, TCG → TTG

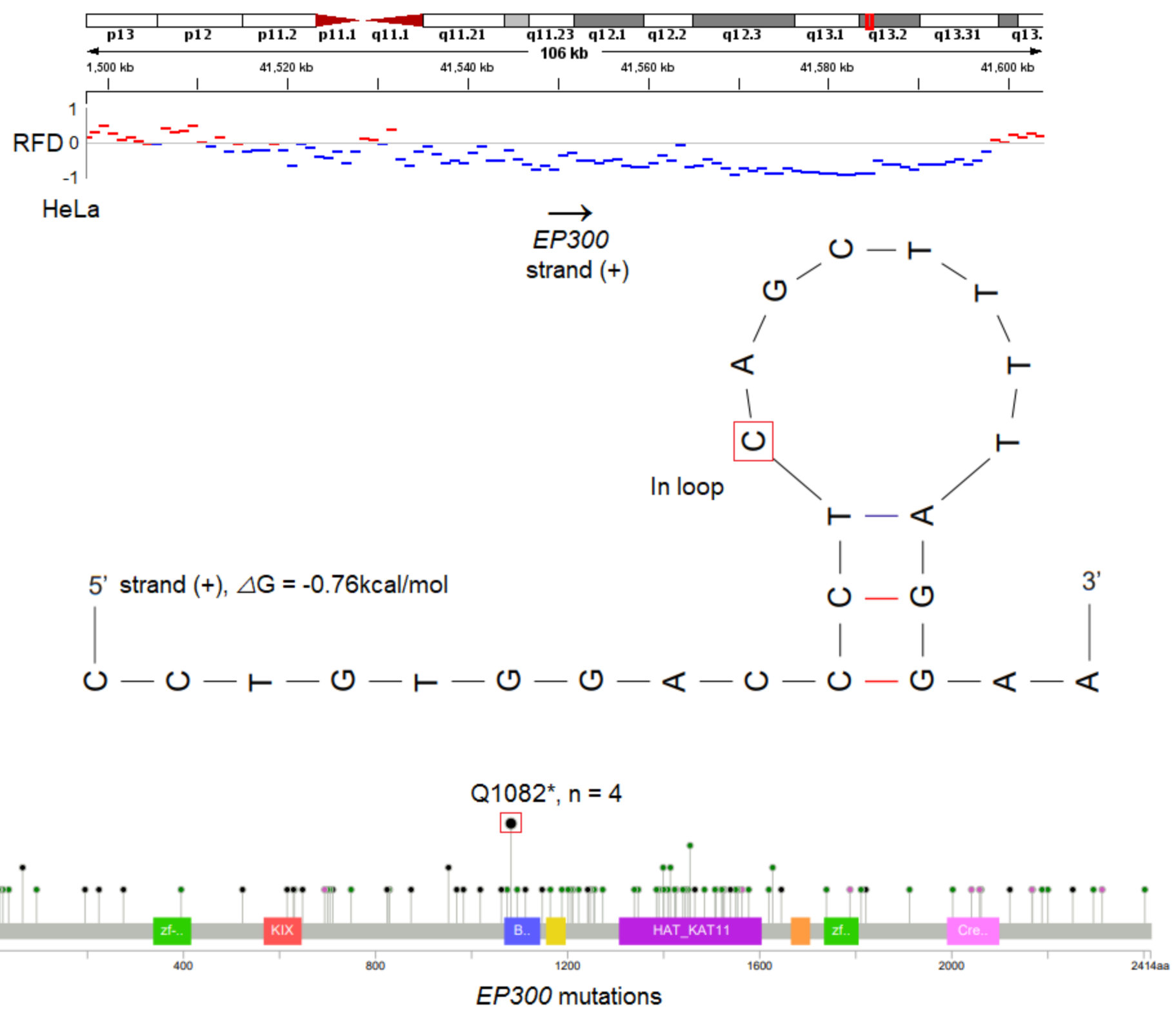


←
 CELSR1
 strand (+)



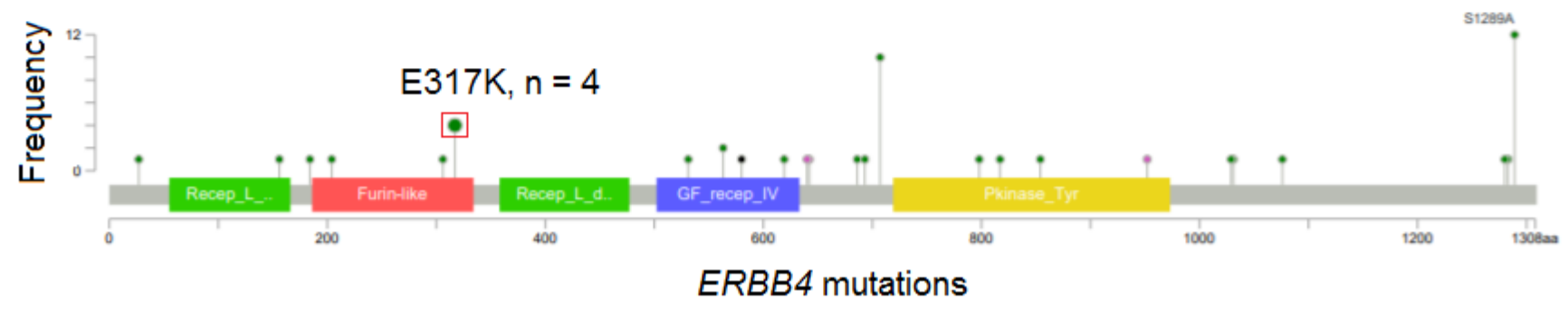
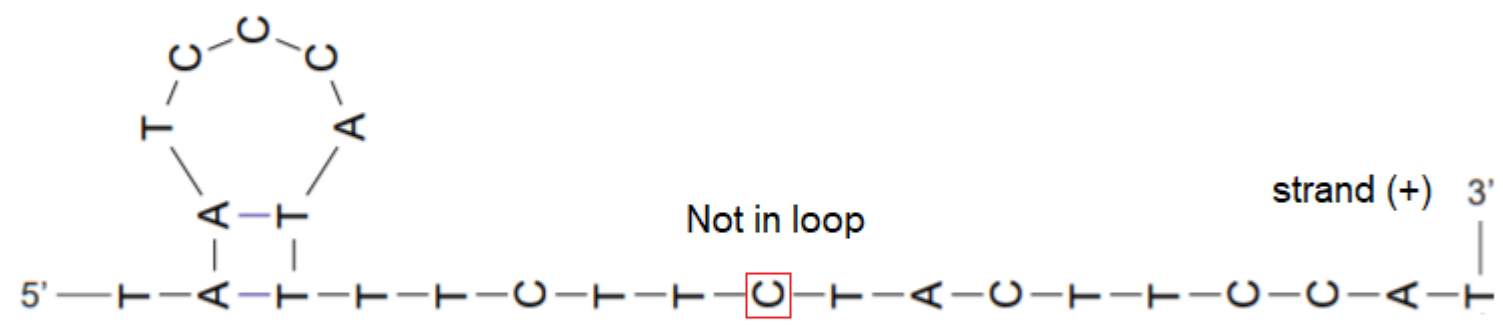
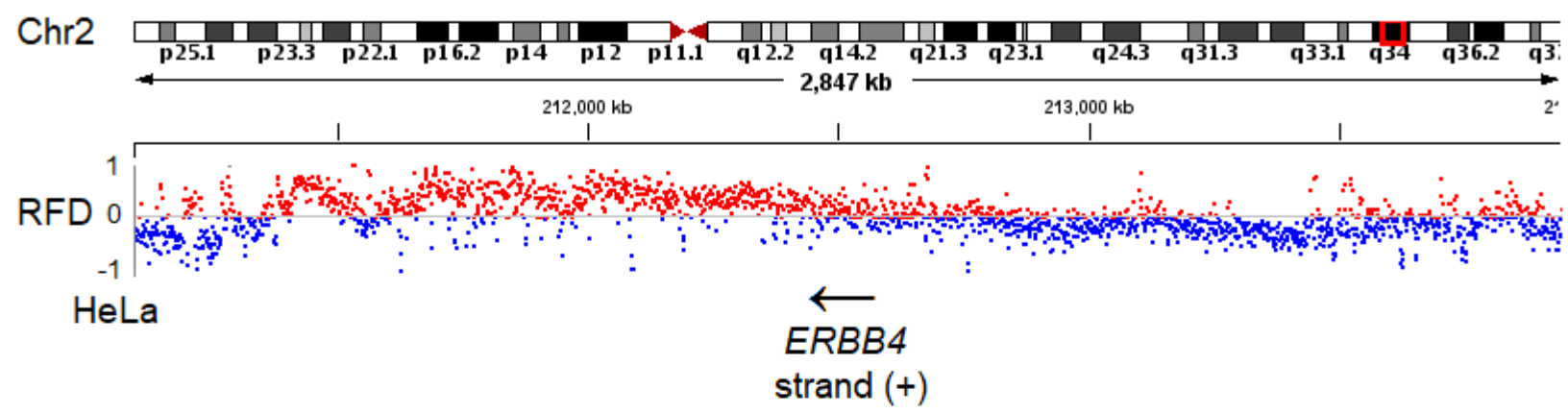
AH

EP300 Q1082*, TCA → TTA



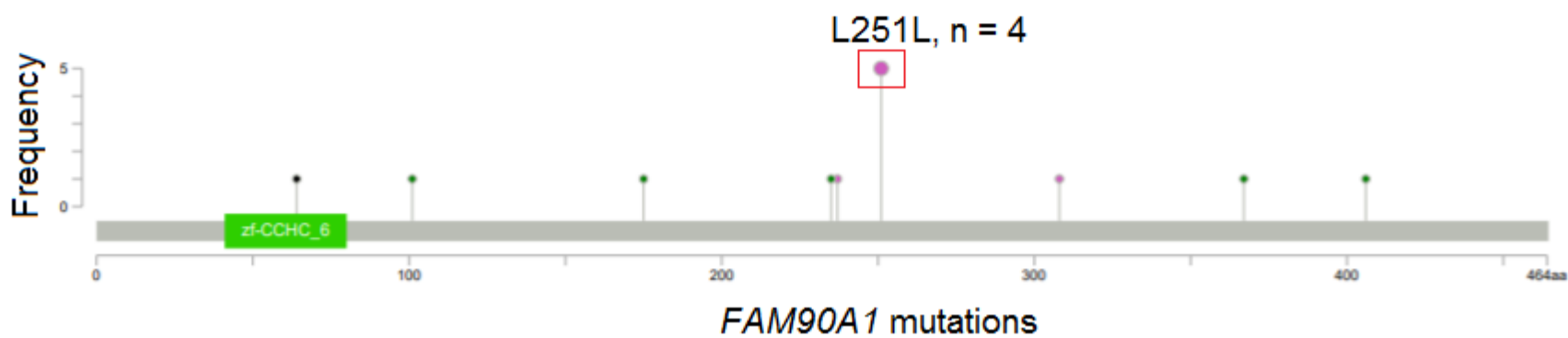
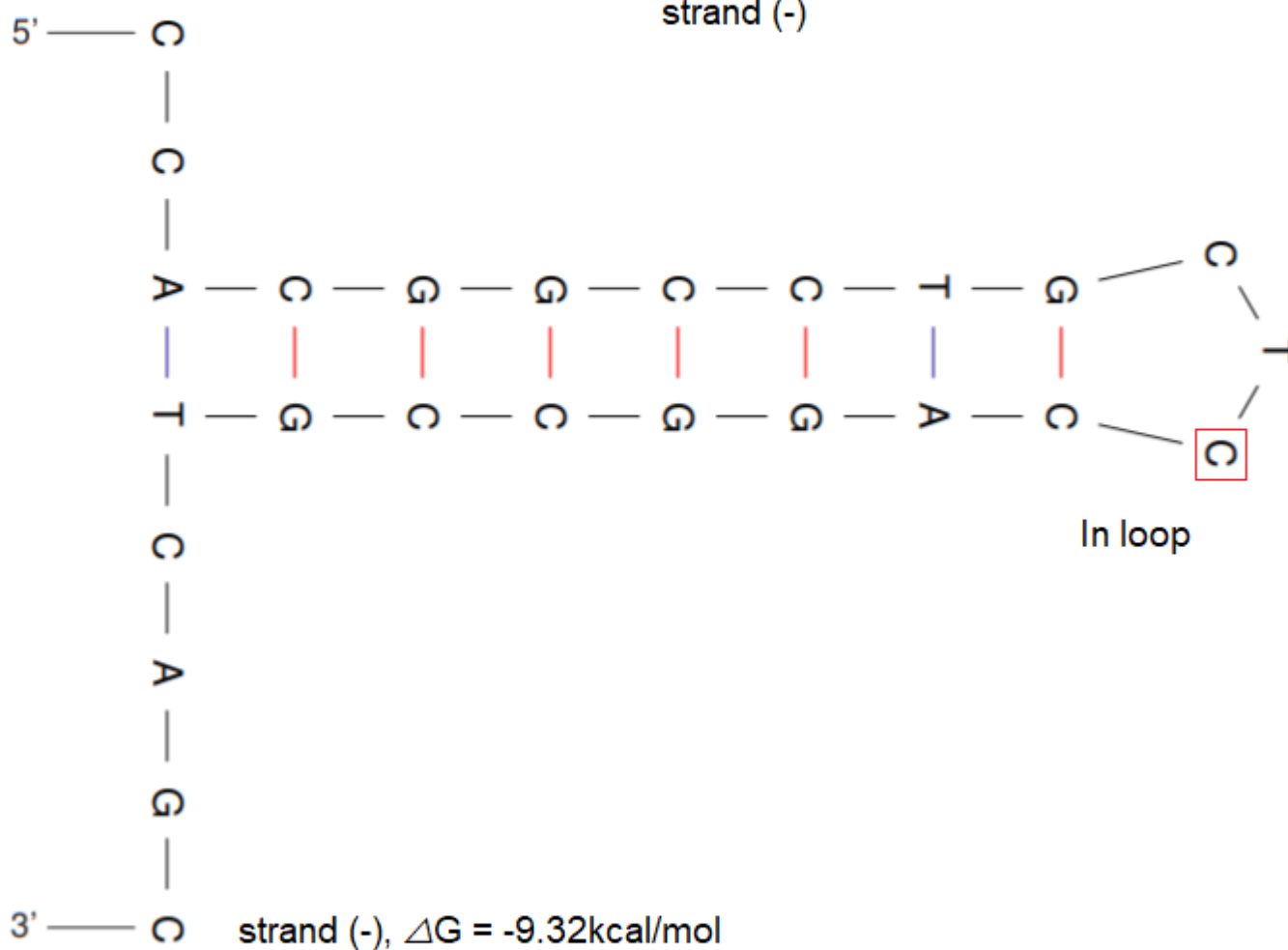
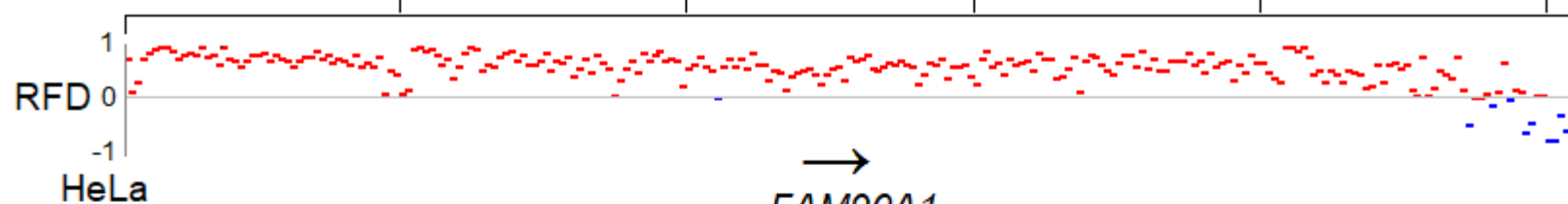
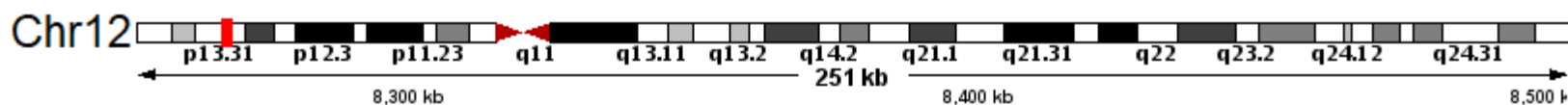
AI

ERBB4 E317K, TCT → TTT



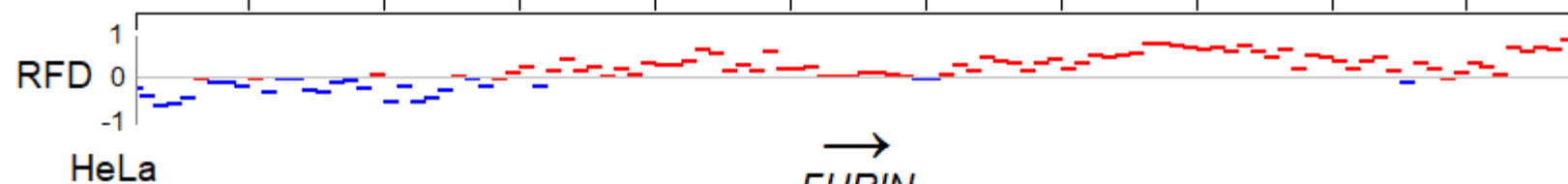
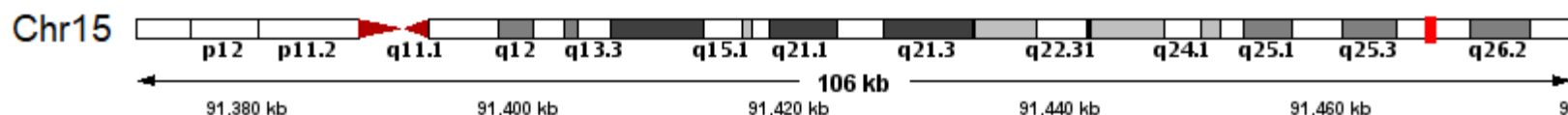
AJ

FAM90A1 L251L, GGA → GCA

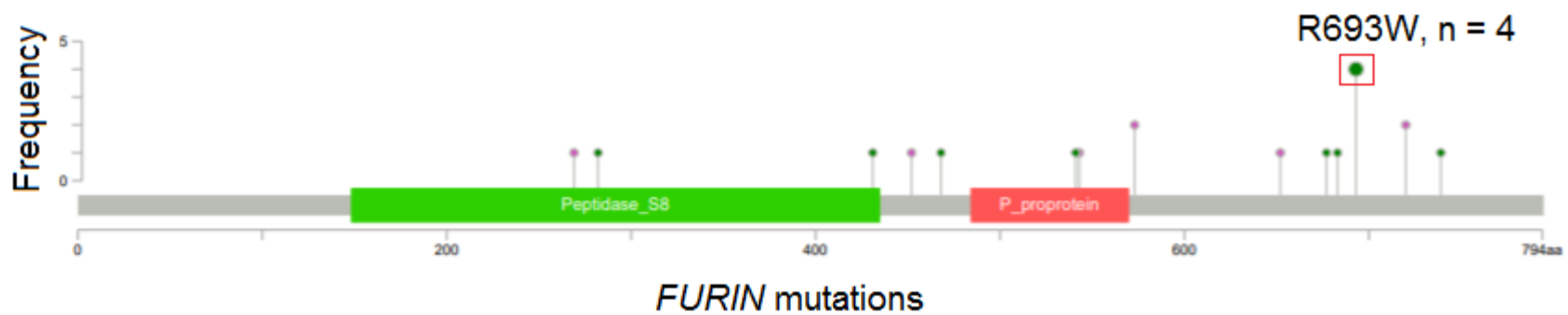
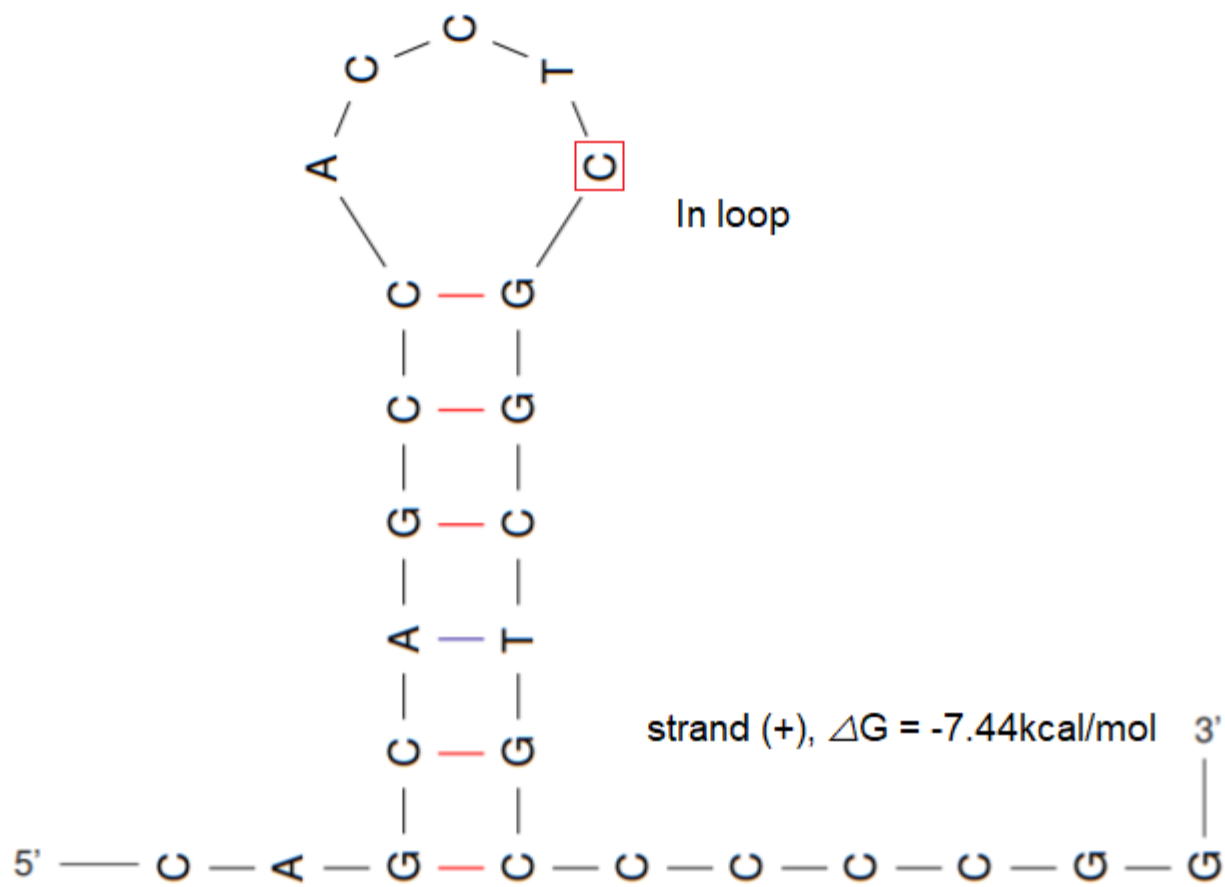


AK

FURIN R693W, TCG → TTG

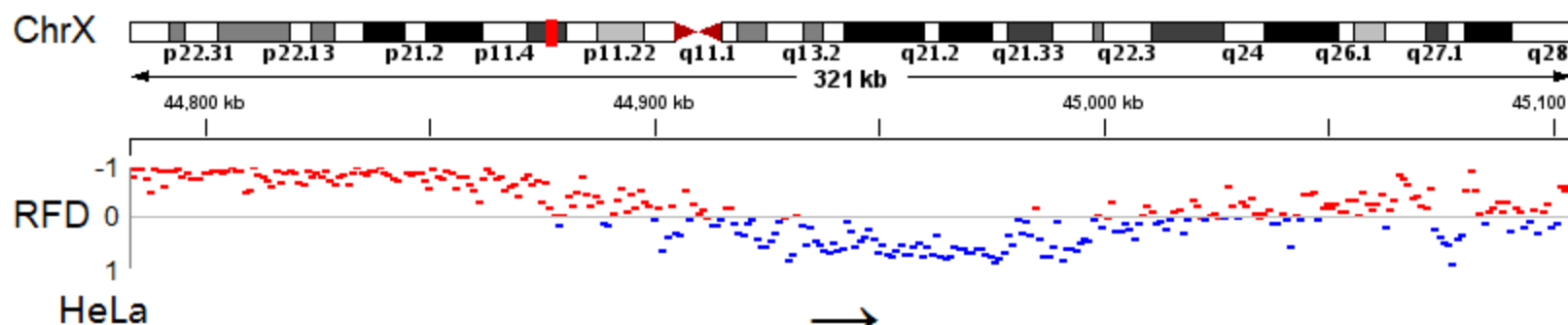


→
FURIN
strand (+)

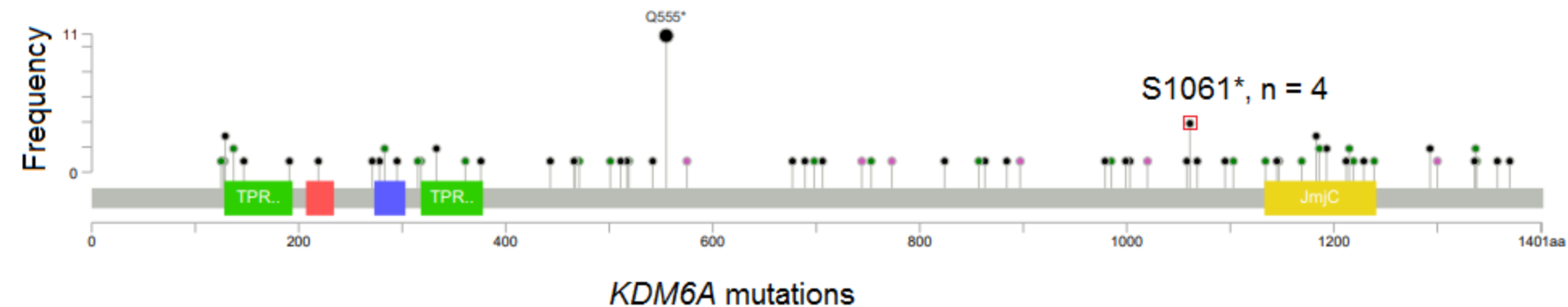
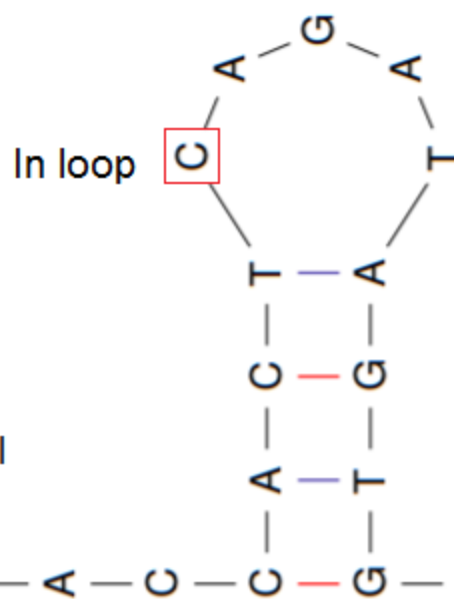


AL

KDM6A S1061*, TCA → TGA

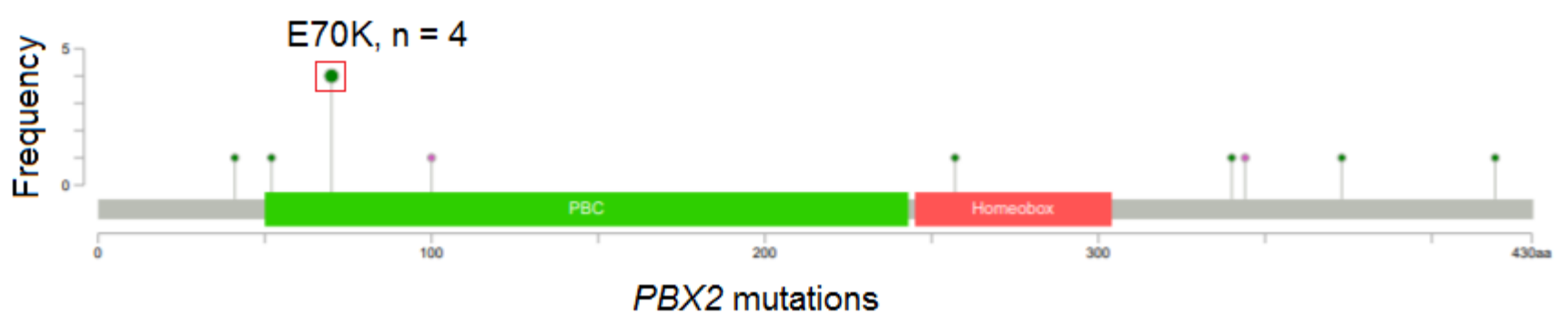
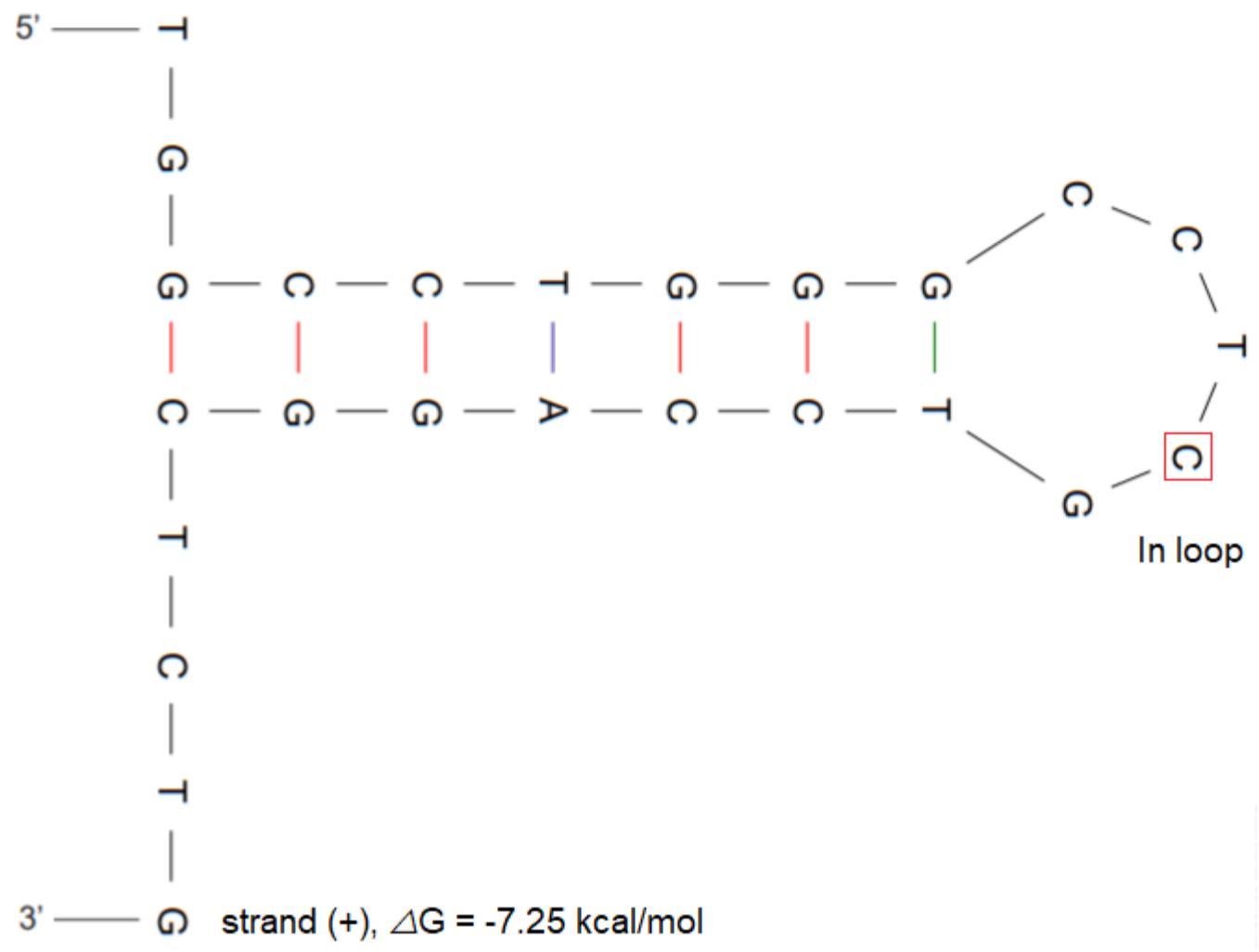
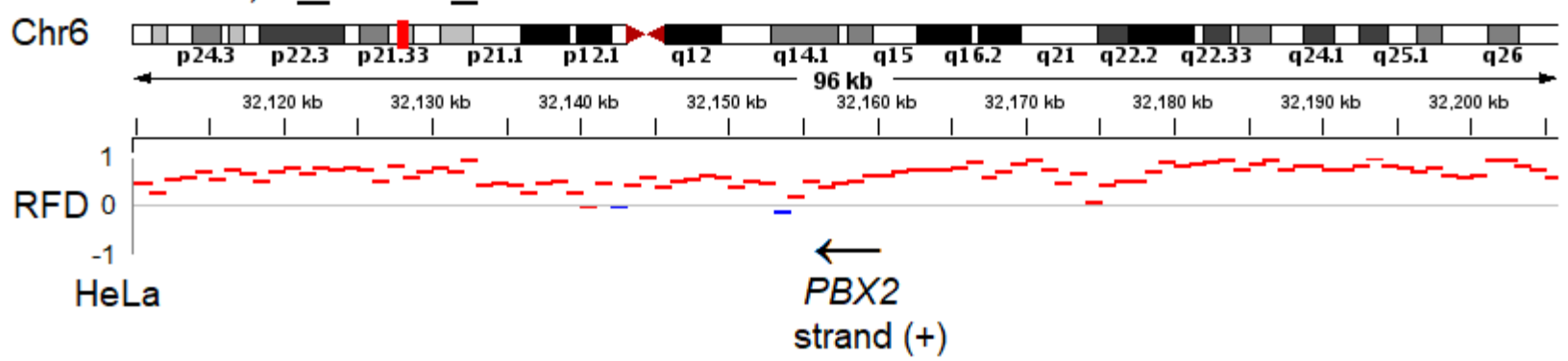


→
KDM6A
strand (+)



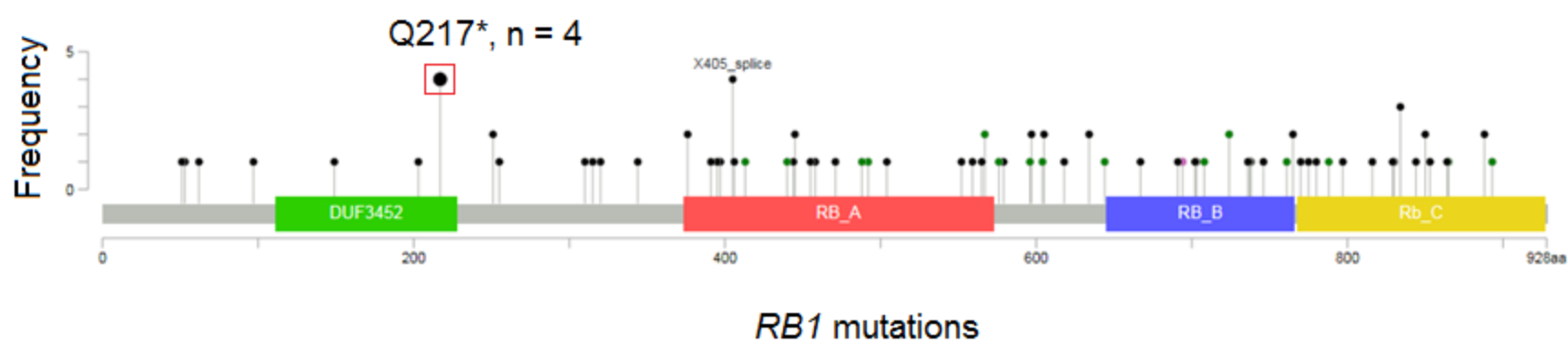
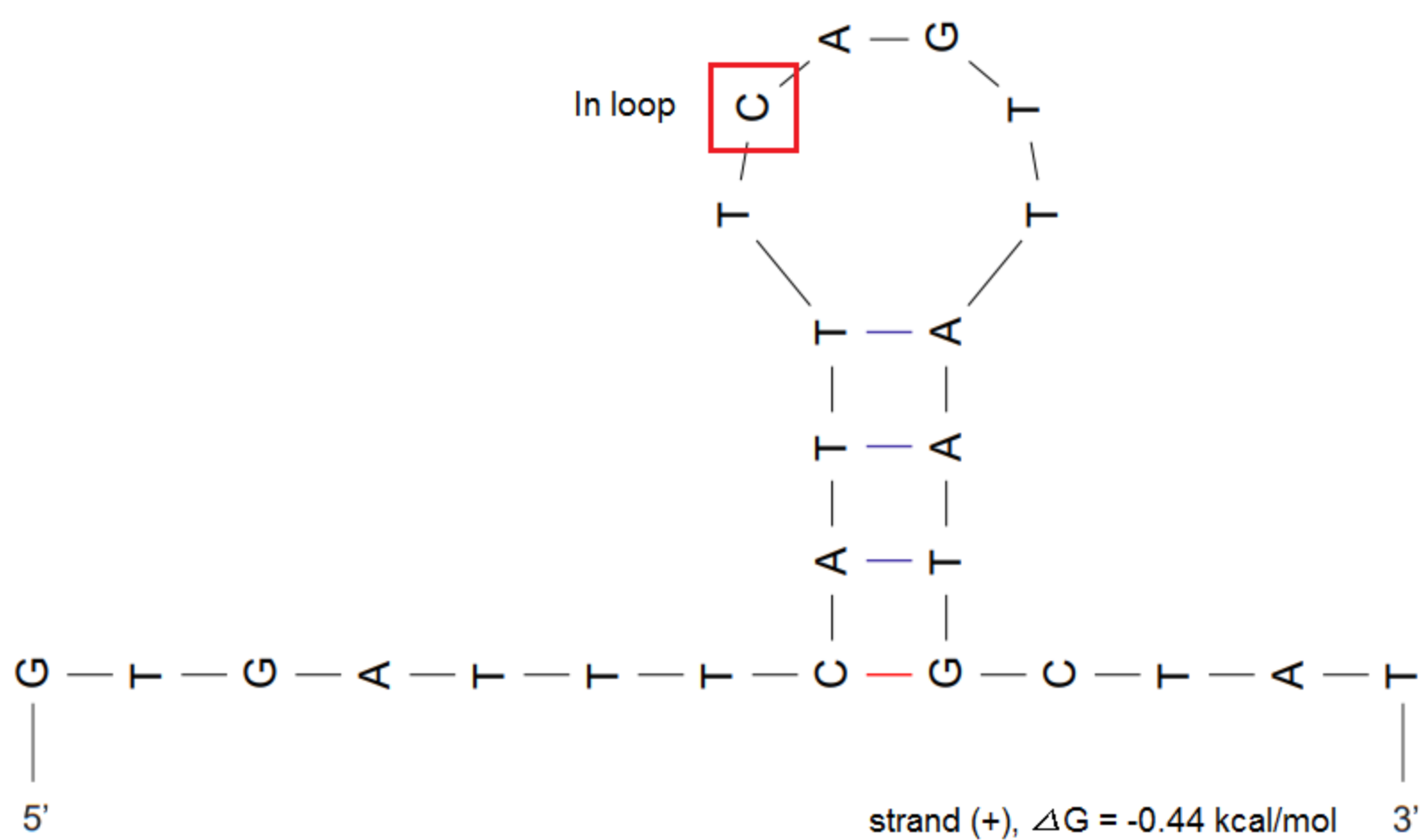
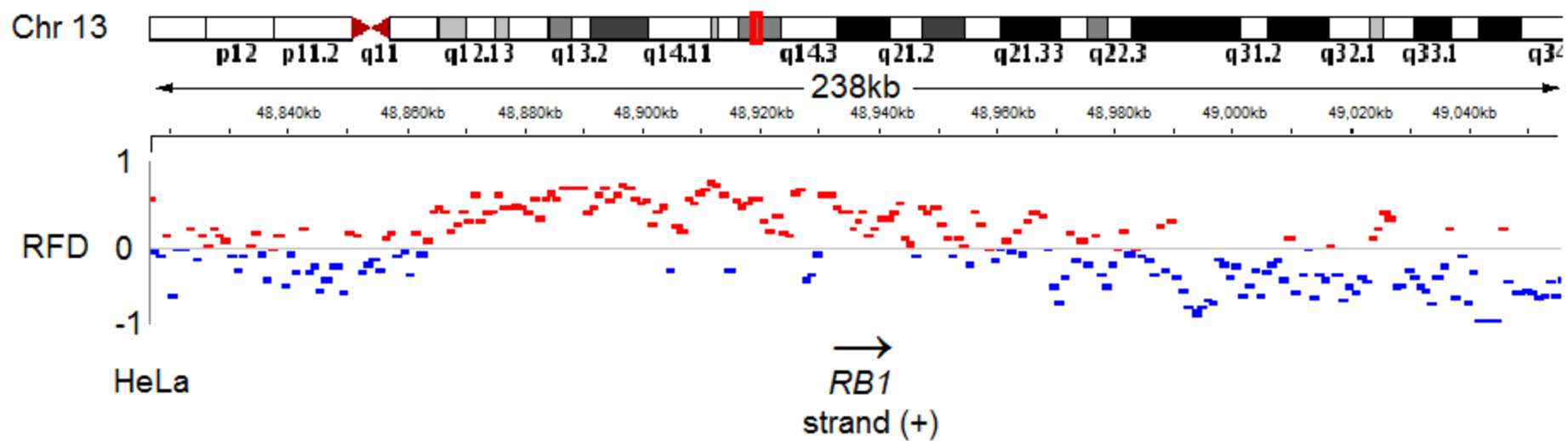
AM

PBX2 E70K, TCG → TTG



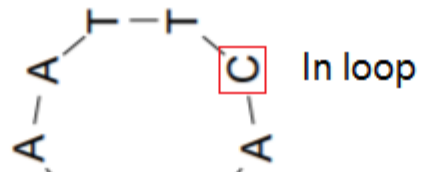
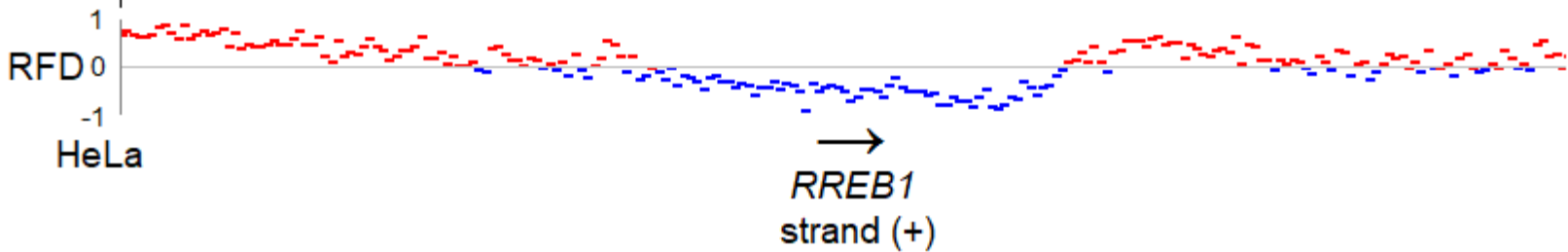
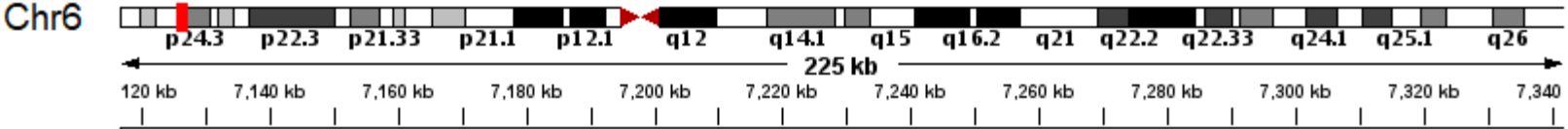
AN

RB1 Q217*, TCA → TTA



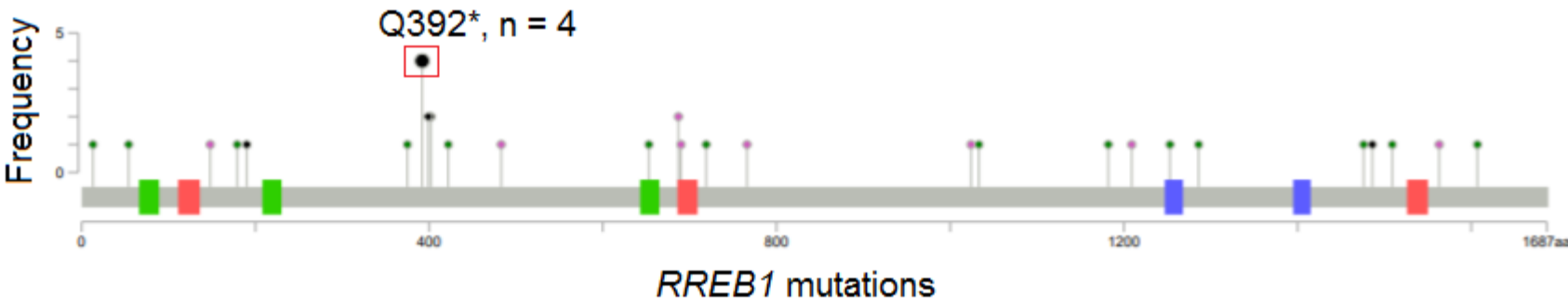
AO

RREB1 Q392*, TCA → TIA

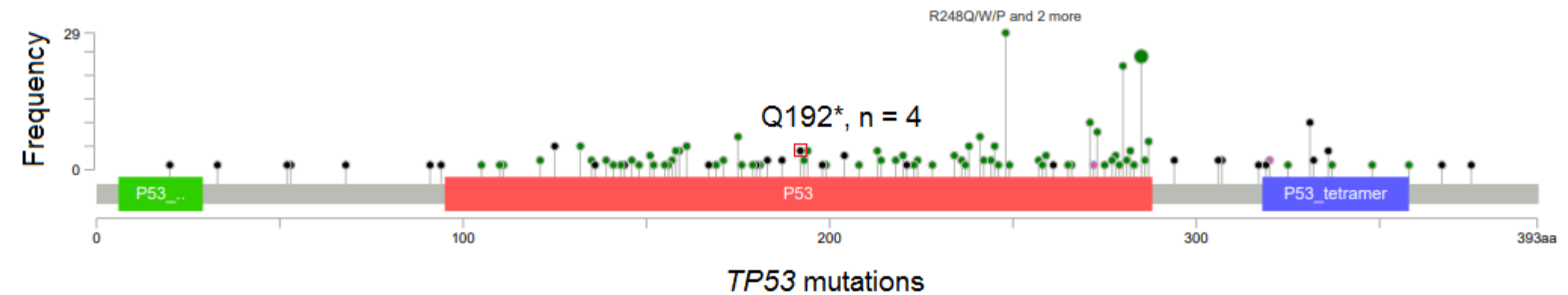
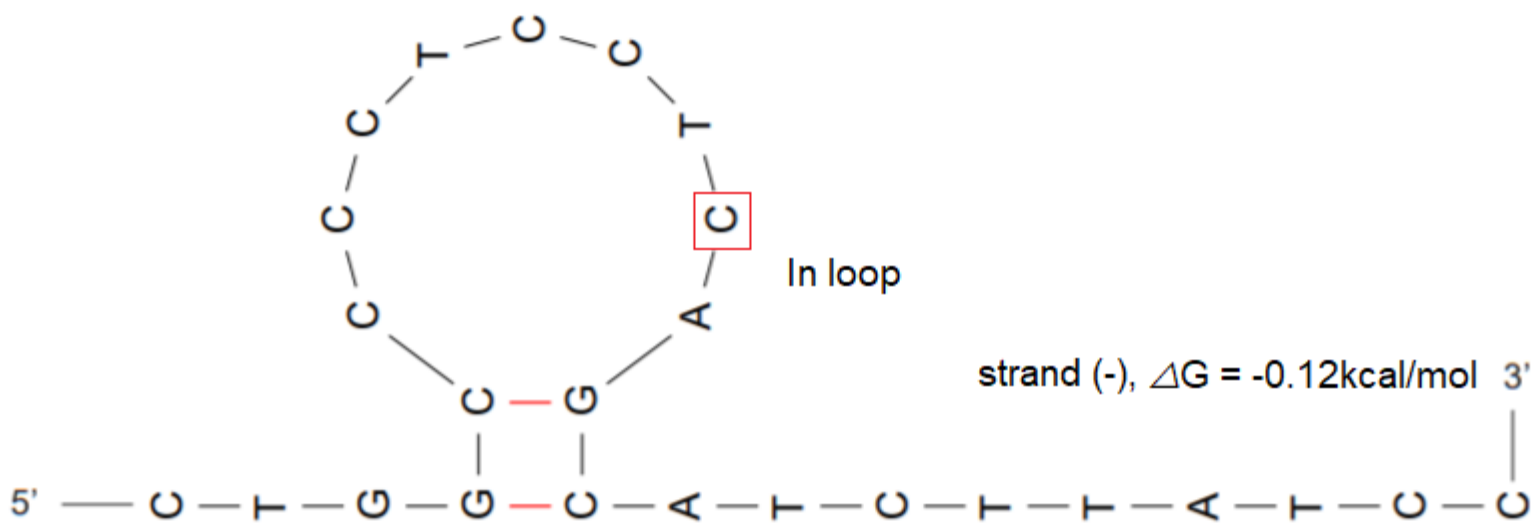
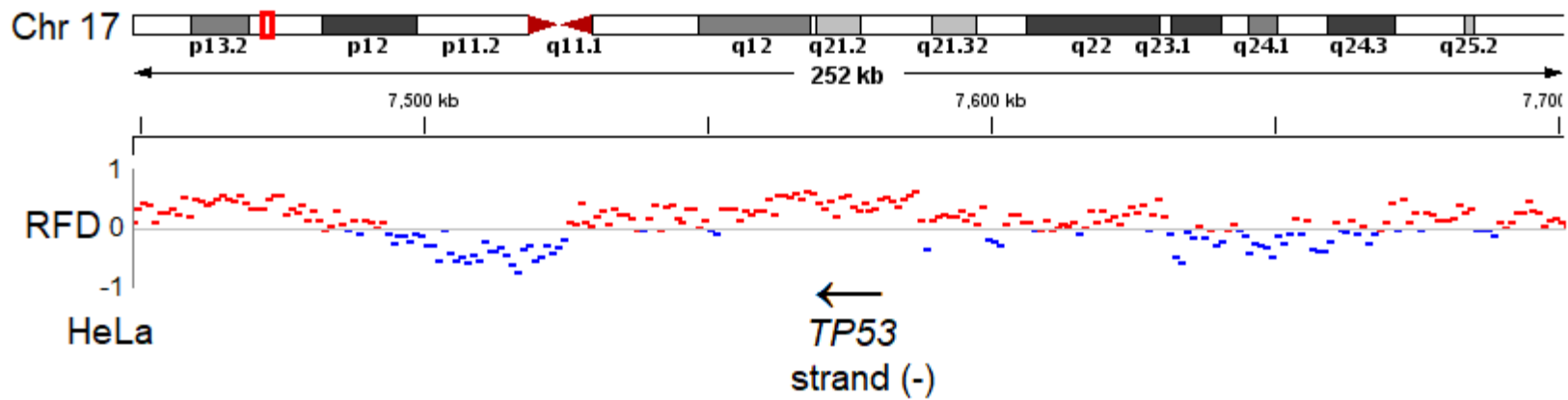


strand (+), $\Delta G = -0.32 \text{ kcal/mol}$ 3'

5' — A — A — C — C — A — G — G — C — T — C — C — A — G — A — C — A — C — 3'



TP53 Q192*, TGA → TAA



AQ

TTC23L Q263Q, AGA → AAA

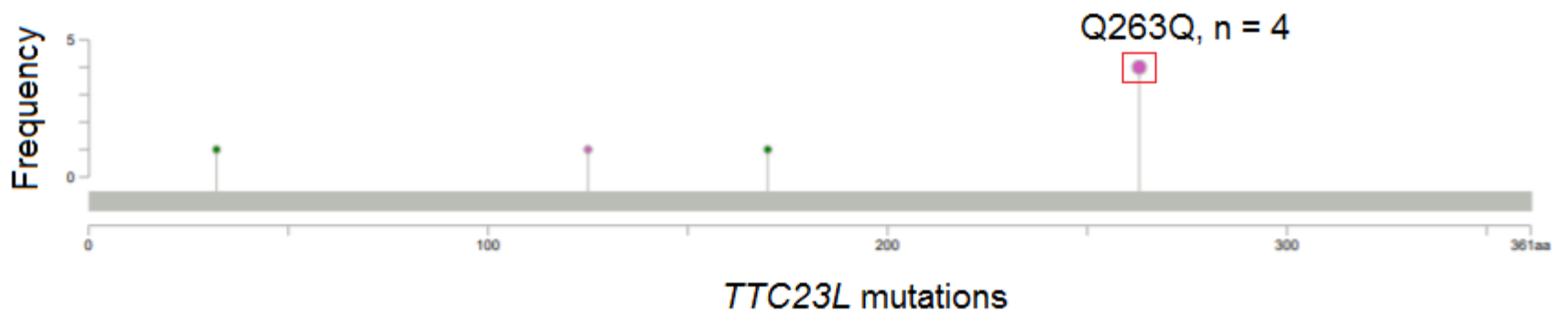
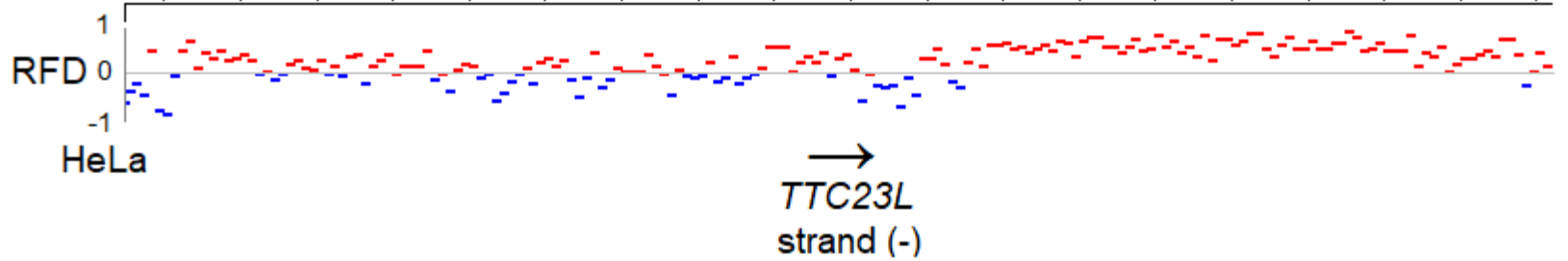
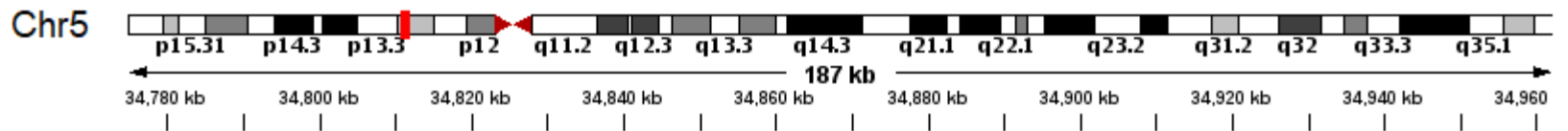
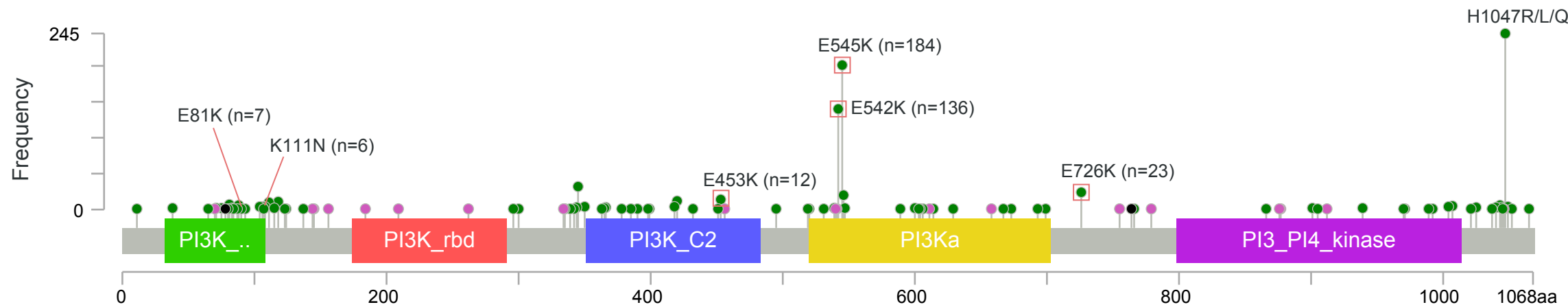
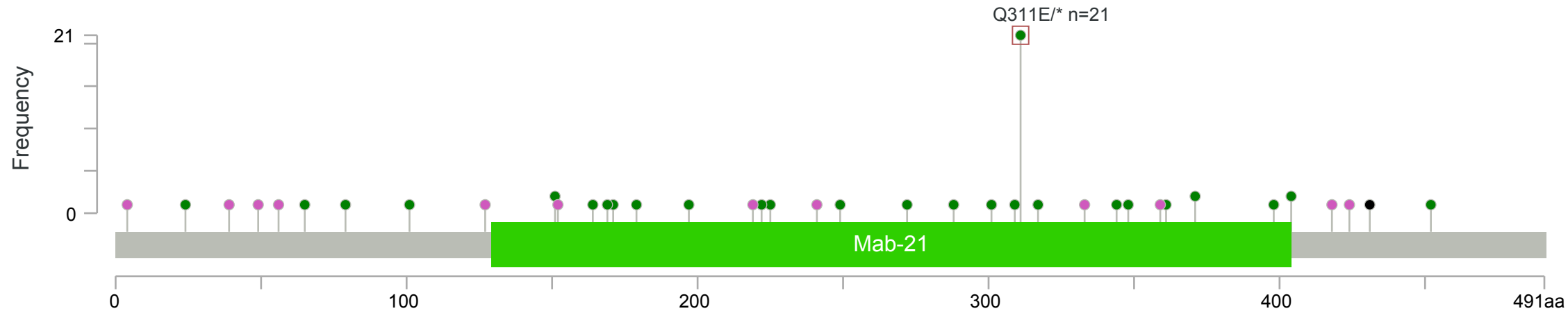


Fig. S7
(Including 55 subfigures)

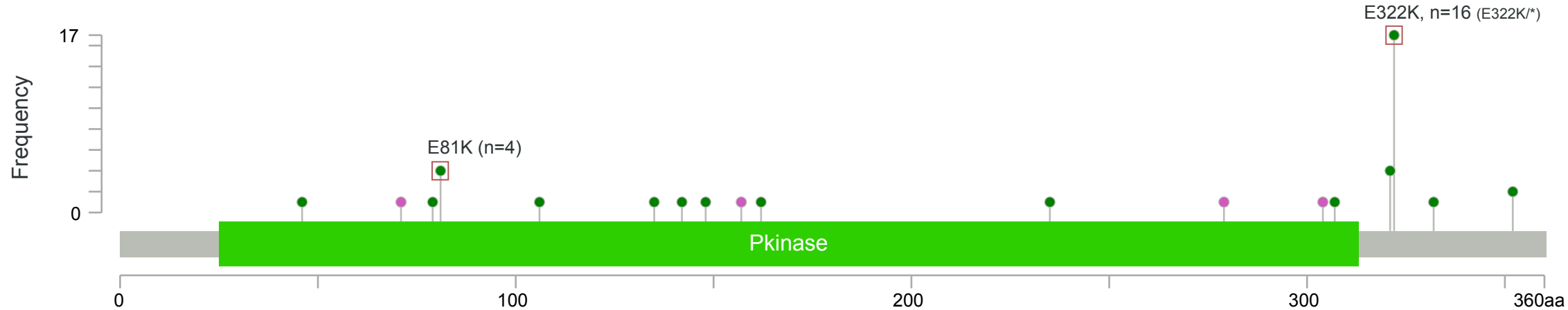
PIK3CA mutations



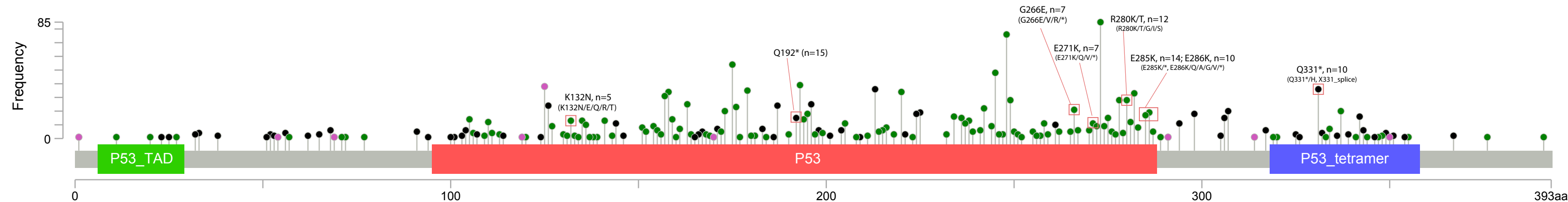
MB21D2 mutations



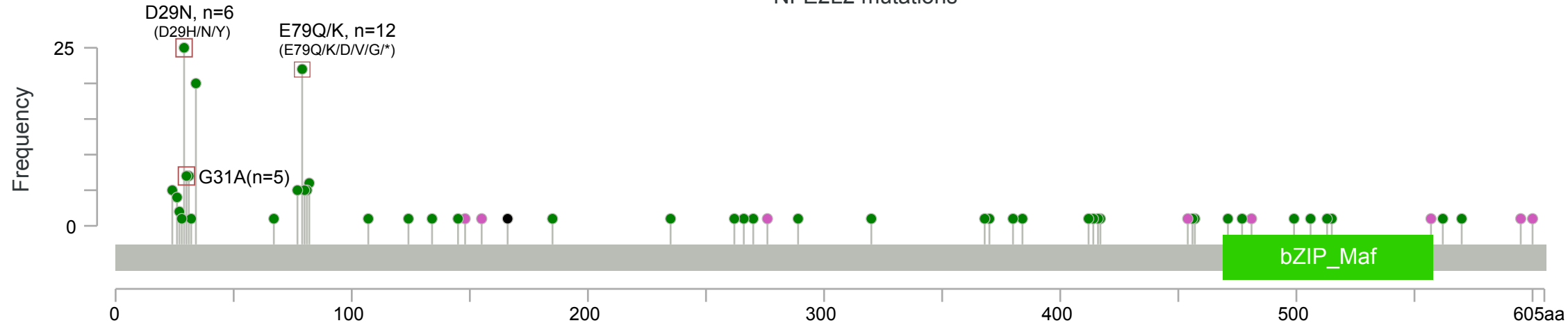
MAPK1 mutations



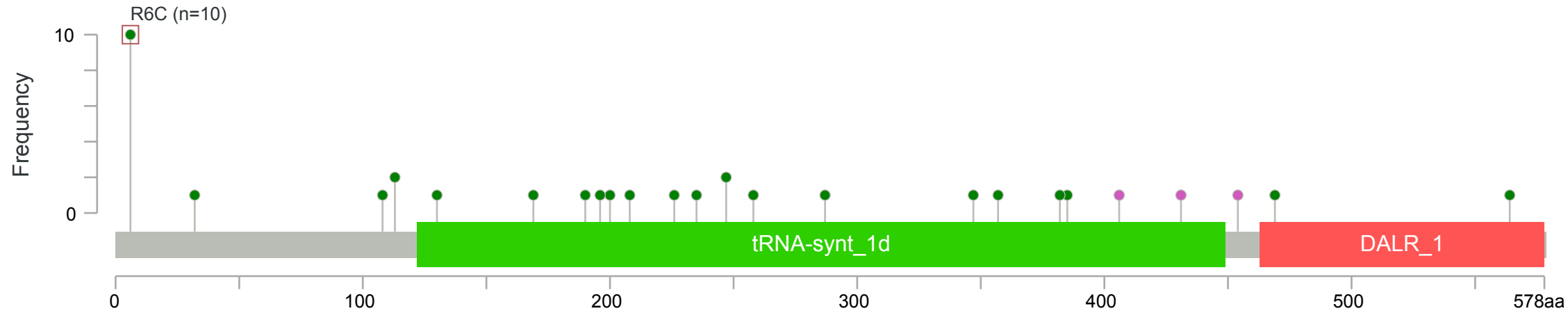
TP53 mutations



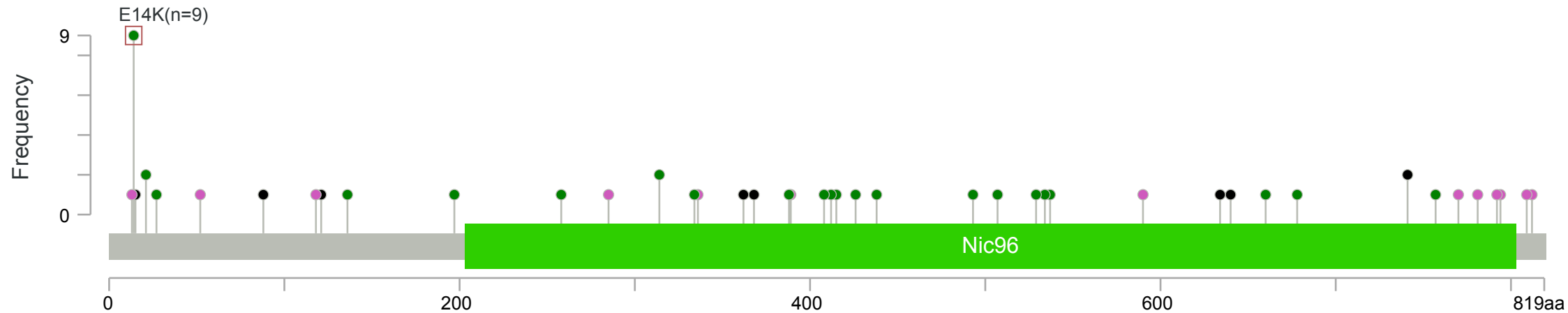
NFE2L2 mutations



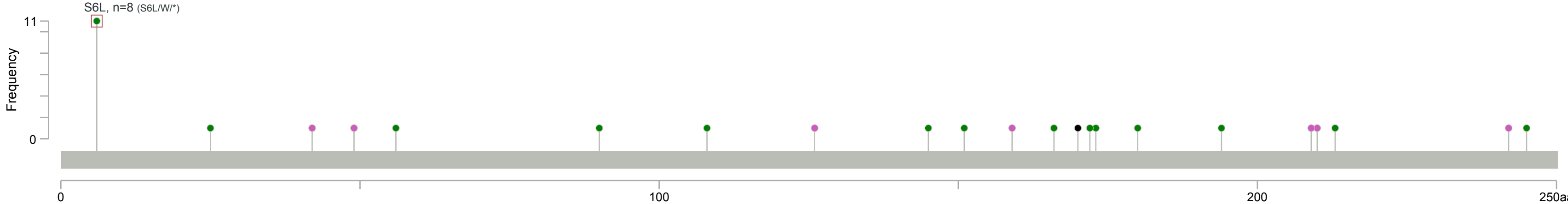
RARS2 mutations



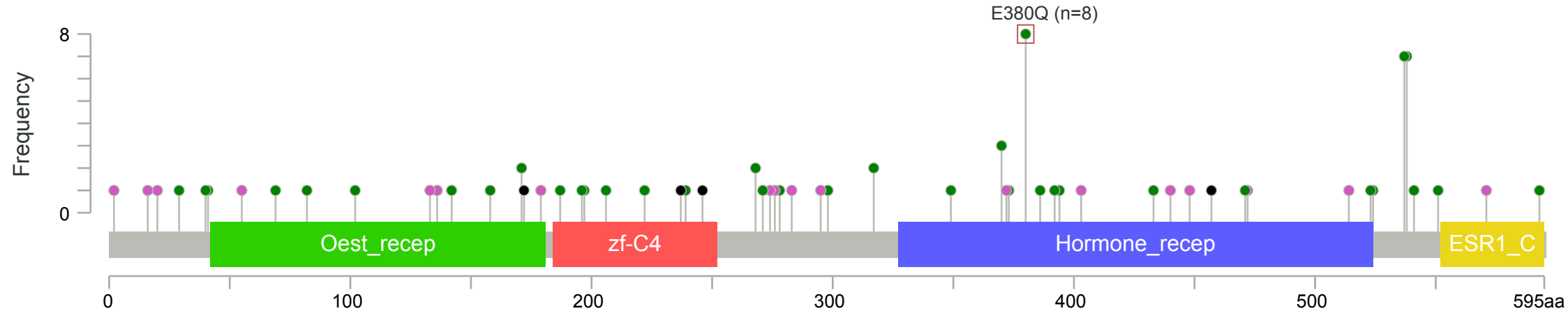
NUP93 mutations



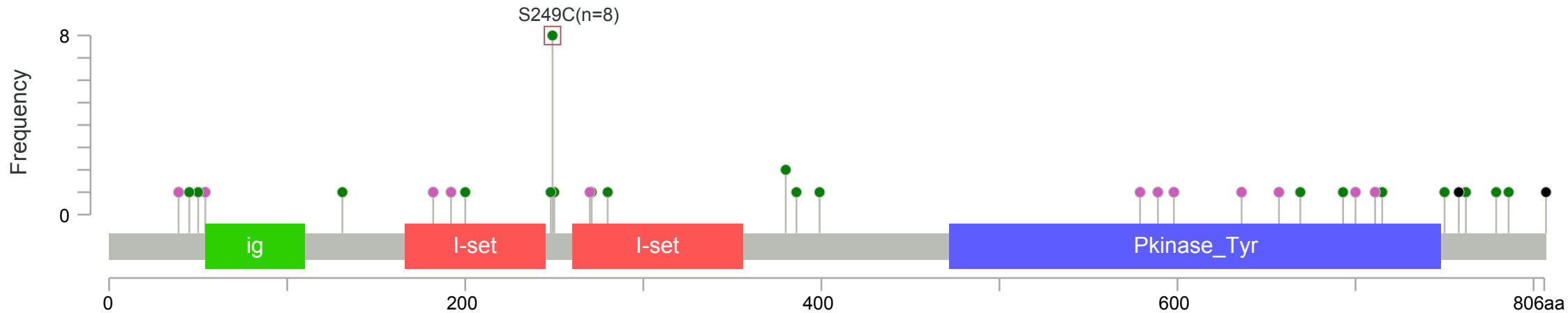
C3orf70 mutations



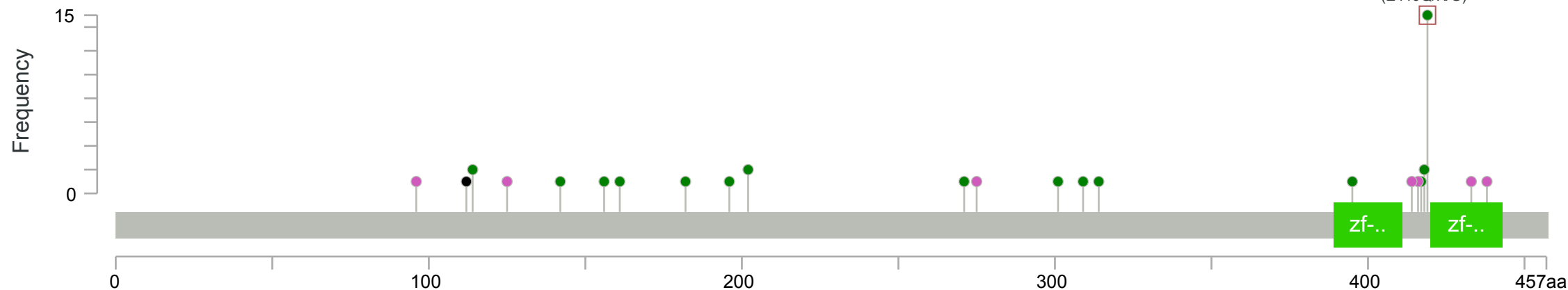
ESR1 mutations



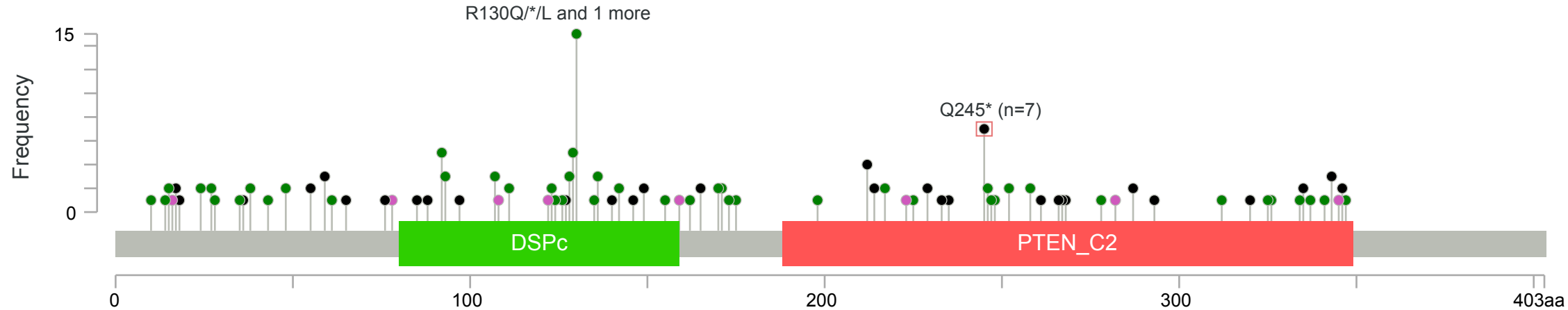
FGFR3 mutations



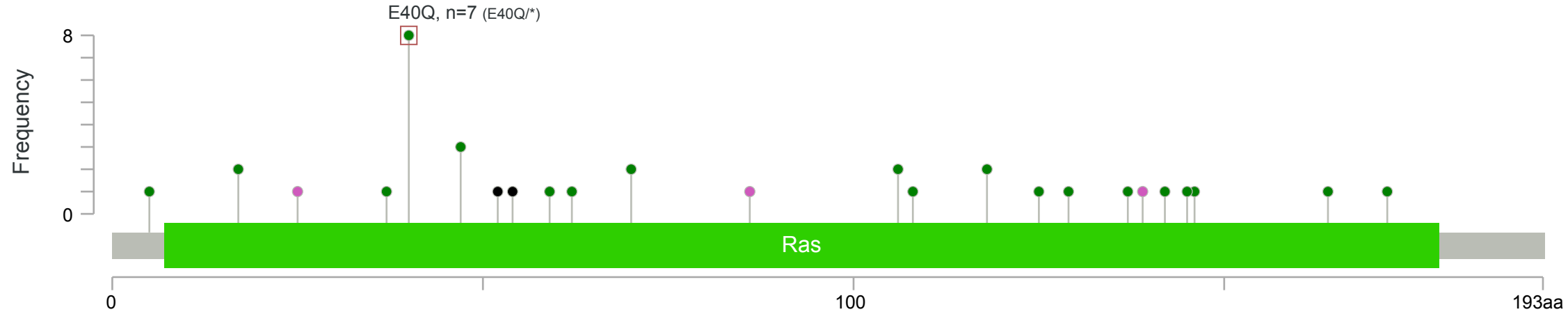
KLF5 mutations



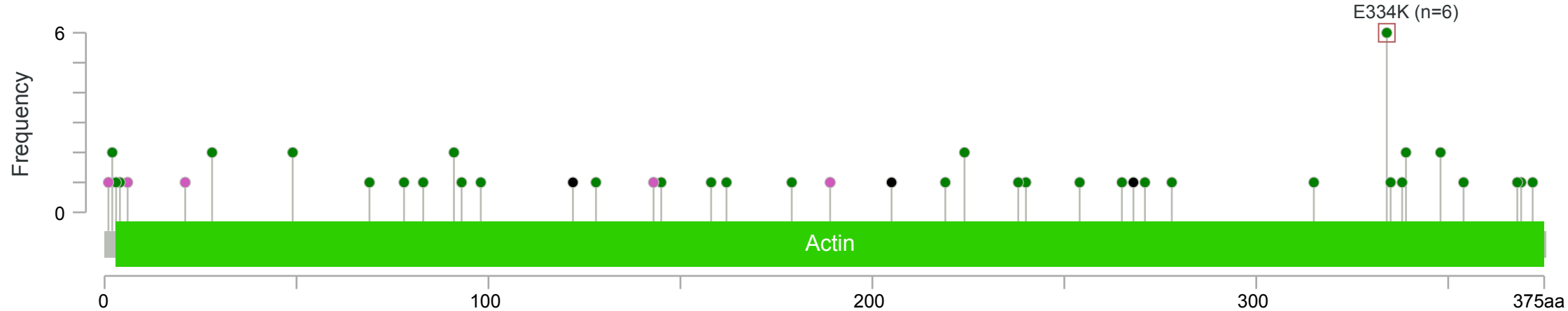
PTEN mutations



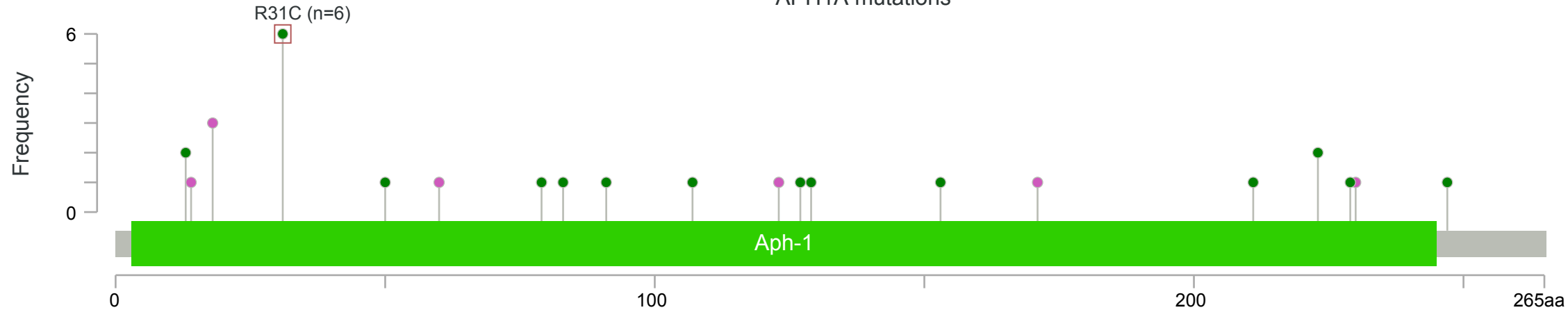
RHOA mutations



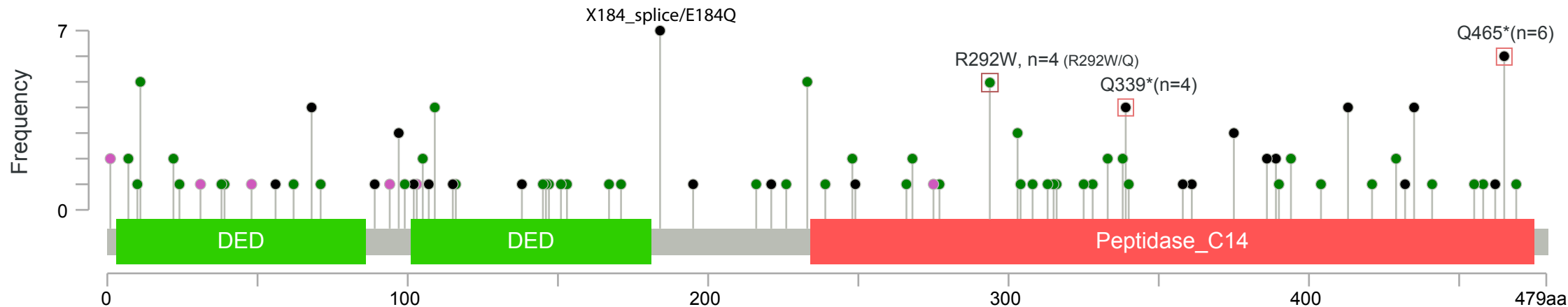
ACTB mutations



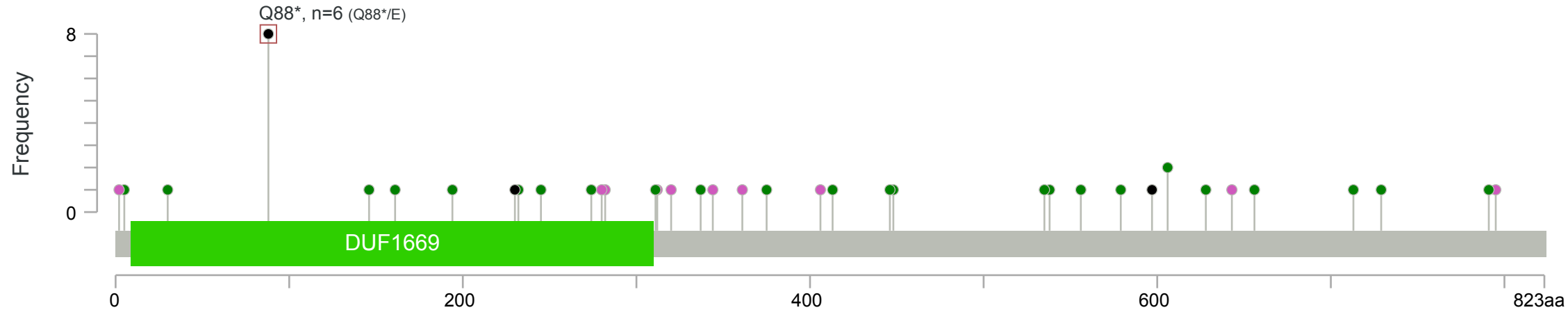
APH1A mutations



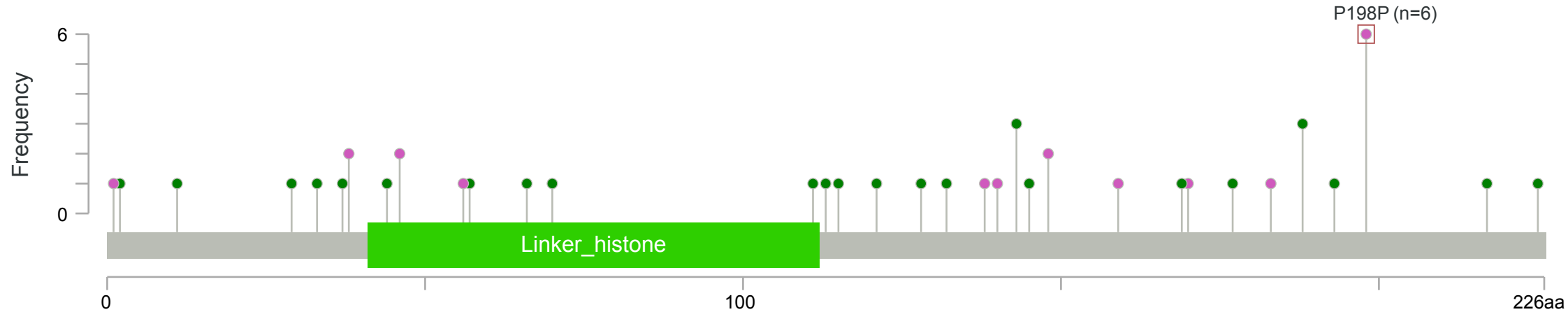
CASP8 mutations



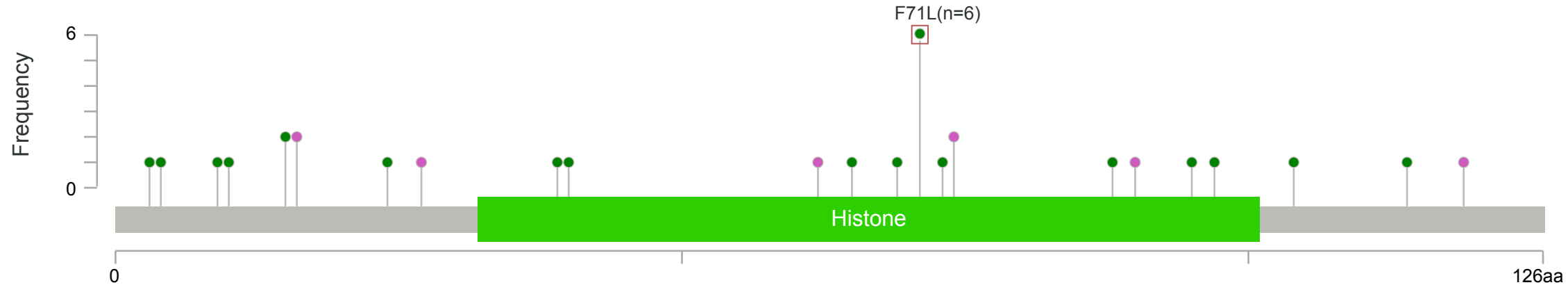
FAM83G mutations



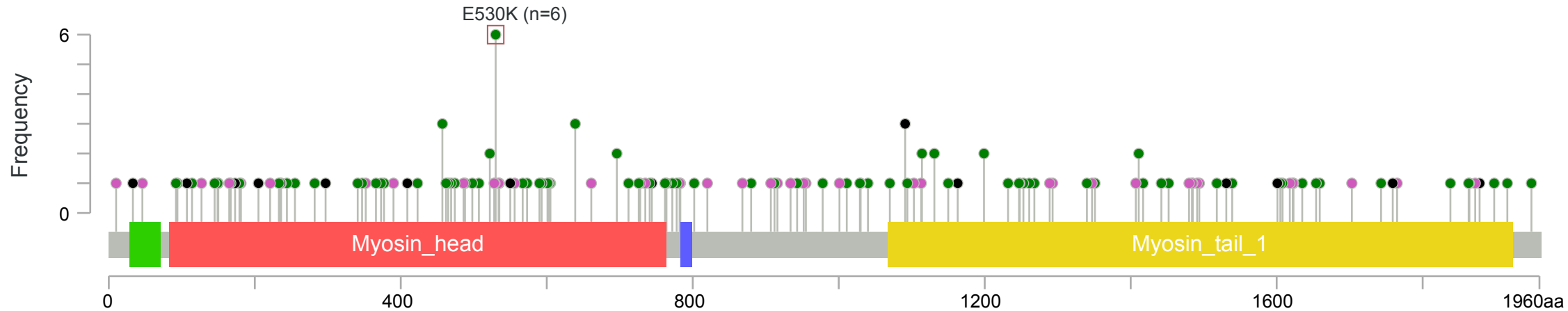
HIST1H1B mutations



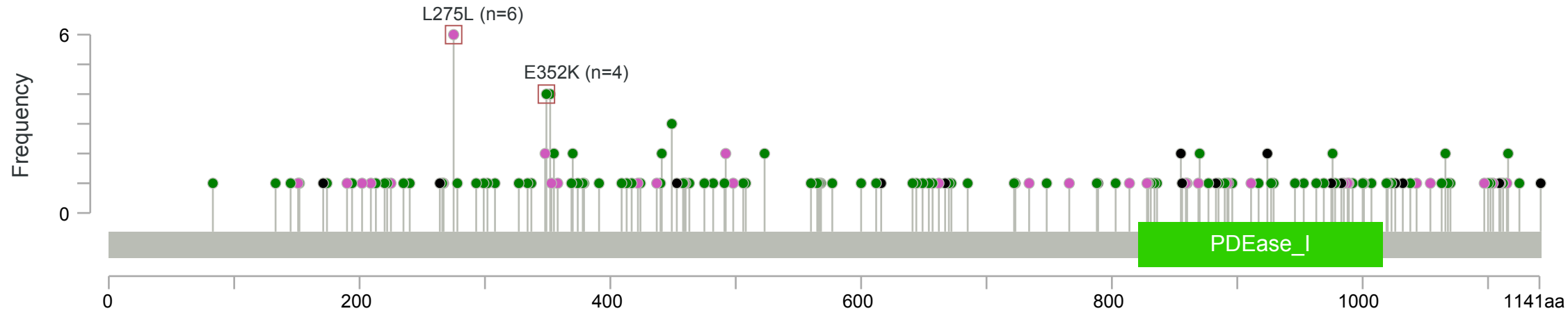
HIST2H2BE mutations



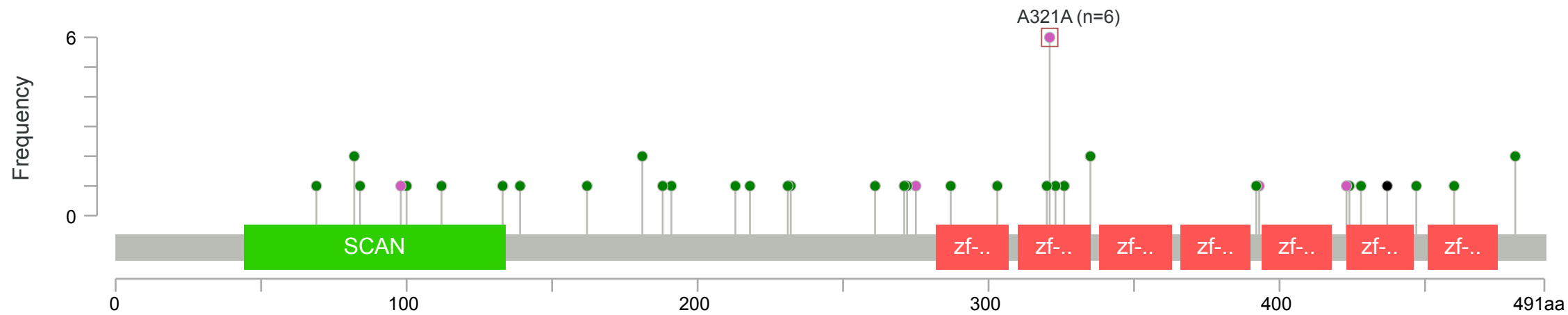
MYH9 mutations



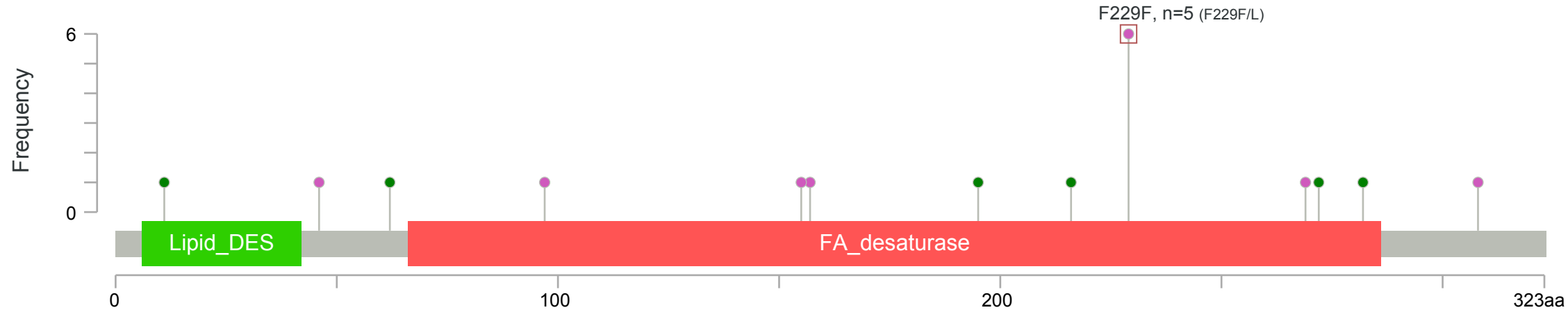
PDE3A mutations



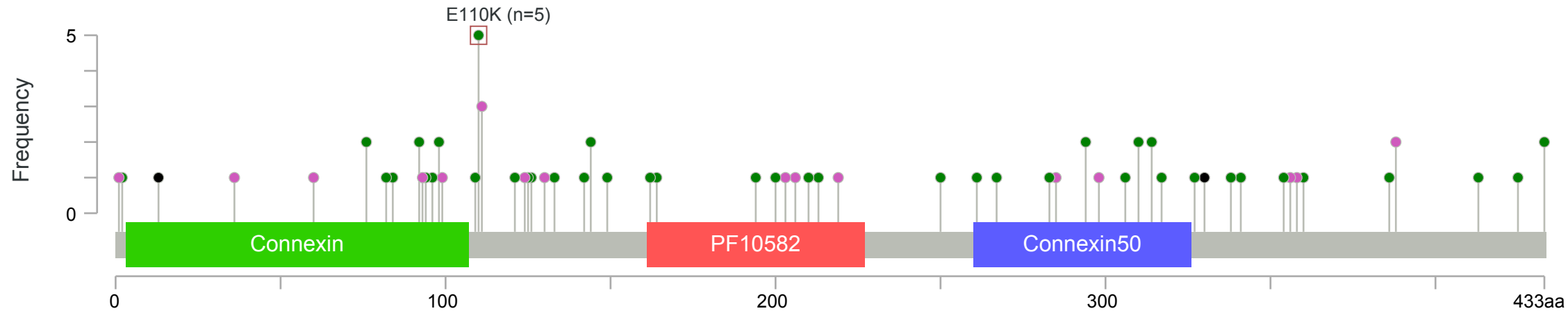
ZSCAN22 mutations



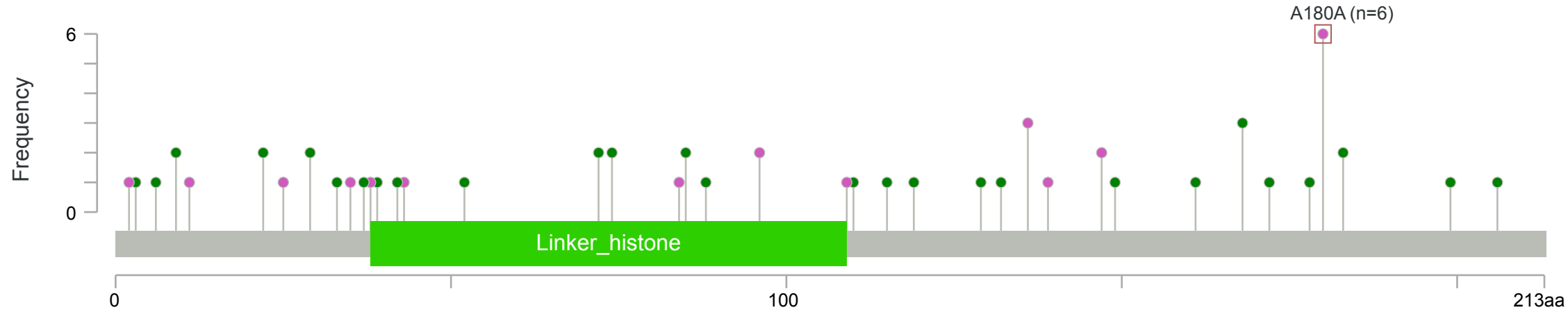
DEGS2 mutations



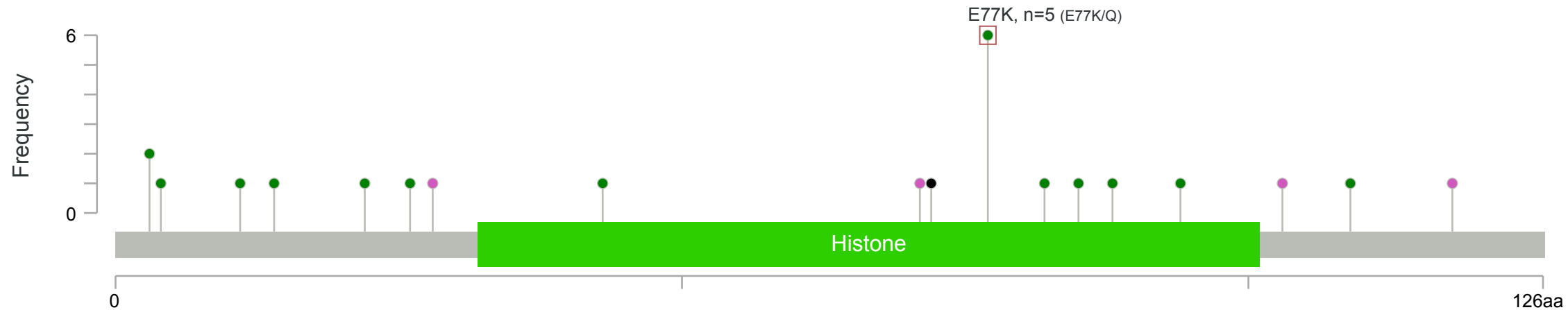
GJA8 mutations



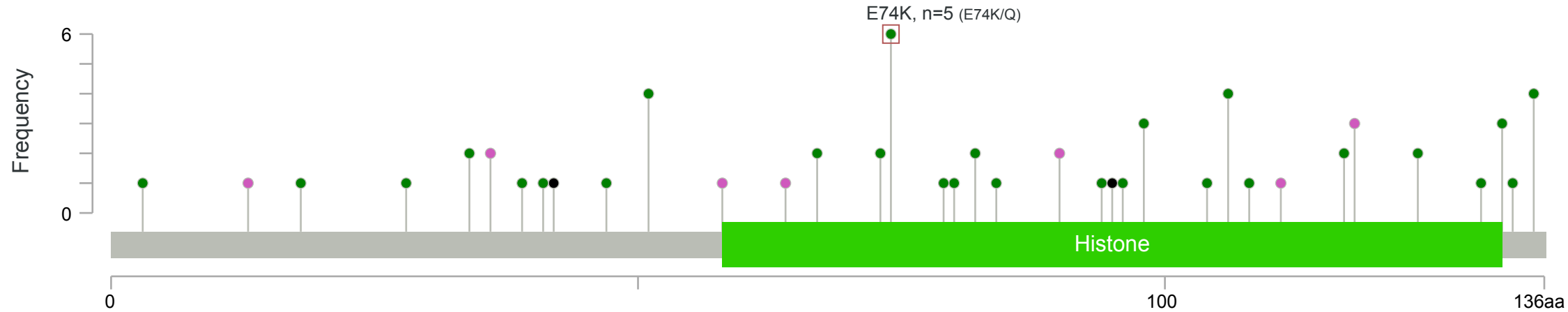
HIST1H1C mutations



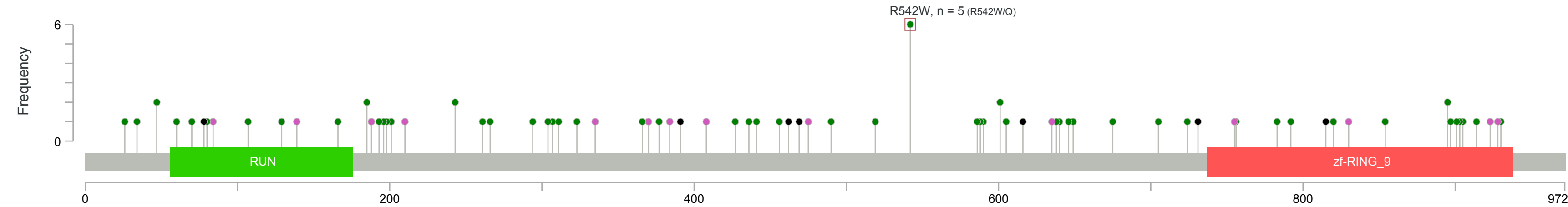
HIST1H2BF mutations



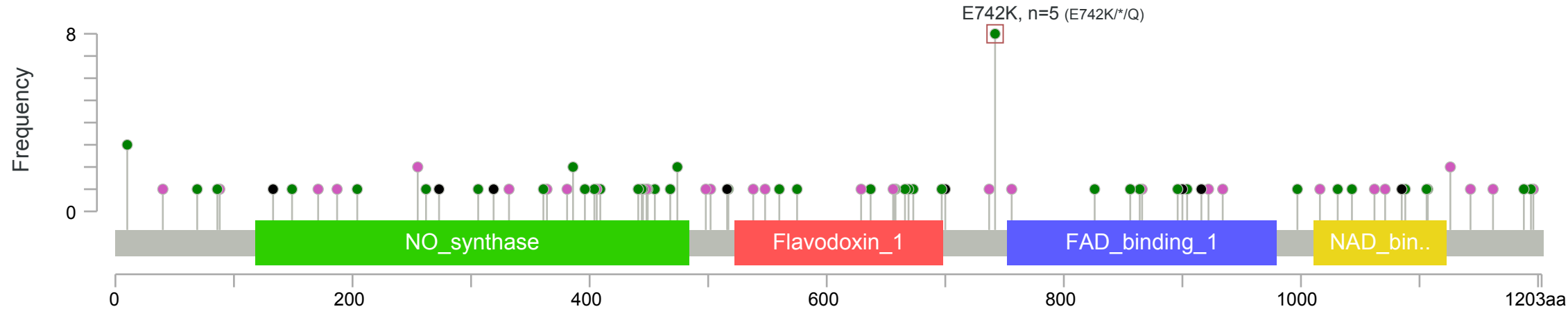
HIST1H3B mutations



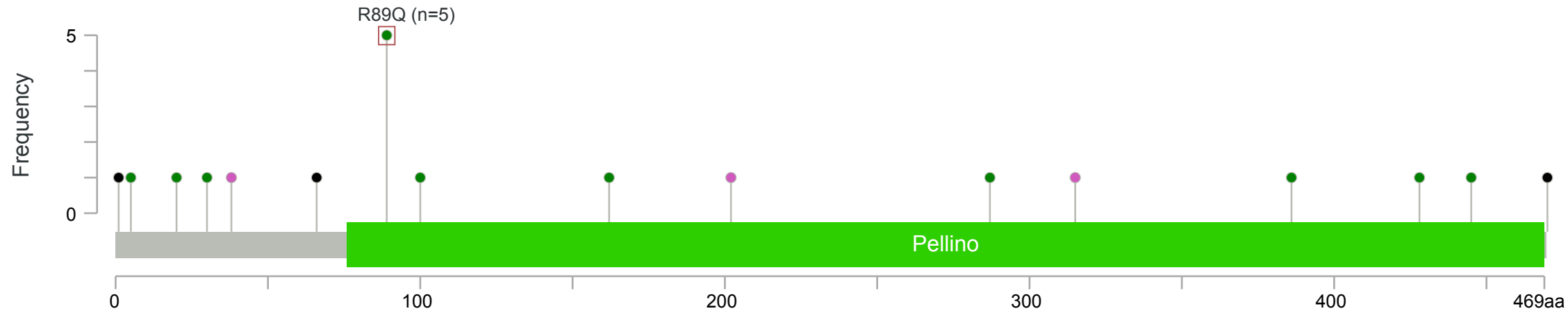
RUBCN mutations



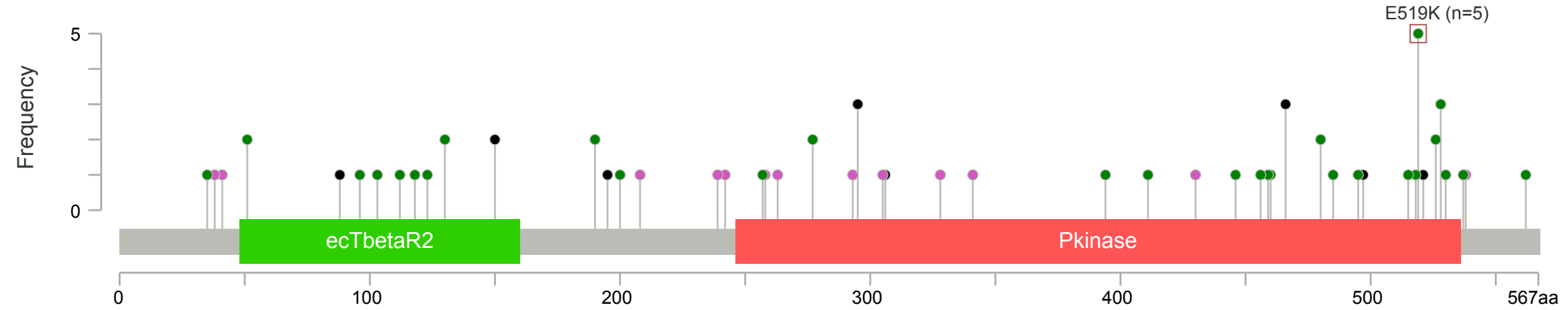
NOS3 mutations



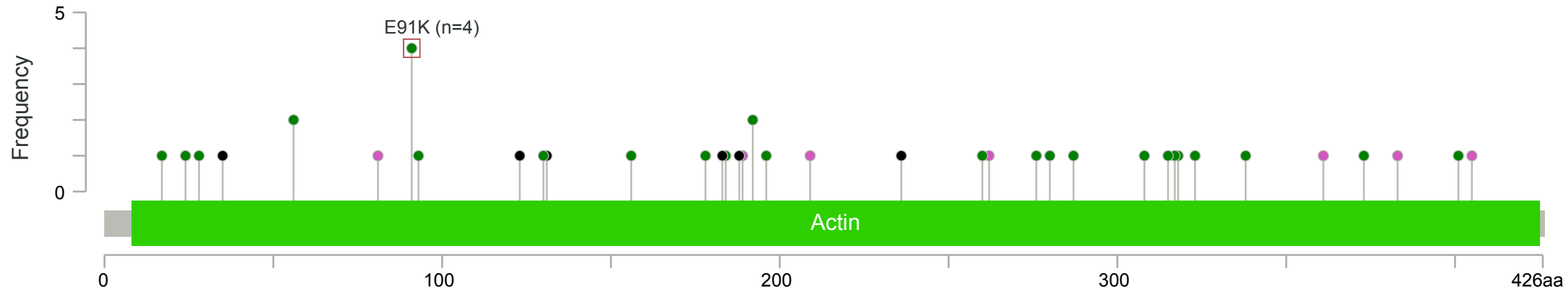
PELI3 mutations



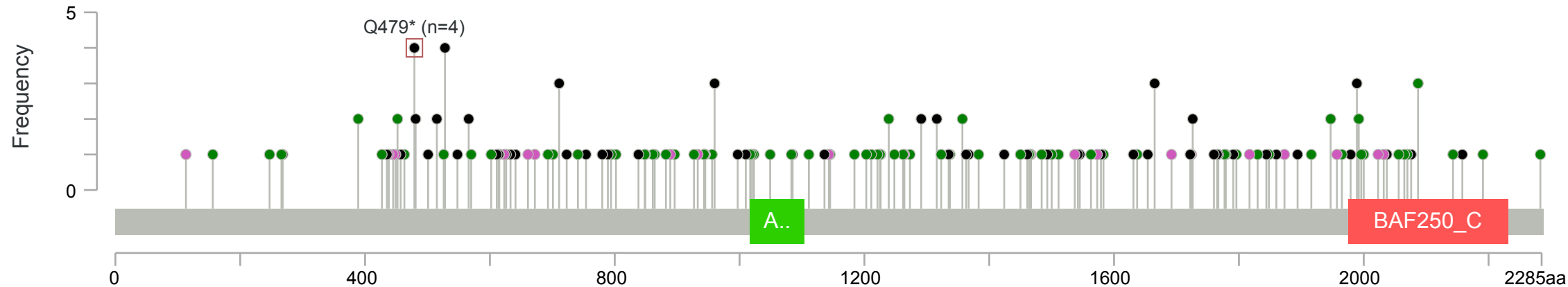
TGFBR2 mutations



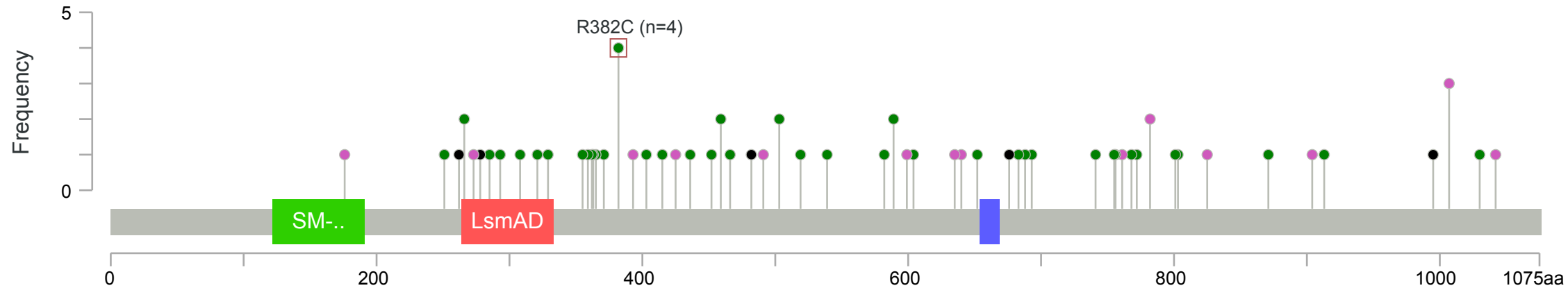
ACTL6B mutations



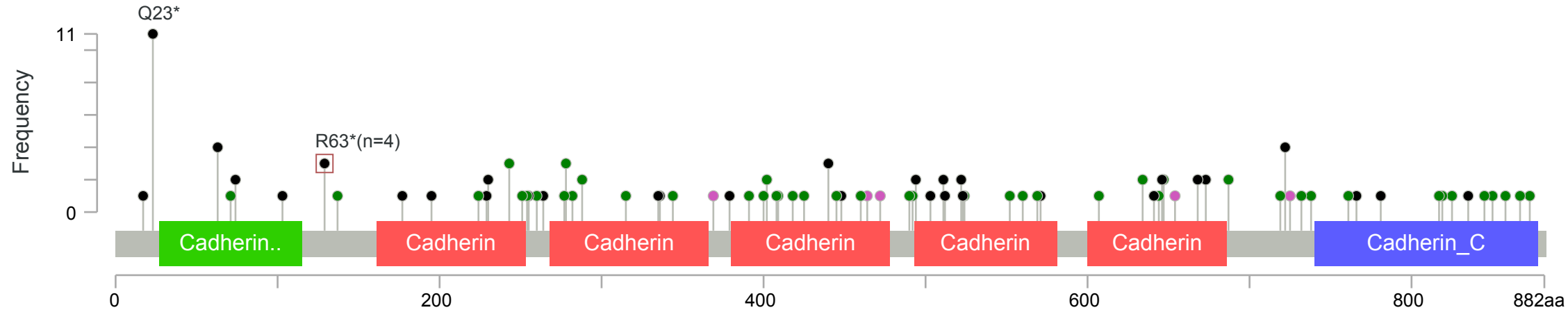
ARID1A mutations



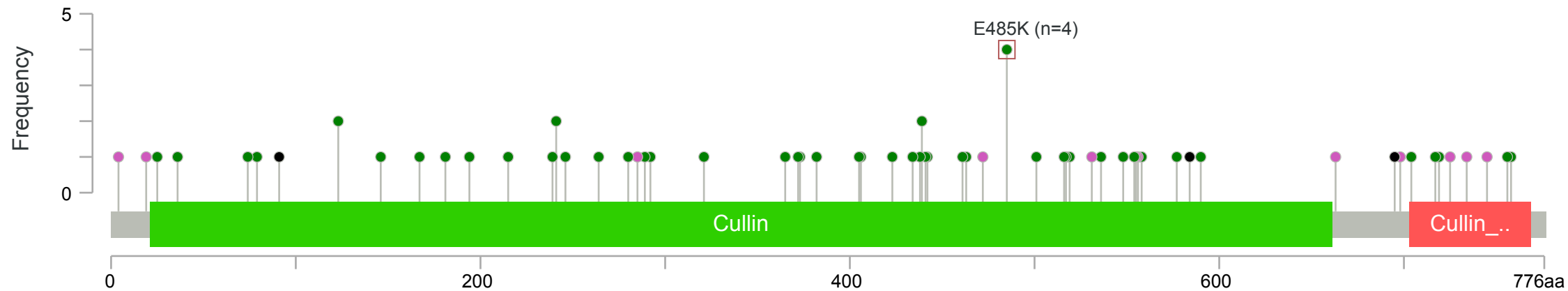
ATXN2L mutations



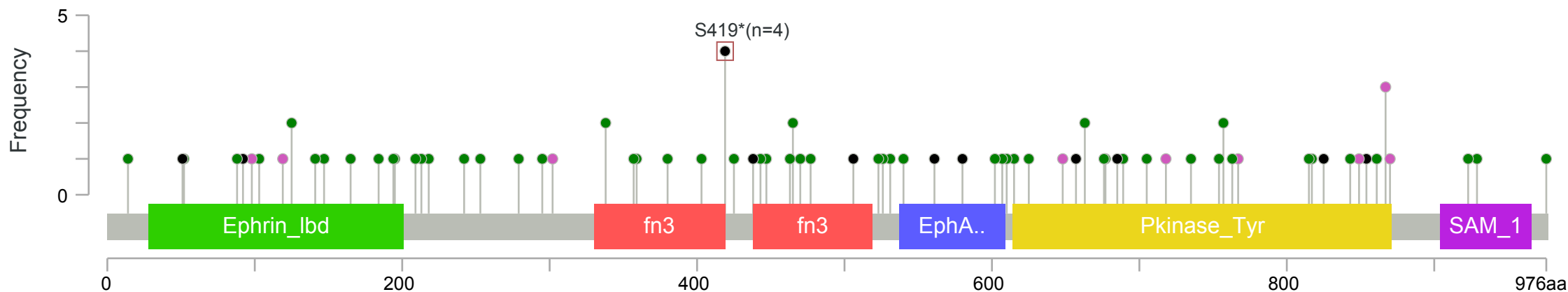
CDH1 mutations



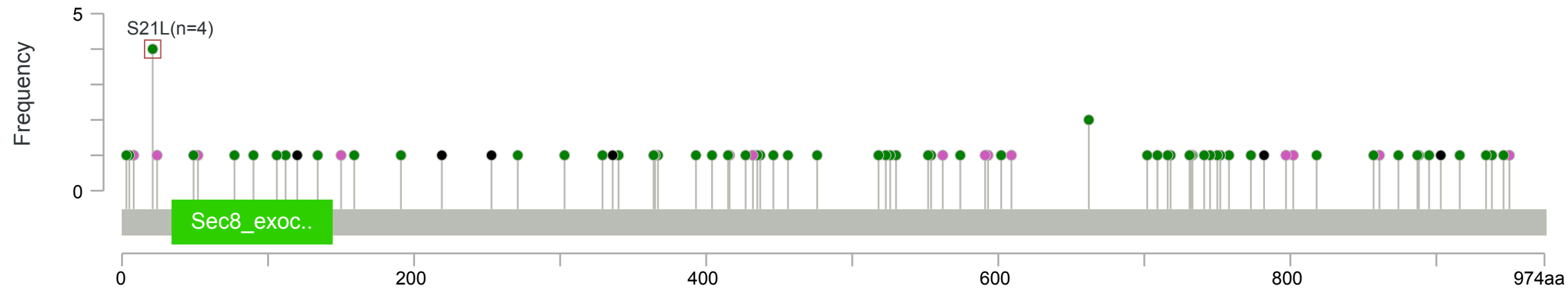
CUL1 mutations



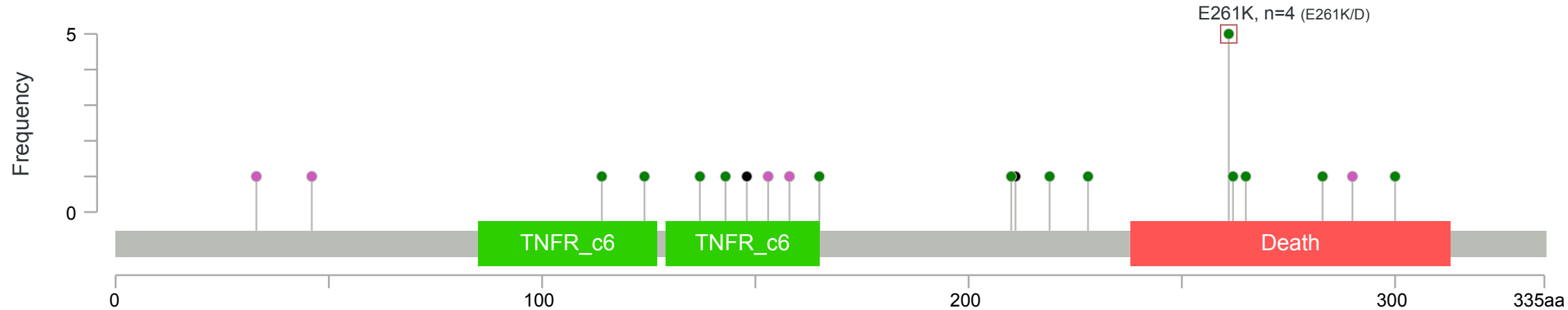
EPHA2 mutations



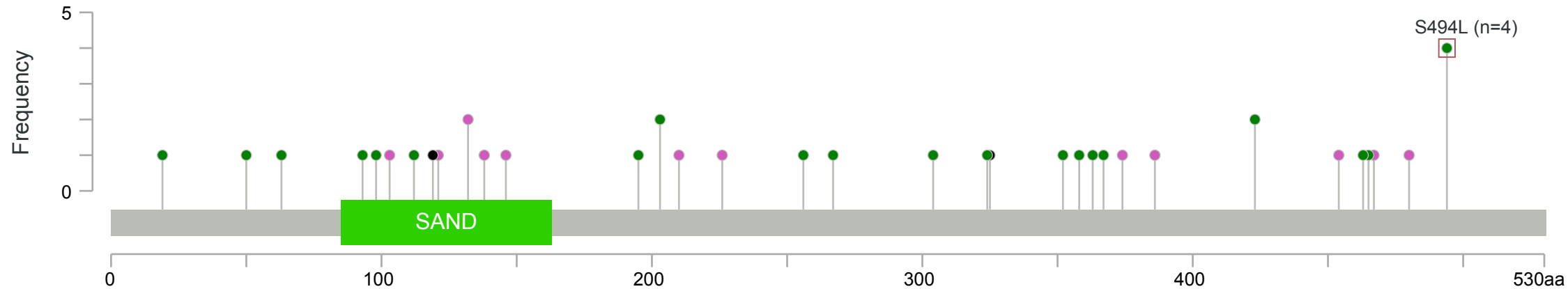
EXOC4 mutations



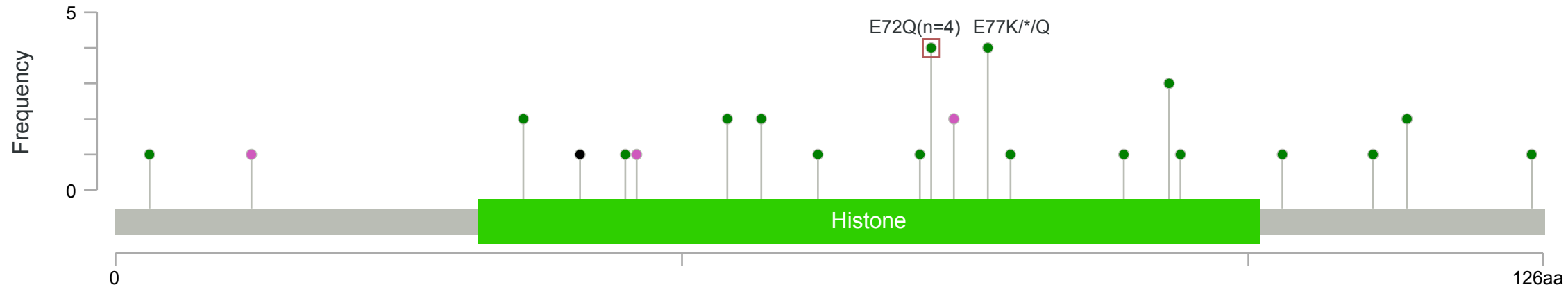
FAS mutations



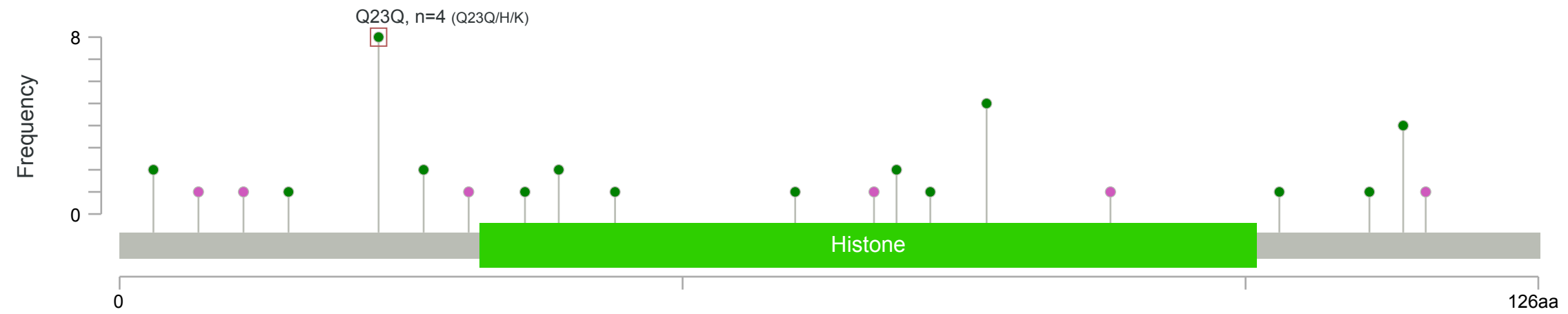
GMEB2 mutations



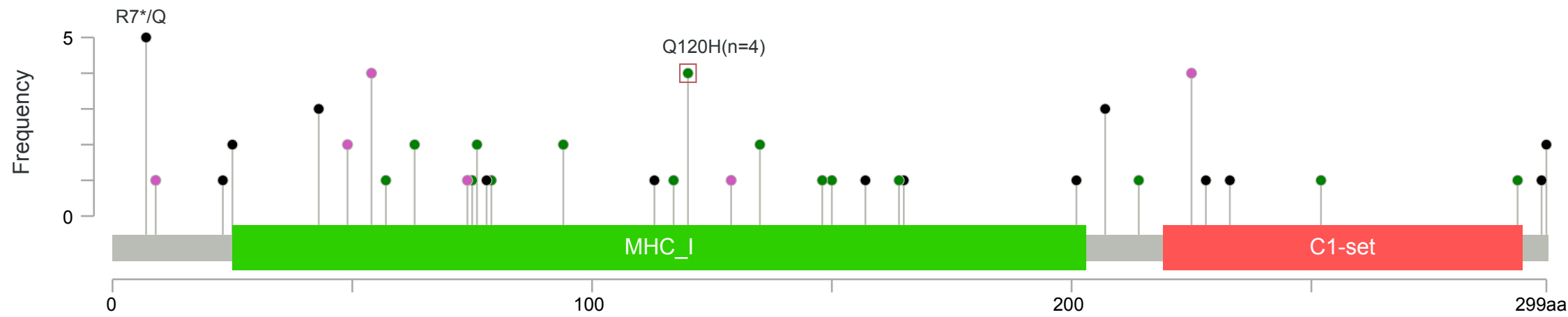
HIST1H2BC mutations



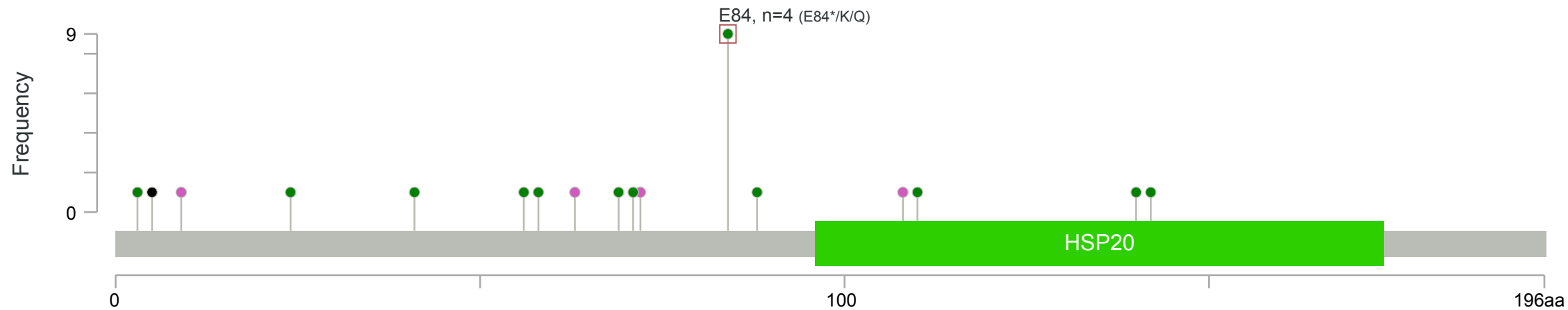
HIST1H2BH mutations



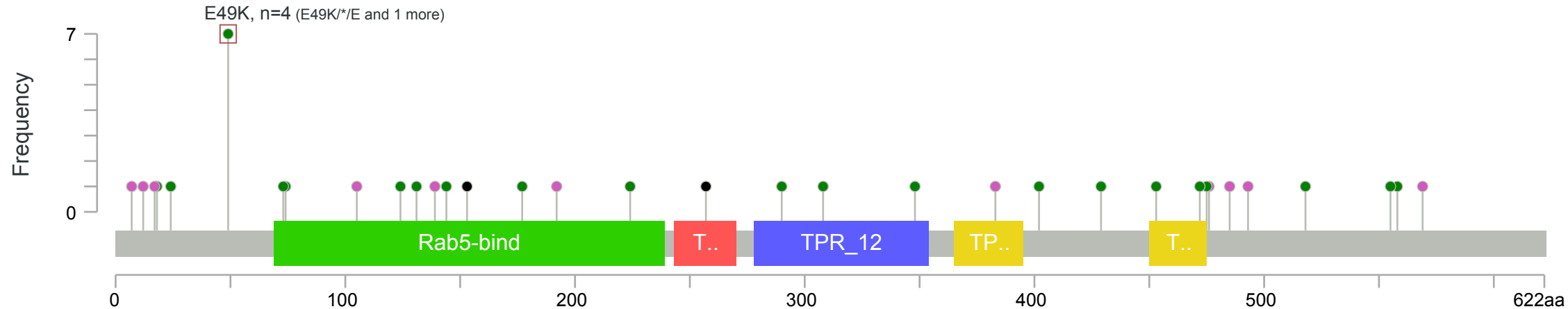
HLA-A mutations



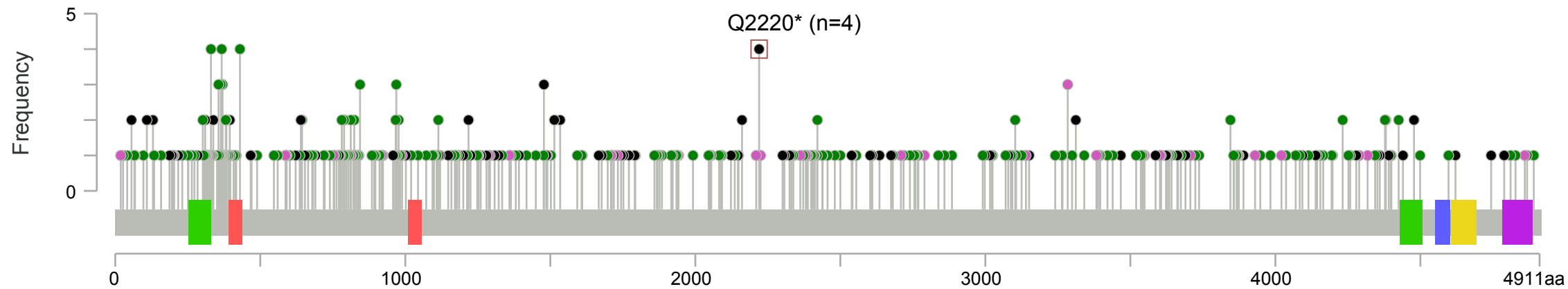
HSPB8 mutations



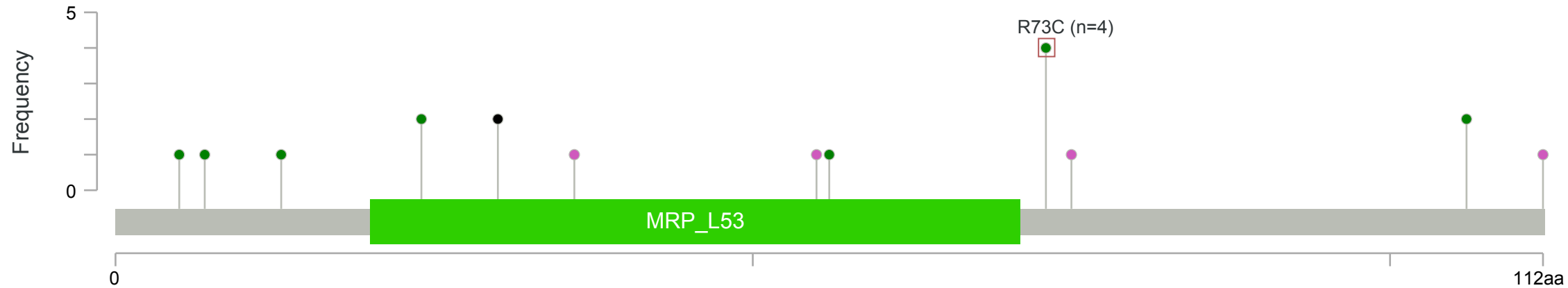
KLC2 mutations



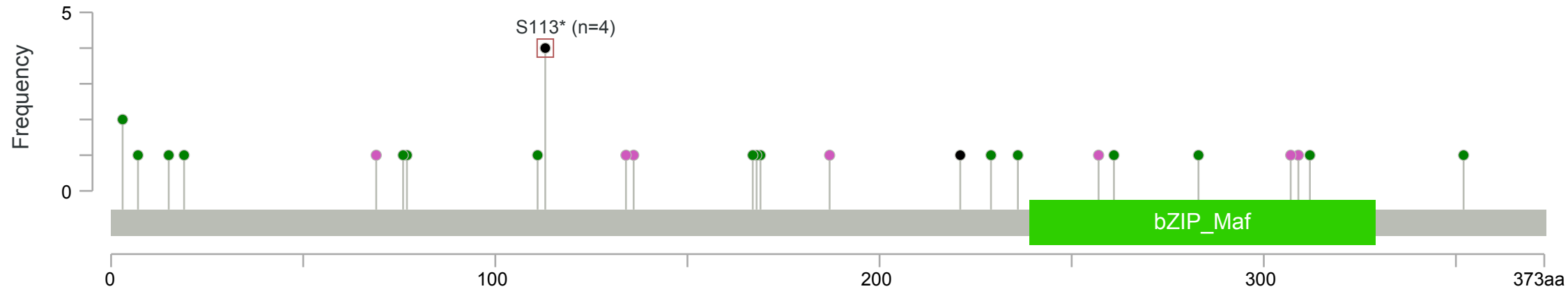
KMT2C mutations



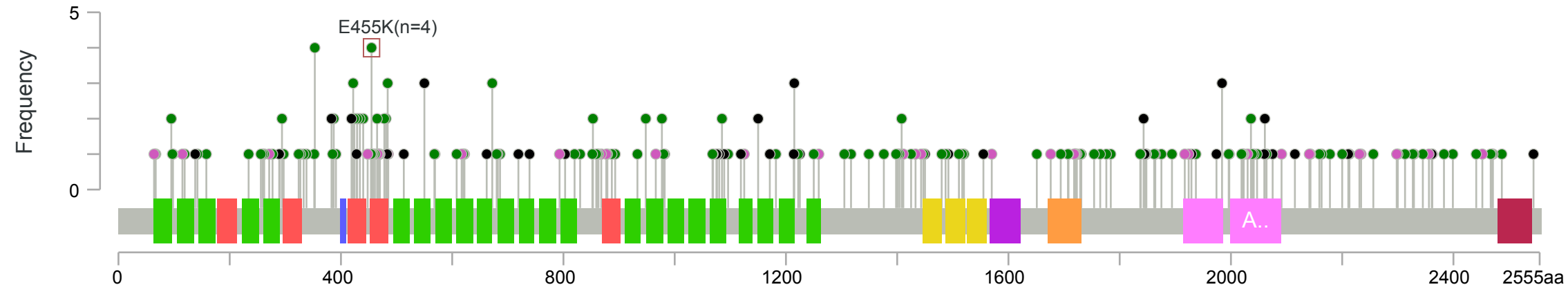
MRPL53 mutations



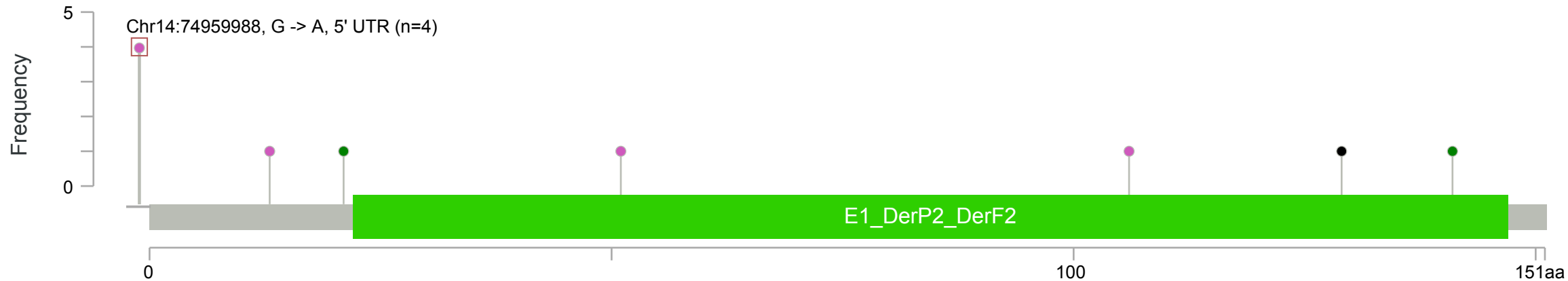
NFE2 mutations



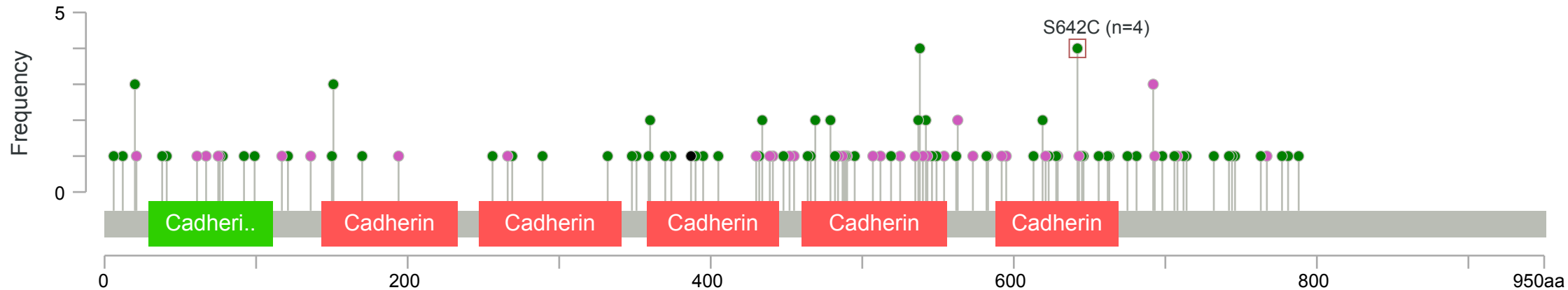
NOTCH1 mutations



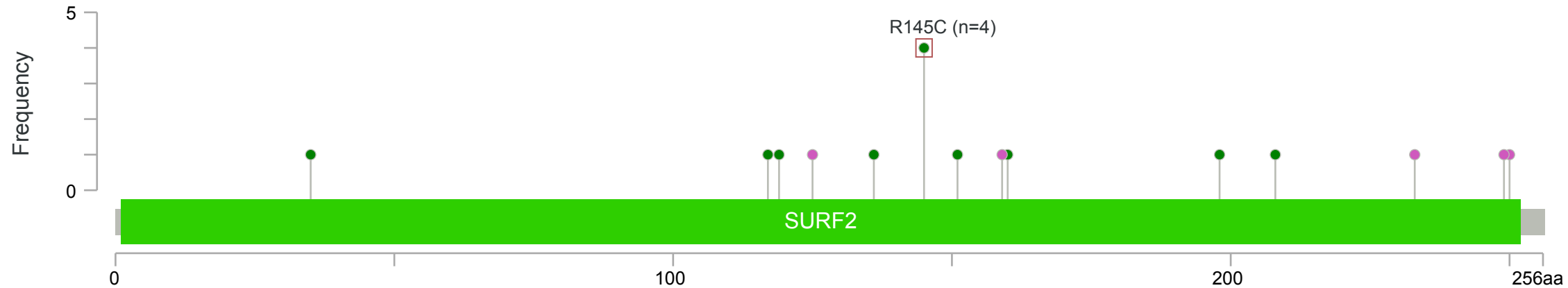
NPC2 mutations



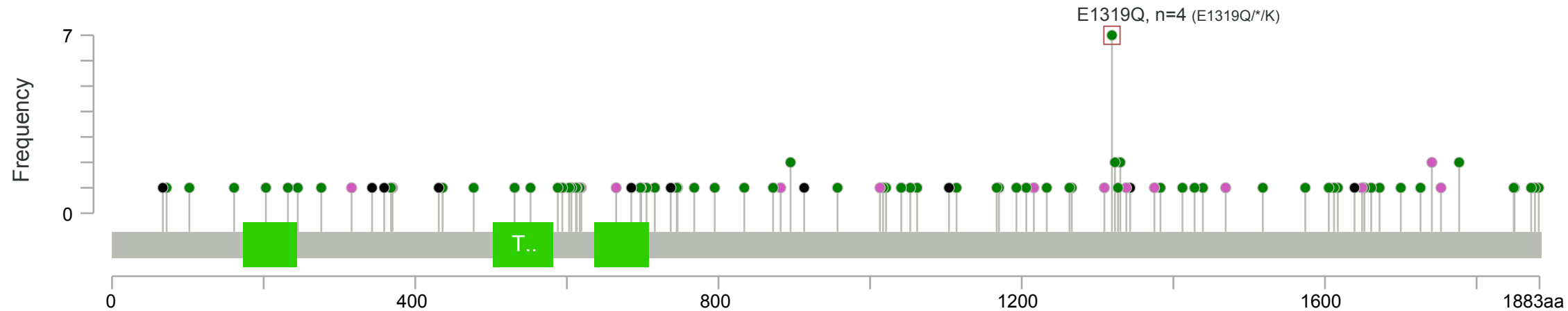
PCDHA8 mutations



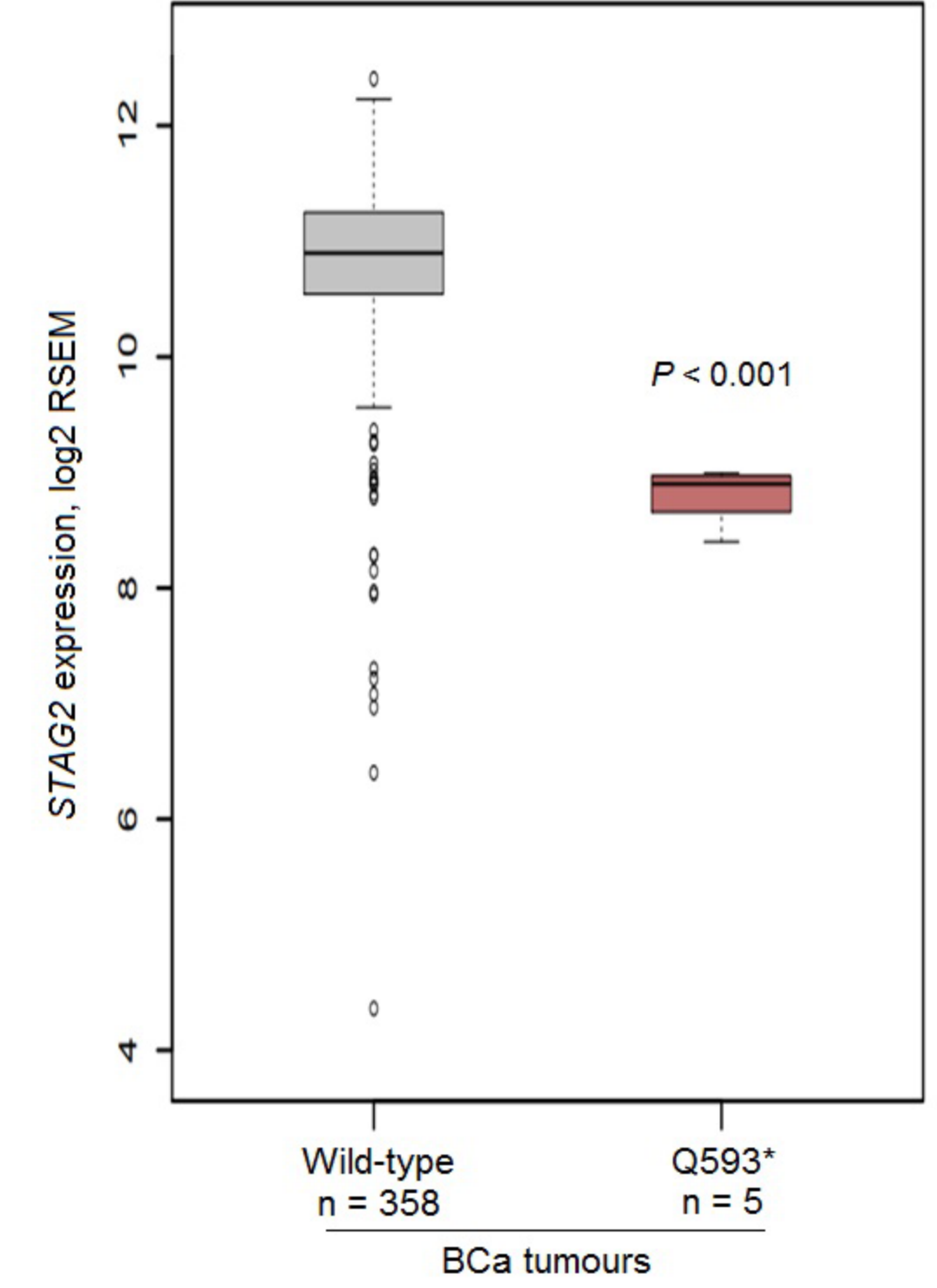
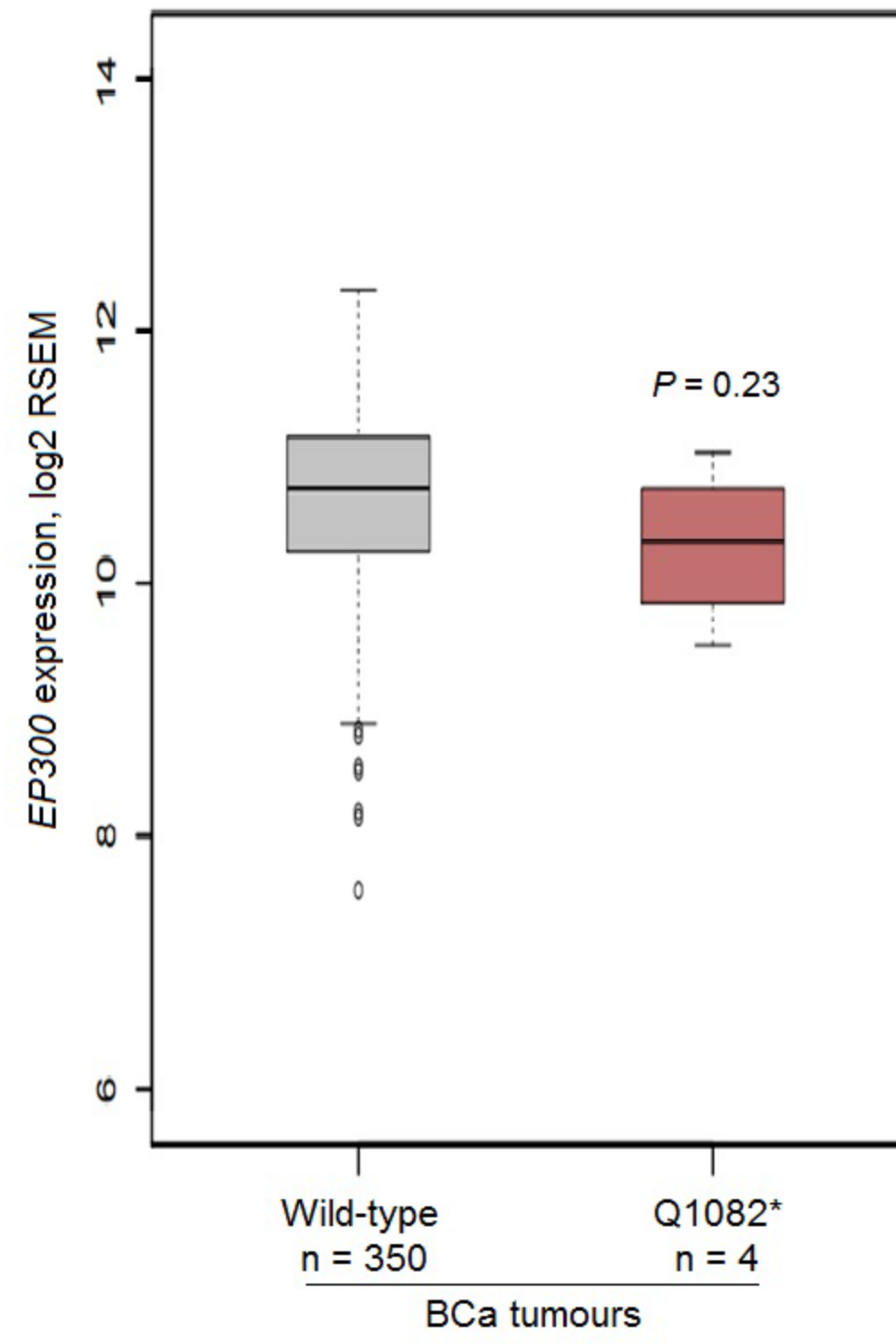
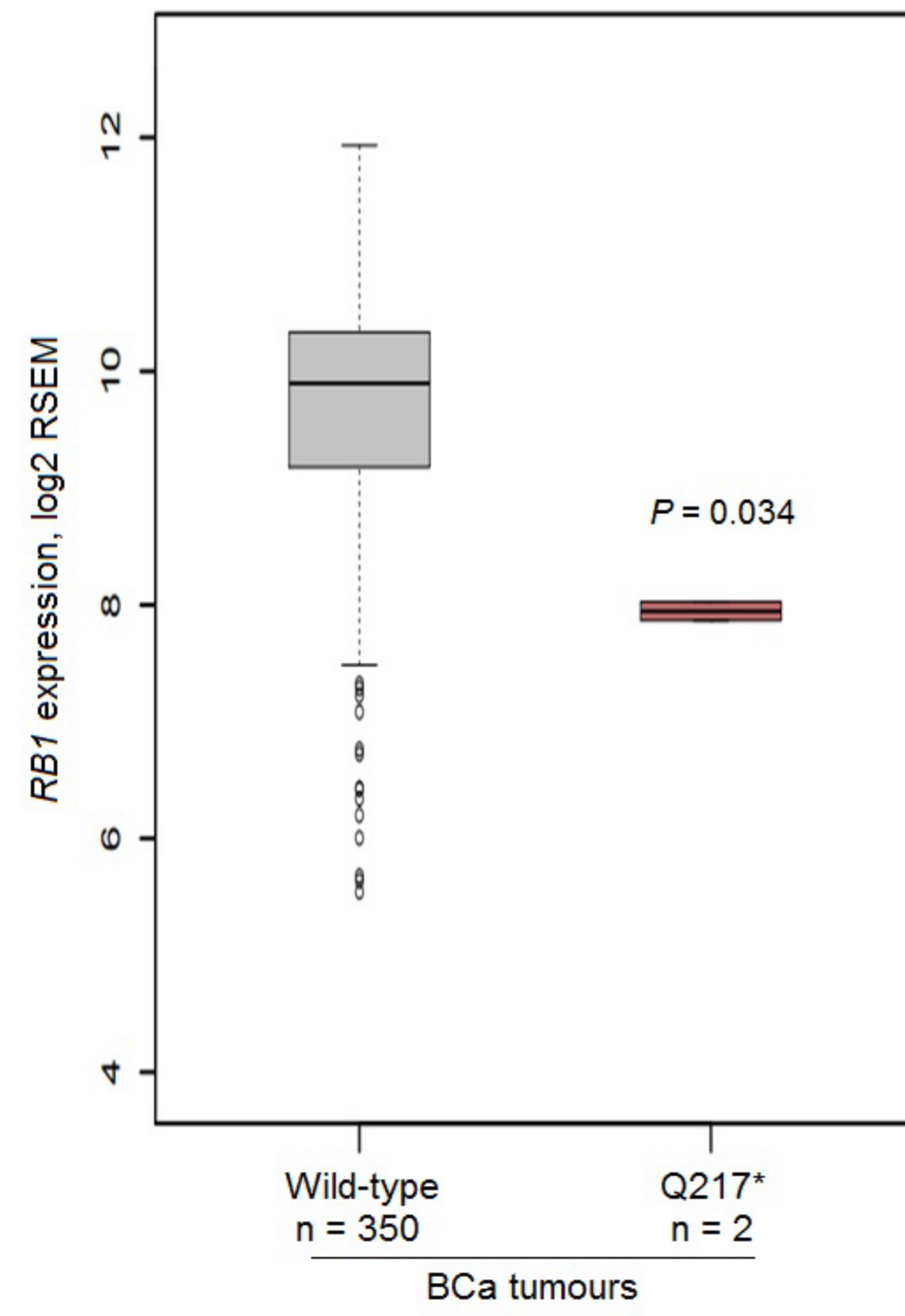
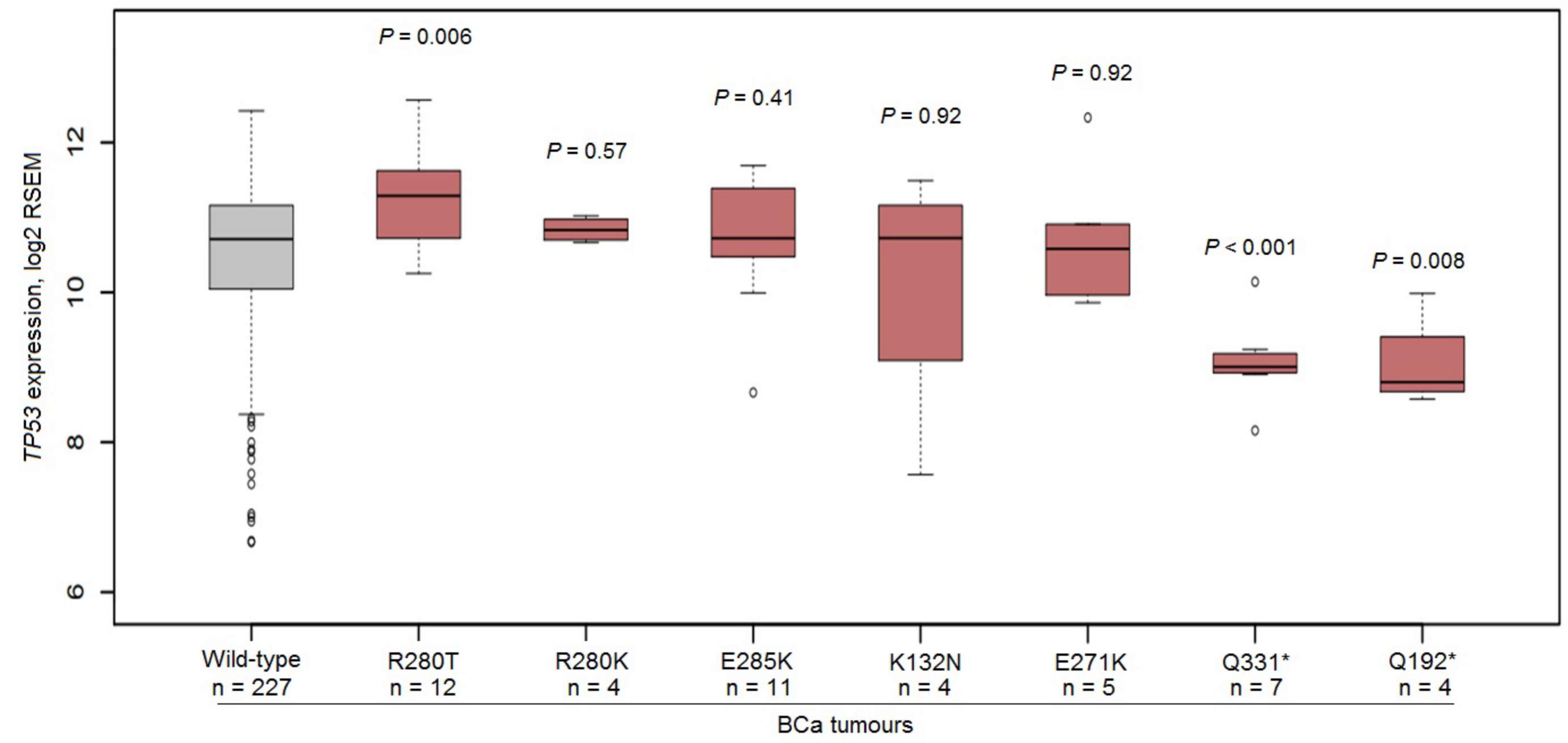
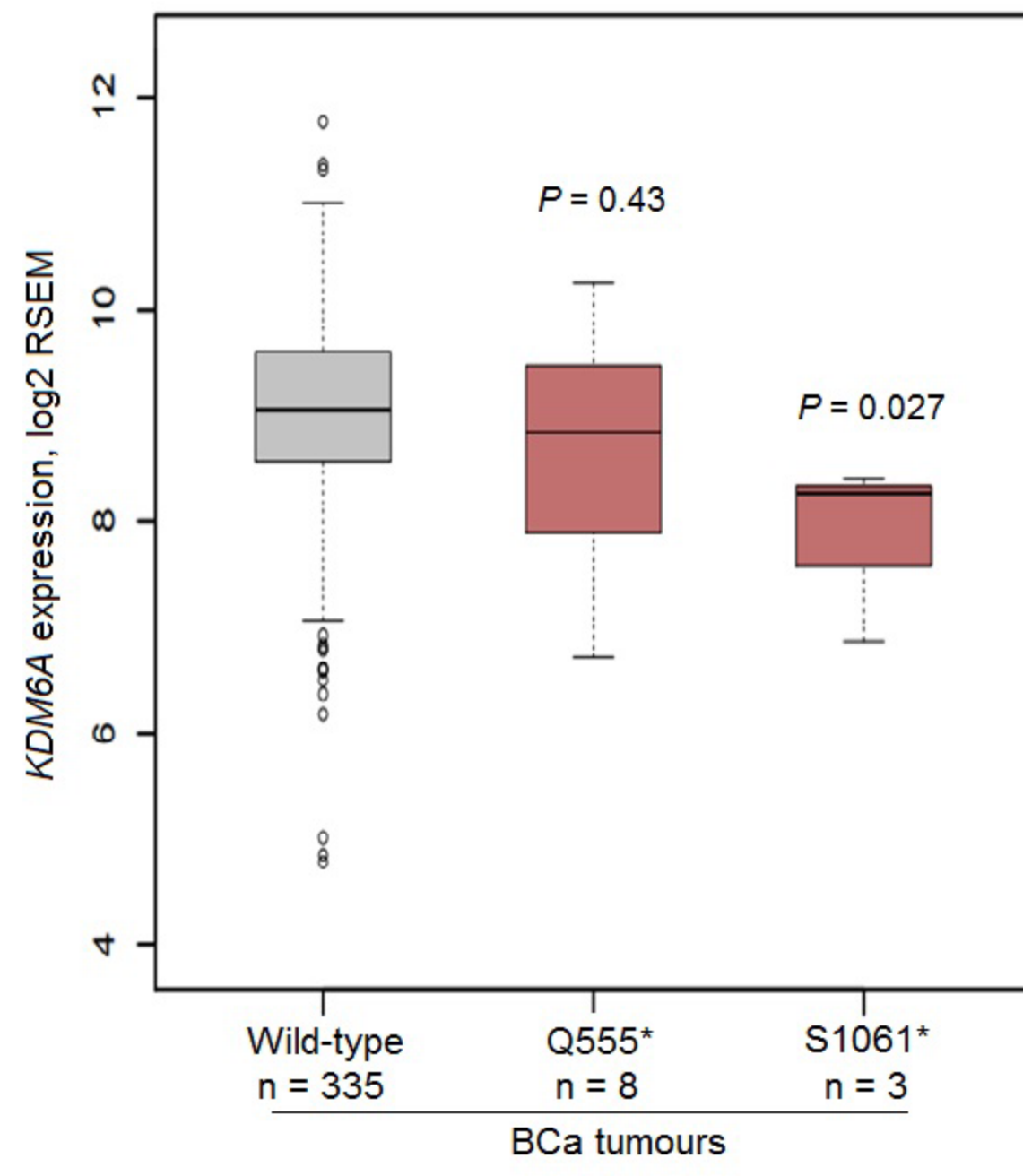
SURF2 mutations



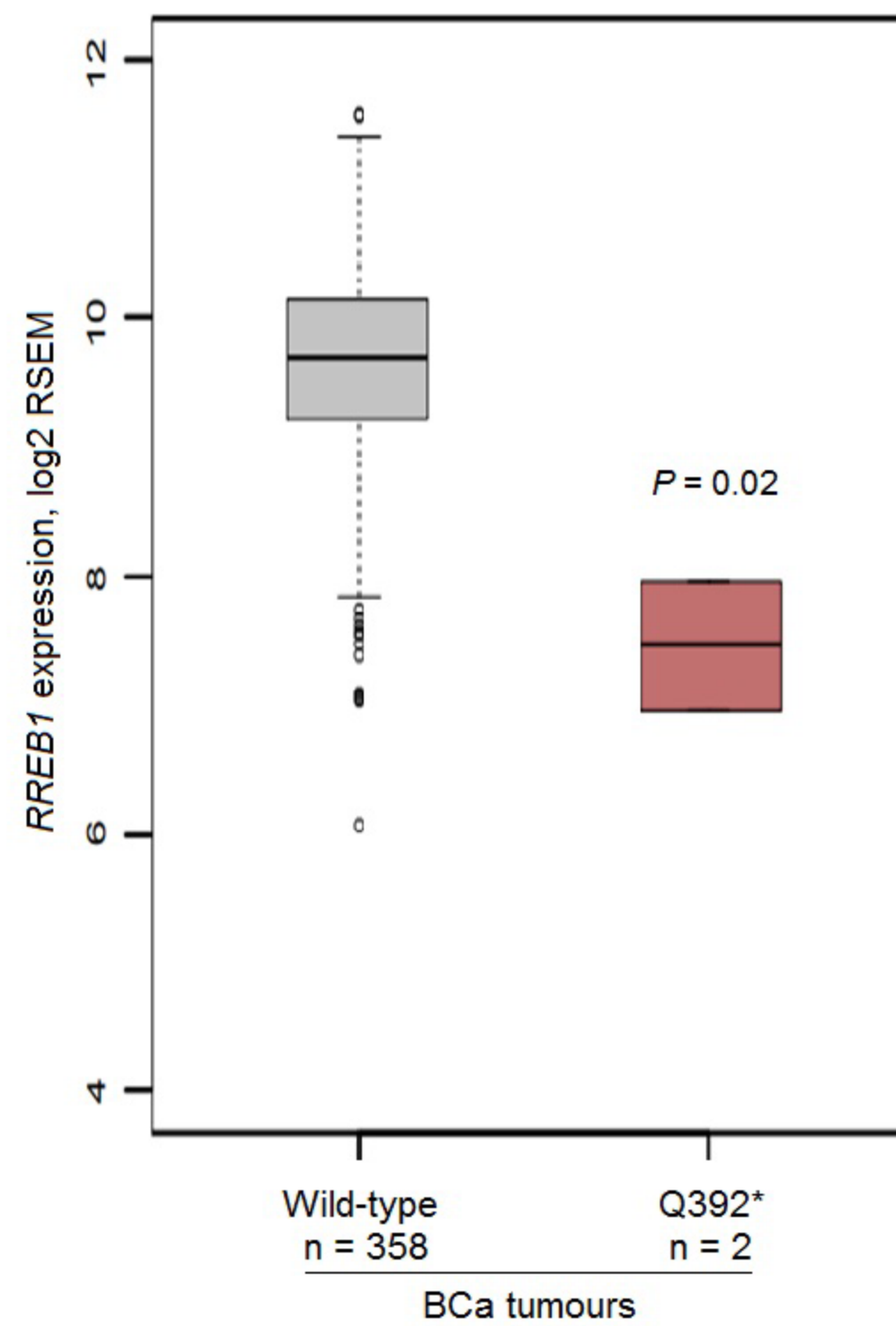
TMEM131 mutations



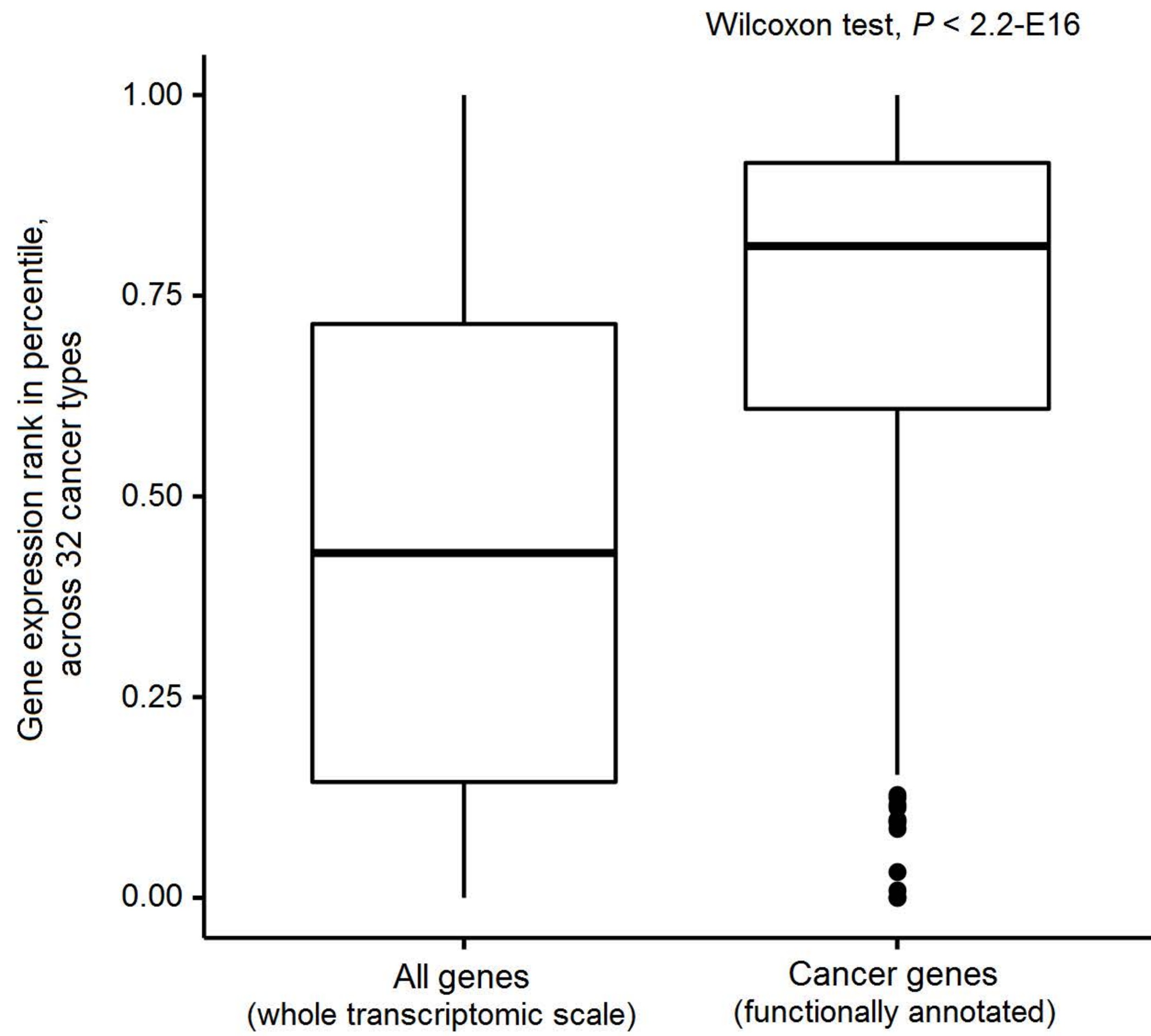
A



B



A



B

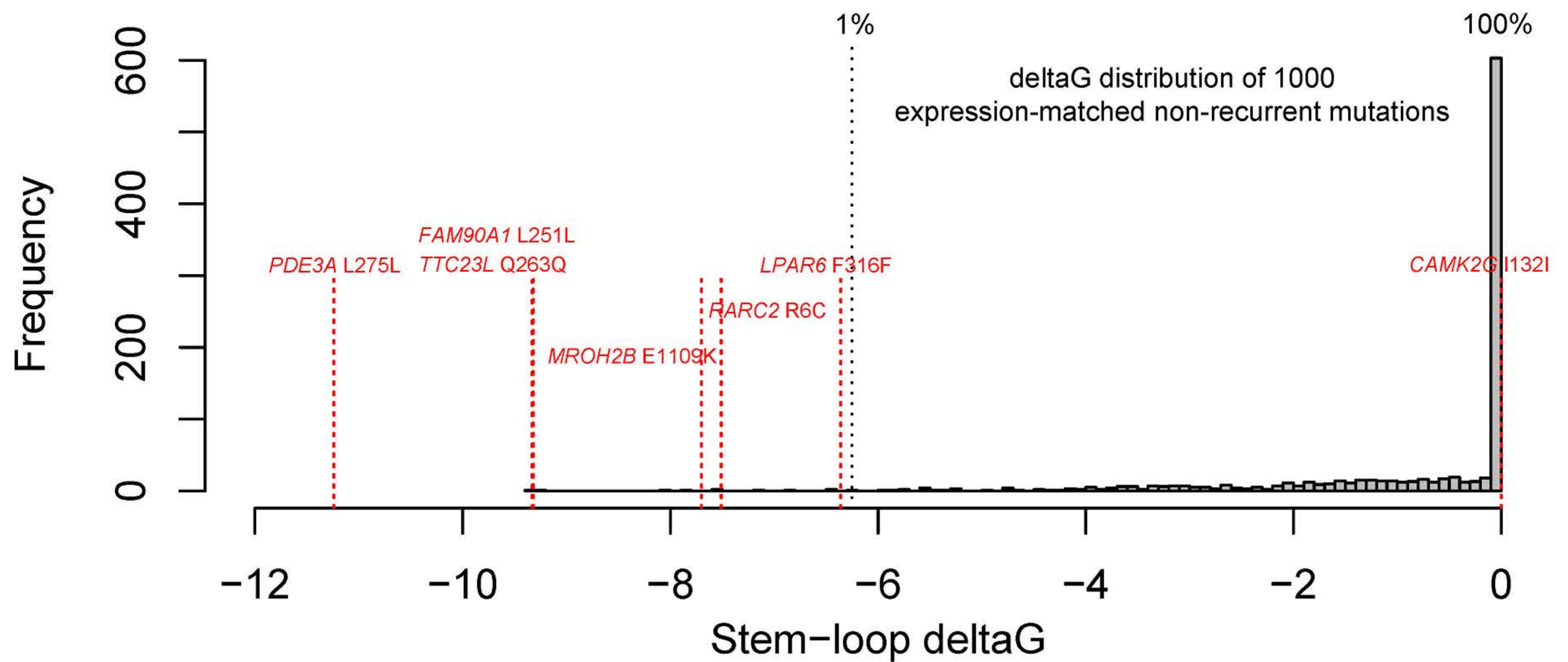
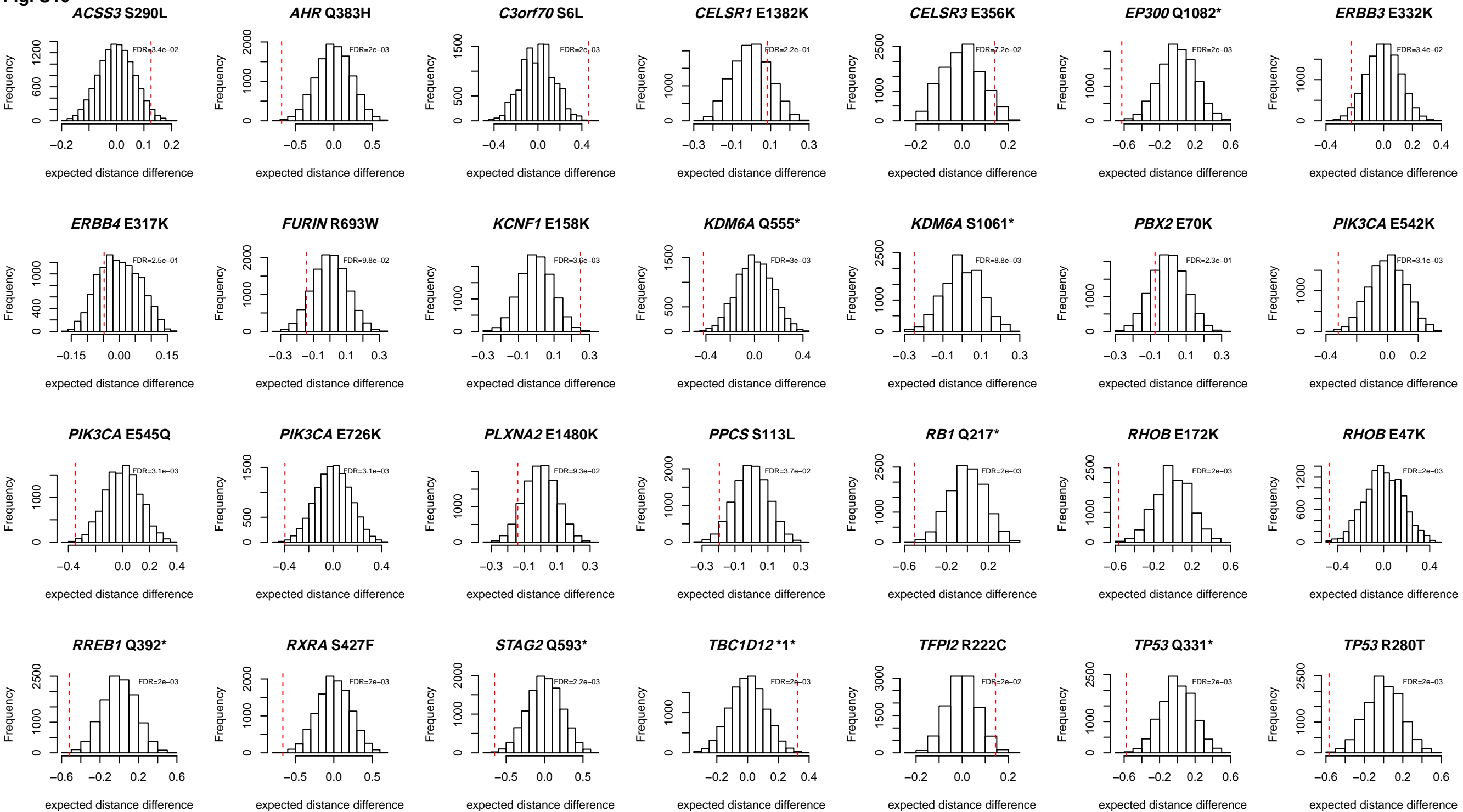
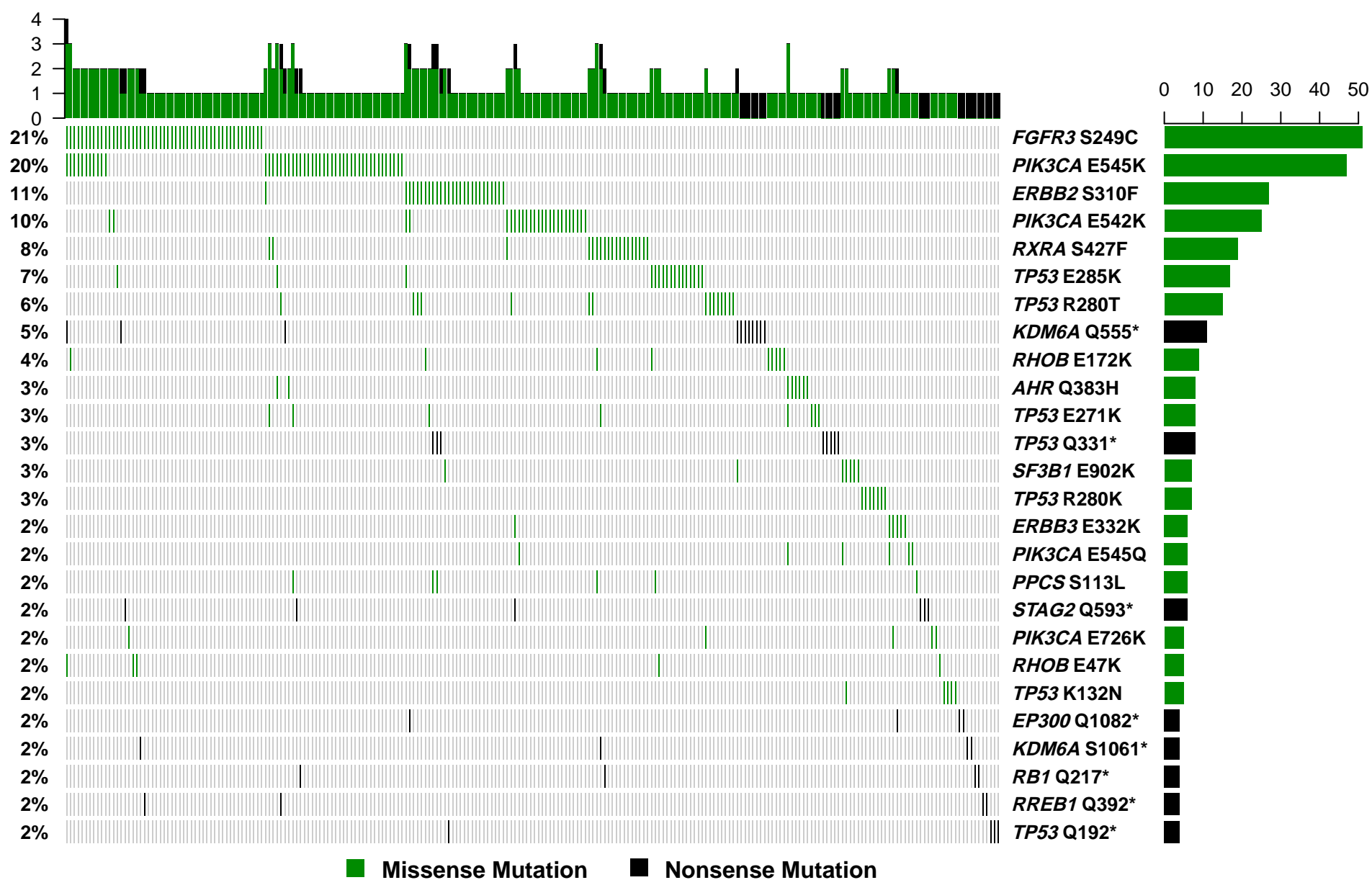
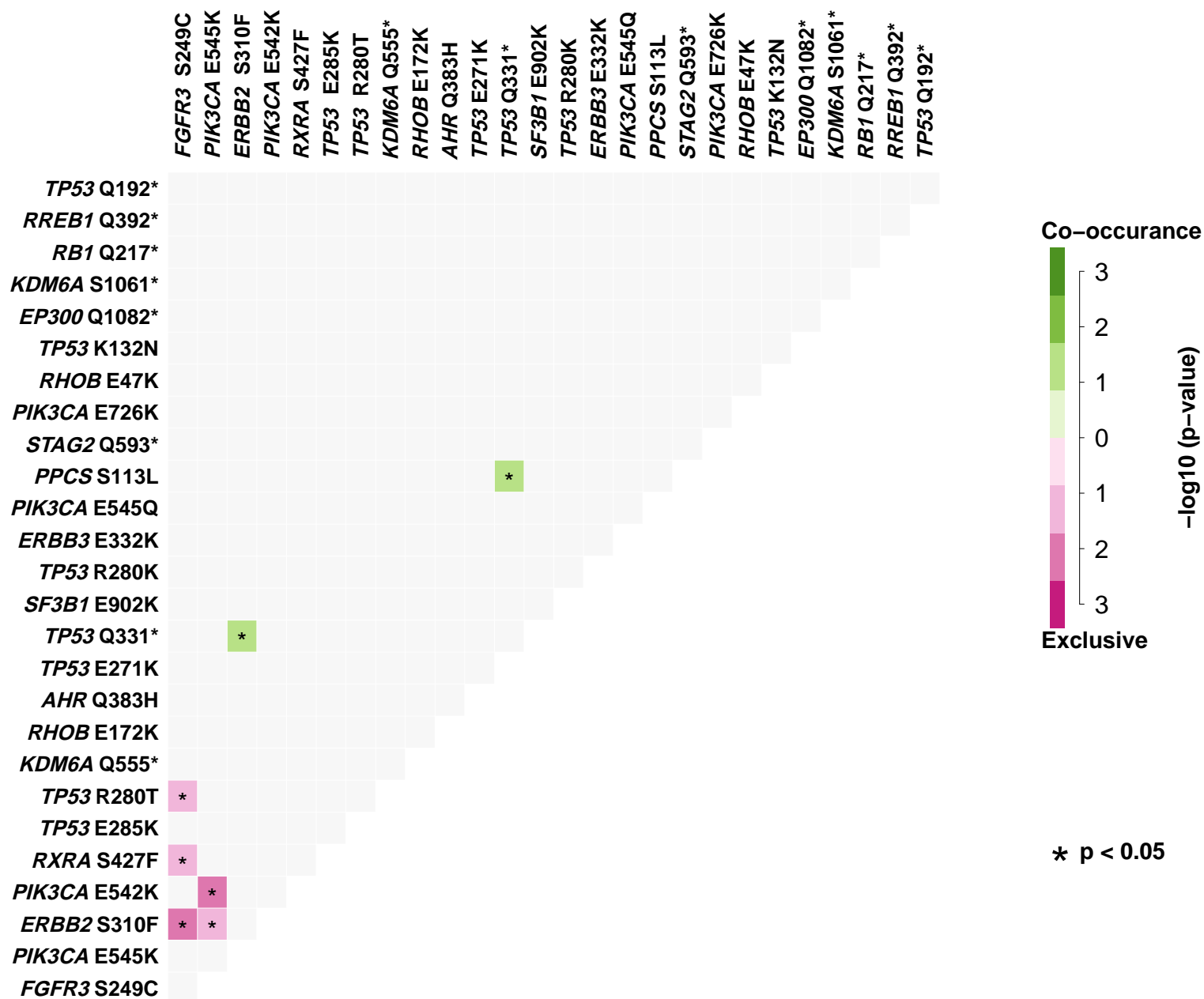


Fig. S10

A

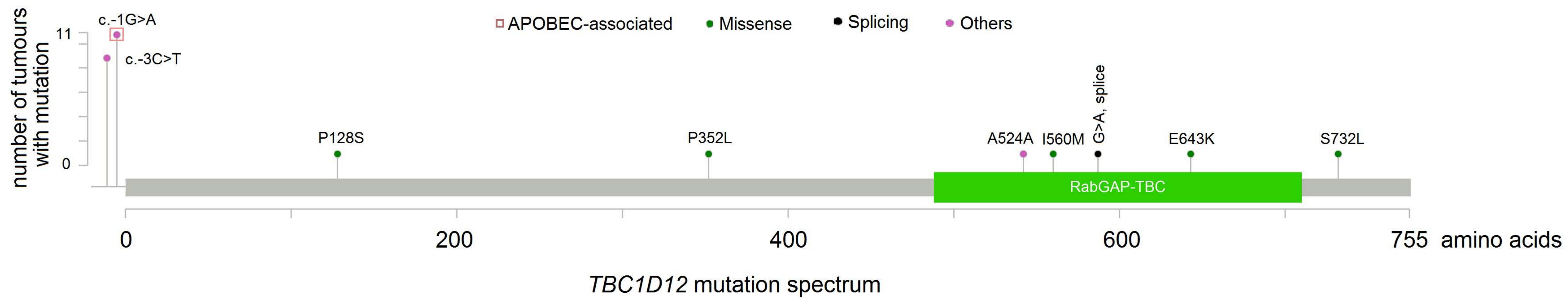


B



* p < 0.05

A



B

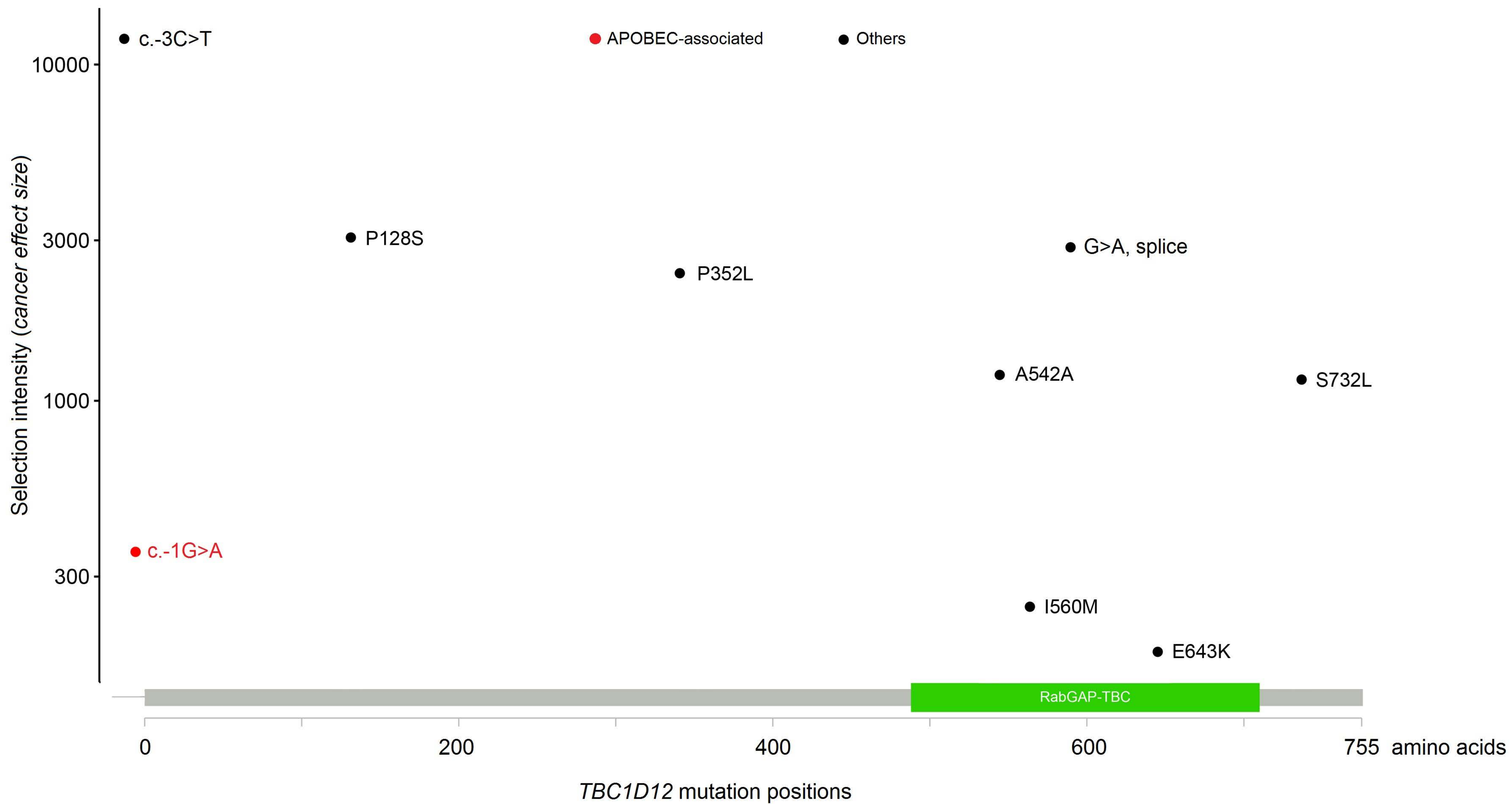


Fig. S13

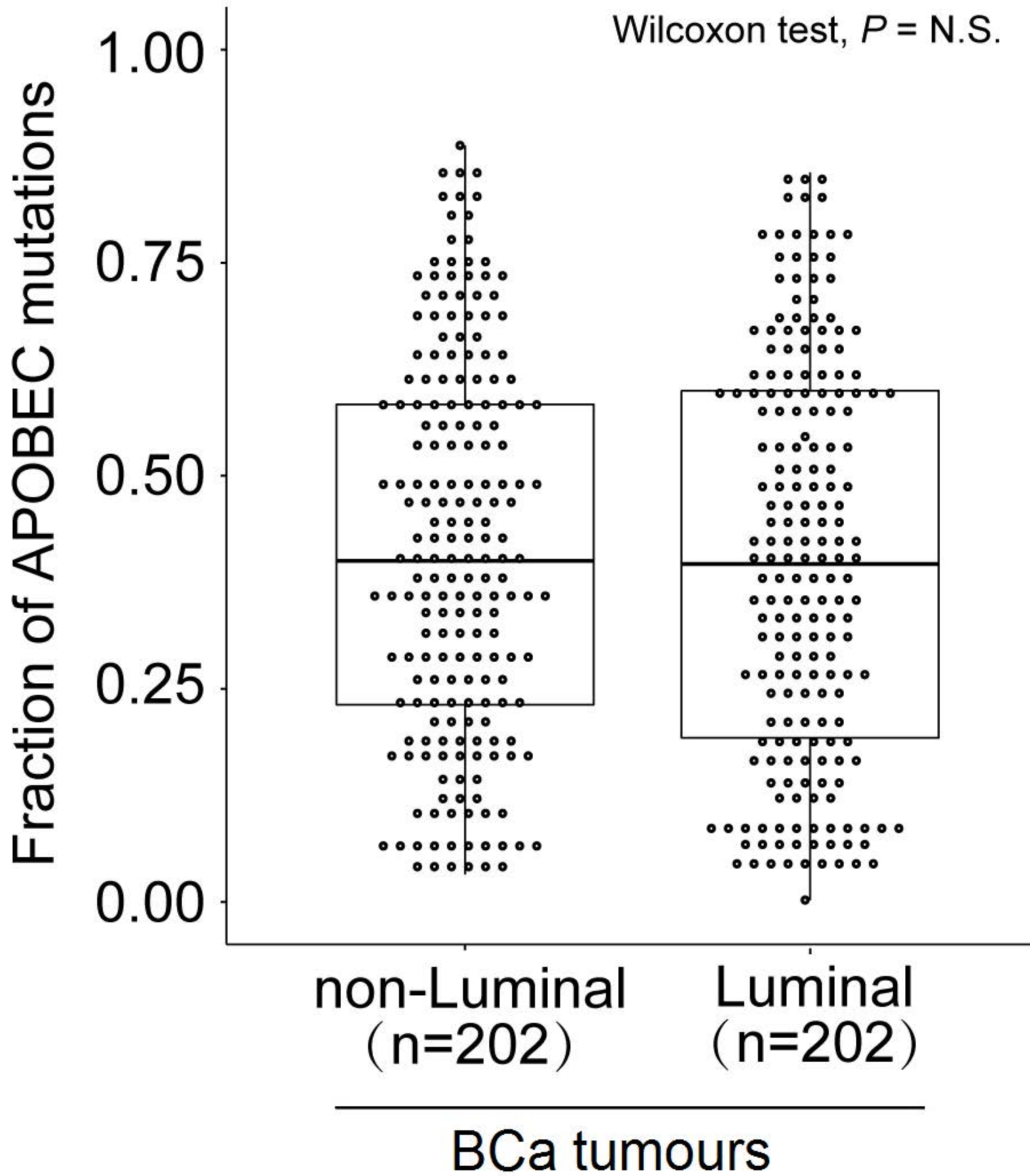


Fig S14

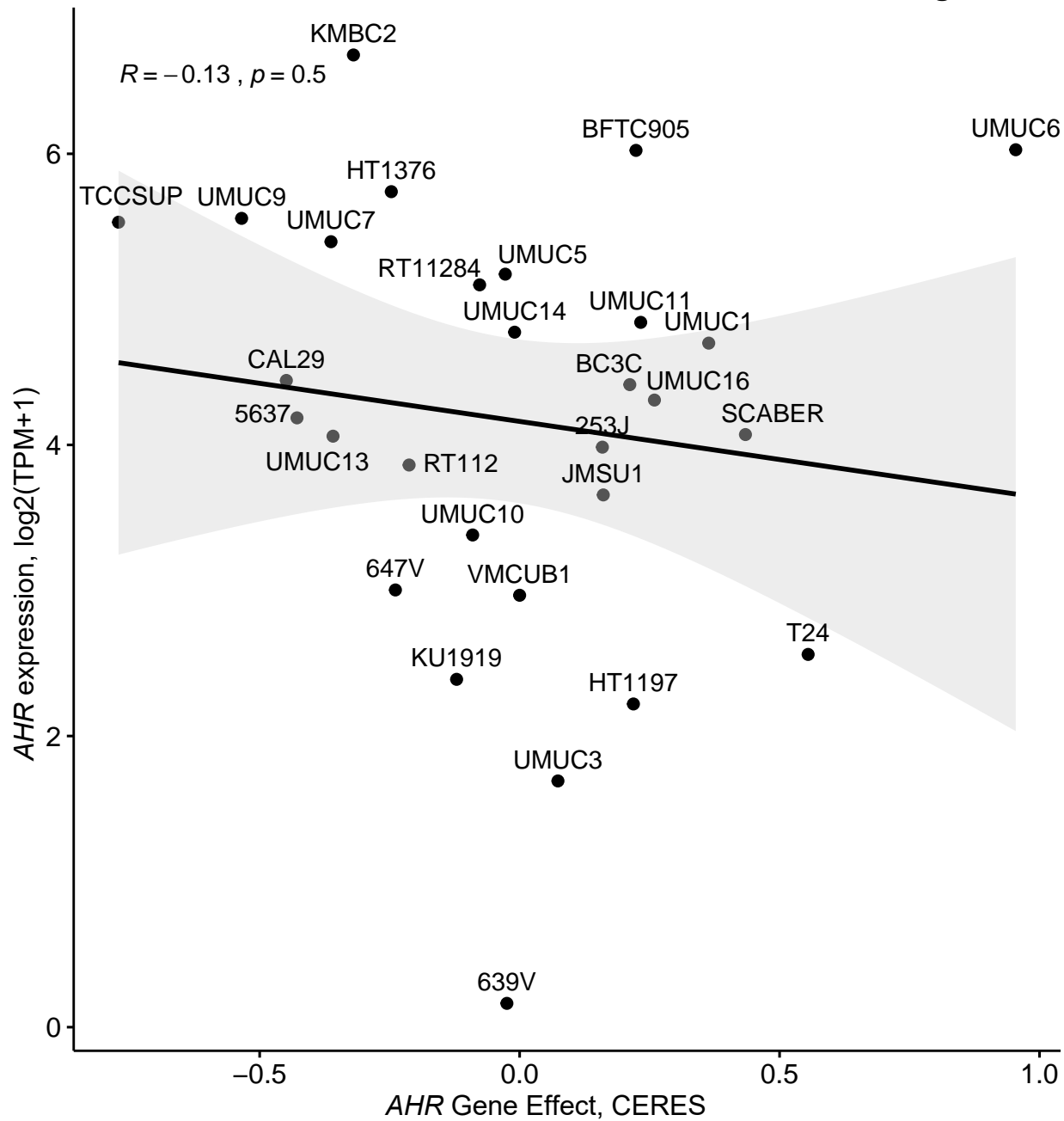


Fig S15

Wilcoxon signed rank test,
 $P = 0.03$

